GREEN SYNTHESIS OF METAL NANOPARTICLES AND THEIR APPLICATIONS AS PLASMONIC SUBSTRATES

A Thesis Submitted to
the Graduate School of Engineering and Sciences of
İzmir Institute of Technology
in Partial Fulfilment of the Requirements for the Degree of

MASTER OF SCIENCE

in Biotechnology

by

Beste ELVEREN

July, 2018

İZMİR

We approve the thesis of **Beste ELVEREN**

Examining Committee Members:

_____

Asst. Prof. Dr. Ahu ARSLAN YILDIZ
Department of Bioengineering, İzmir Institute of Technology

_____

Prof. Dr. Erdal BEDİR
Department of Bioengineering, İzmir Institute of Technology

_____

Prof. Dr. Elif ŞAHİN ILGIN
Department of Chemistry, Dokuz Eylül University

5 July 2018

_____

Asst. Prof. Dr. Ahu ARSLAN YILDIZ
Supervisor, Department of Bioengineering
İzmir Institute of Technology

_____

Asst. Prof. Dr. Ümit Hakan YILDIZ
Co-Supervisor, Department of Chemistry
İzmir Institute of Technology

_____

Assoc. Prof. Dr. Engin ÖZÇİVİCİ
Head of the Department of Biotechnology
and Bioengineering

_____

Prof. Dr. Aysun SOFUOĞLU
Dean of the Graduate School of
Engineering and Sciences

ACKNOWLEDGEMENT

First of all, I would like to acknowledge the constant support and advice from my thesis advisor Asst. Prof. Dr. Ahu ARSLAN YILDIZ, and co-advisor Asst. Prof. Dr. Ümit Hakan YILDIZ. Their support, guidance, encouragement and patience has so much value for me.

I would like to thank my family for supporting my academic career and being there for me every step of the way. I am so lucky that I have such good parents and a sister that trust me.

In addition, I would like to acknowledge 116Z547 project supported by The Scientific and Technological Research Council of Turkey (TÜBİTAK), and the Scientific Research Project 2016IYTE70 by İzmir Institute of Technology. Also, special thanks to Izmir Institute of Technology, Centre for Materials Research (MAM) and Biotechnology and Bioengineering Applications and Research Centre (BİYOMER) for their contribution.

Besides, I would like to thank to Biomimetics and BioSens&BioApps family for their friendship. All the fun we had and all the friendships I gained, has special place in my heart.

Lastly, I am very grateful of my friends, who have supported me while I had difficult times through my thesis and life, and helped me overcome them. So thank you my dears, Cansu UÇAR, Rojda CAN, Özge GÜZEL, Fazilet GÜRER, and Seda DUMAN. And, do not get spoiled over writing your names here. I would also thank to my other friends whom I could not write their names. Moreover, my boyfriend Bashir İbrahim YABANİ, I cannot explain how important your support was, so thank you.

ABSTRACT

GREEN SYNTHESIS OF METAL NANOPARTICLES AND THEIR APPLICATIONS AS PLASMONIC SUBSTRATES

Gold nanoparticles (GNPs) have been widely used in diagnostic, tissue engineering, and drug delivery fields, in the last decades. Generally, reducing gold salts to zero valent gold has been accomplished by harsh chemicals and strong reducing agents, which cause toxicity and eventually limiting the bioapplications. Green synthesis is a newly developing methodology to synthesize GNPs. Especially natural products and plants extracts are commonly preferred for green synthesis based on their natural content. Biological molecule-capped GNPs, are more biofriendly and biocompatible nano-materials that can be used for varied applications.[1-3] Sensor applications; varying from biosensing to environmental analysis, are an important field that GNPs were intensively utilized.[4-5]

Cyanide ion (CN^-) has been considered as one of the main pollutants of water, because of its rapid discharge. CN^- is currently being used in industry such as; polymer synthesis[6], noble metal mining[7], pest control[8], plastics production etc., at large scale. However, there is an unmet need for CN^- detection and monitoring. Colorimetric detection of CN^- that utilizes GNPs has been done by several researchers.[9-10] However, in all these studies reduction of GNPs were done by strong reducing agents. Green synthesis of GNPs eliminates the toxic side-products that can be harmful to both environment and human health. To overcome this problem green synthesized GNPs were used to establish the sensor platform, which can be further employed for CN^- detection. Oxidation of GNPs in the presence of cyanide molecules is a direct-forward, colorimetric and optical method that requires no toxic chemicals; therefore it is a greener approach towards CN^- detection in water resources.

ÖZET

METAL NANOPARÇACIKLARIN YEŞİL SENTEZİ VE BUNLARIN PLAZMONİK SUBSTRAT OLARAK UYGULAMALARI

Altın nanoparçacıklar (GNP'ler) son yıllarda tanı, doku mühendisliği ve ilaç iletimi alanlarında yaygın olarak kullanılmaktadır. Genel olarak, altın tuzlarının sıfır değerlikli altınlara indirgenmesi, sert kimyasallar ve güçlü indirgeyici ajanların kullanılmasıyla yapılmasından kaynaklı toksisiteye neden olur ve sonuç olarak biyo-uygulamalarını sınırlar. Yeşil sentez, GNP'lerin sentezlenmesi için yeni bir metodolojidir. Özellikle doğal ürünler ve bitki özleri, doğal içeriğine göre yeşil sentez için tercih edilir. Biyomoleküler kaplı GNP'ler, çeşitli uygulamalar için kullanılabilen biyouyumlu nanomalzemelerdir.[1-3] GNP'lerin yoğun kullanım alanları sensör uygulamaları ve biyosensörden çevre analizine kadar değişkenlik gösterir.[4-5]

Siyanür iyonu (CN^-), hızlı deşarjı nedeniyle suyun ana kirleticilerden biri olarak kabul edilir. CN^- farklı sektörlerde kullanılmaktadır: Polimer sentezi[6], soy metal madenciliği[7], böcek kontrolü[8], plastik üretimi, vb. Bununla birlikte, CN^- tespit ve izleme için karşılanmamış bir ihtiyaç vardır. GNP'ları kullanarak siyanürün kolorimetrik belirlenmesi pek çok araştırmacı tarafından yapılmıştır.[9-10] Bununla birlikte, tüm bu çalışmalarda, GNP'lerin indirgenmesi güçlü indirgeyici maddeler tarafından yapılmıştır. GNP'ların yeşil sentezi, hem çevreye hem de insan sağlığına zararlı olabilecek zehirli yan ürünleri ortadan kaldırır. Yeşil sentezlenmiş GNP'ların CN^- algılamasında kullanılması, tüm bu sorunları çözebilmek amaçlı yeni bir platform oluşturur. Sodyum oksitlerin varlığında GNP'ların oksidasyonu, toksik kimyasallar gerektirmeyen doğrudan kullanılabilir, kolorimetrik ve optik bir yöntemdir; bu nedenle su kaynaklarında CN^- tespiti için daha yeşil bir yaklaşımdır.

To my family

TABLE OF CONTENTS

LIST OF FIGURES

Figure **Page**

LIST OF TABLES

Table **Page**

CHAPTER 1

INTRODUCTION

1.1 Scope of the Thesis

Green synthesis of GNPs is a newly developing technique that provides more benefits compared to other GNP synthesis methodologies, which uses harsh chemicals. *Melissa officinalis* (Lemon Balm), *Punica granatum* (Pomegranate), and *Salvia officinalis* (Sage) plants are used as mild reducing agents in this work. Characterization of green synthesized GNPs is done by well-known techniques; such as UV-Vis Spectroscopy, FTIR, SEM, AFM.

Cyanide (CN^-) is one of the main pollutants in water because of its constant and rapid discharge to environment. Here green synthesized GNPs were immobilized onto solid platform and that plasmonic platform was utilized as a CN^- sensor for CN^- detection in water.

1.2 Nanoparticles and Their Plasmonic Properties

Nanoscience is considered to be the manipulation of materials in nano-scale.[11] It is considered as a nano-scale when at least one dimension of a material is in the range of 1-100 nm.[12] The continuous developments in nanoscience, and the applications on biomedical areas have huge role in the fields of drug delivery, sensing, tissue engineering, and diagnosis.

There are different kinds of nanomaterials produced from variety of chemicals, which are; metals, polymers, ceramics, metal-oxides, carbon, silicates and biomolecules like liposomes. Nanoparticles (NPs) are currently the preferable materials because of the size and easy to manipulate surface properties. Some metal NPs have plasmonic properties which put them in a very unique position.

Plasmon is the quantum of plasma oscillation, and it is created by the quantization of oscillations.[13] When plasmons couple with photons, they cause the

generation of polaritons. Surface plasmon resonance (SPR) is the resonance emission of conductive electrons at the interface between the excited negative and positive permittivity of material, excited by incident light, which is an optical method commonly used in sensor applications. SPR spectroscopy uses this phenomenon to observe the bio-affinity of two components; one of which is immobilized to the metal surface and the other one passes through the flow cell.[14] SPR property can also be observed on the nanoparticle surfaces and can be utilized for solution-based assays. Localized Surface Plasmons (LSPRs) are excited, by the wavelength smaller than, the diameter of the nanoparticle and conduction electron vibration frequencies in the NPs.[15] The LSPR effect depends also on the size, shape and electromagnetic properties of the NPs. Measurement of these plasmons is called Localized Surface Plasmon Resonance (LSPR) Spectroscopy. Similarly, LSPR is highly sensitive to the refractive index change of the medium. Only some metals show plasmonic properties as listed on Table 1.

Table 1. Plasma Frequencies of metals

Metal	**Plasma Frequency**
Lead, Pb	Ultra-violet
Indium, In	Ultra-violet
Mercury, Hg	Ultra-violet
Tin, Sn	Ultra-violet
Cadmium, Cd	Ultra-violet
Gold, Au	Visible
Cupper, Cu	Visible
Silver, Ag	Visible

Nanoparticles have unique optical properties because of their size and structures, which limit their electrons and create quantum effects. To illustrate; gold nanoparticles appear wine-red in solution[9]. For the materials that consist of nanoparticles, the absorption of continuous light is higher than the thin films of the material.[10] The core-shell nanoparticles can boost, both electric and magnetic resonances, at the same time, showing unique properties when compared with the normal studies.[11] Differently; superparamagnetism, quantum confinement of semiconductor particles and SPR properties depend on the size of the nanoparticle. Particle size, capping agent,

interparticle distance, and, shape of the nanoparticle, have a huge role on the physical properties of nanoparticles. Different shapes have been found in literature which are named using nano prefix before the geometrical shape, like, nanorods, nanocubes, nanostars, nanoplates, nanoshells and nanoclusters.[13] The shape of the nanoparticle, also, affects the surface properties and functionalization conditions. Different shapes can be used for different applications, including diagnosis, and sensor technologies.

1.2.1 Nanoparticle Synthesis Methods

Nanoparticle synthesis is an important step of nanoscience, since most of the surface properties are fixed at that stage. Several methods for NP synthesis have been developed over the past couple of decades, which are categorized as two groups; top down and bottom up approaches.

As seen from Table 2, top down approaches include, chemical etching, laser ablation, mechanical miling and sputtering, while bottom up approaches consists of aerosol processing, atomic condensation, electrochemical precipitation, biological process, laser pyrolysis, sol-gel process and vapor deposition.[16]

Top down approaches involves mechanical/thermal cycles causing broad size distribution (1 nm-1 μm), and varied shapes. This limits the applications to nanocomposites and nano-grained bulk materials.[17] Differently, bottom up approaches have higher control over the reaction kinetics and controlled size generation, which makes them much more preferable than top down approaches.

Surface of the metal nanoparticles can be easily functionalized especially with biomolecules for biosensing, diagnosis, and detection applications. They are also as an agent for drug delivery systems and gene transportation.[15] The applications of nanoparticles using SPR technology vary from biosensing to adsorption studies.[16-18] Lipid vesicles are used for the adsorption studies[19], while other nanoparticles can be used for the signal enhancement processes.[20]

1.2.2 Gold Nanoparticles

Gold is an universally enquired nanomaterial for the last couple of decades, since the metal has very low toxicity to biological environment, and unique surface,

plasmonic, and chemical properties, as well as good stability and biocompability.[18-20] Addition to its biocompability, GNPs are considered to be inert, as well. The applications of GNPs can range from imaging, therapeutic to diagnostics fields since their physical properties can be precisely controlled. This control over GNPs; also, contributes to its optical and physiochemical properties. Different shapes (Table 3) and different sizes of GNPs; also, contributes to these properties.

Table 2. Nanoparticle synthesis methods

Top Down Approaches	**Bottom Up Approaches**
Etching (chemical)	Aerosol process
Laser ablation	Atomic condensation
Mechanical miling	Electrochemical precipitation
Sputtering	Biological process
	Laser pyrolysis
	Sol-gel process
	Vapor deposition

In literature, it is observed that the first GNP synthesis is performed by Faraday[21], using auric chloride ($AuCl_4$) as precursor and phosphorus (P) as reducing agent. This study opened a new era in GNP synthesis and his successors developed new methods as the area expanded.

In 1951, the Turkevich method is founded using citrate as mild reducing agent.[22] The method then became one of the commonly used methodologies for GNP synthesis *in situ*. The synthesis is done under 100 °C by the addition of trisodium citrate dihydrate ($Na_3C_6H_5O_7$) to auric acid ($HAuCl_4$). A wine red color and monodispersed 20 nm GNPs are synthesized. When investigated by Frens[23], it is found that the size of the particles can be adjusted from 15 to 150 nm in varied ratios of citrate and auric acid.

Another well-known method is the Brust-Schiffrin[24] method that uses thiolate ($C_{10}H_{10}O_4S_3$) to generate relatively smaller particles. Particle size for this method ranges from 2 to 5 nm, and this provides thermal stability to particles along with easy functionalization and modification properties. Thiol groups cap the GNPs in a way that is uniquely close packed which is called self-assembly monolayer (SAM). This

phenomenon is caused by the empty p orbitals on both gold (Au) and sulphur (S). Functionalization of gold surfaces with thiolates can also be observed from different studies.[25-27]

In a study by Liang et. al a cyclic arginine-glycine-aspartic acid [c(RGDyC)] – gold nanoclusters (AuNCs) were synthesized by using aqueous $HAuCl_4$ solution.[28] Gold solution was added to the peptide solution and as a stabilizer, NaOH solution was introduced 2 min later to arrange the pH of the mixture between 12-13.

Table 3. Dimensional Shape Separation of NPs

Zero dimensional	One dimensional (1D)	Two dimensional (2D)	Three dimensional (3D)
• Nanoparticles • Quantum dots	• Nanorods • Nanowires • Nanotubes • Nanobelts	• Nanostars • Nanopentagons • Nanoplates	• Nanotadpoles • Branched NPs • Nanodumbells • Nanopods

In another study, water-soluble 3-nm gold NPs were synthesized using one of the ligands; thiol ligands 2-(2- mercaptoethoxy)ethanol or ligand 2-[2-(2-mercaptoethoxy)ethoxy]ethanol.[29] $HAuCl_4$ was dissolved in 2-propanol, obtaining a yellow solution. Using one of the ligands, gold solution was mixed and to this solution,$NaBH_4$ solution in methanol was added rapidly with stirring, resulting in a color change from yellow to dark purple.

As the size of the particle continues to reach the bulk limit, the surface plasmon resonance wavelength moves toward the Infra-Red region of the spectrum and the most visible wavelengths are echoed, so that the NPs turn into an open or semi-transparent color as shown in Table 4.[30] Size or the shape of the nanoparticle can be tuned for specific surface plasmon resonance values, leading to unique optical properties adjusted for just different applications.

1.2.3 Green Synthesis of Metal Nanoparticles

Different sorts of metal nanoparticle synthesis methods have been developed over the last decade. Most methods use harsh chemicals for the reduction of metals.

The side-products of these chemicals are toxic to both environment and human health.[31] Currently nanoparticle synthesis methods include biological processing, namely "green synthesis" started to become more preferred method over using harsh chemicals. Biological process uses yeast, bacteria, fungi, algae, or plant to initiate the reaction.[32] While yeast, bacteria, algae and fungi uses their own bioprocesses to reduce the metal salts, plants are being used as cell-free extracts. Figure 1 shows the suggested reaction between phenolic molecules, which will be explained further in the chapter, that are contributing to reduction with gold primer.

Table 4. Maximum wavelength values of GNPs depending on size

Diameter	**Nanoparticles/ mL**	**Peak SPR Wavelength**	**RGB code of the color**
5 nm	$5.47x10^{13}$	515-520 nm	#1fff00 - #36ff00
10 nm	$5.98x10^{12}$	515-520 nm	#1fff00 - #36ff00
15 nm	$1.64x10^{12}$	520 nm	#36ff00
20 nm	$6.54x10^{11}$	524 nm	#46ff00
30 nm	$1.79x10^{11}$	526 nm	#4eff00
40 nm	$7.15x10^{10}$	530 nm	#5eff00
50 nm	$3.51x10^{10}$	535 nm	#70ff00
60 nm	$1.96x10^{10}$	540 nm	#81ff00
80 nm	$7.82x10^{9}$	553 nm	#adff00
100 nm	$3.84x10^{9}$	572 nm	#e7ff00

Green synthesis of NPs is a new methodology developed to reduce the toxicity of NPs. Most of the applications of NPs are in the areas where there is a relationship between these particles and a biological system.[33]

Green synthesis has been applied to various metals and metal-oxides using different parts of plants like; root, stem, fruit, leaf, seed, callus and/or flowers.[11] The method induces biomolecule or bio-based capping around nanoparticles. Biomolecules induces the production of harmless materials and makes the NPs bio-friendly and biocompatible. Utilization of the plant extracts for GNP synthesis provides kinetic control over metallization process, contributing to the growth mechanism of NPs.[34]

According to Luty-Błocho et. al GNPs synthesis with mild reducing agents, occurs in three steps; first one is the reduction step (Eqn. 1.1), second one is the nucleation (Eqn. 1.2) and final step is the autocatalytic growth step (Eqn. 1.3).[35]

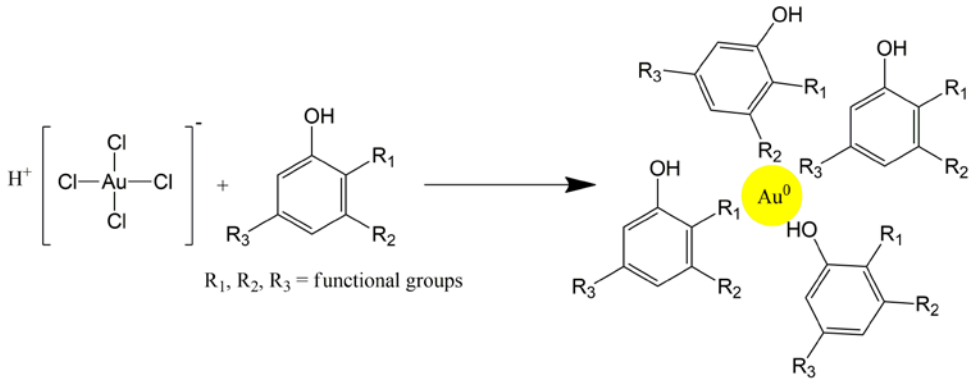

Figure 1. Reduction of gold via phenolic content of plant extracts

$$\text{Au(III) + plant extract} \xrightarrow{k_1} \text{Au(I) + products} \qquad (1.1)$$

$$\text{Au(I) + plant extract} \xrightarrow{k_2} \text{Au}^0\text{ + products} \qquad (1.2)$$

$$\text{Au(I) + Au}^0\text{ + plant extract} \xrightarrow{k_3} \text{2 Au}^0\text{ + products} \qquad (1.3)$$

Nucleation step can be considered as the rate-determining step, since temperature and reducing agent change results in different shapes and sizes. In this case, k_2 is the rate constant of the complete reaction mechanism. Slow reduction (at least 24 hours) occurs for green synthesis of GNPs that cause slow nucleation, and Ostwald ripening which eventually cause different sizes/shapes.[36]

For instance, Mukherjee et al. reported a green synthesis method for GNPs by using green tea derivatives.[37] In another study, green synthesis was done by using different fruit juices.[38] Similarly, poly-phenolic components of tea extracts were used for synthesizing nanoclusters which was investigated the inhibition of cell proliferation and stimulation of apoptosis for cancer cells.[39] In varied studies it was shown that, utilization of green synthesized GNPs as a sensing platform can be a rapid and cost-effective, most importantly an environmentally friendly alternative to the traditional chemical methodologies.

Fang et al. synthesized GNPs both directly on glass surface and on gold nanosphere surface to observe the difference between two models.[40] For the growth on glass surface they used seed mediated method, generating different shaped nanoplates; hexagonal, triangular, circular and truncated triangular. Differently, growth on nanospheres, which are citrate capped, was performed by using hydrogen peroxide.

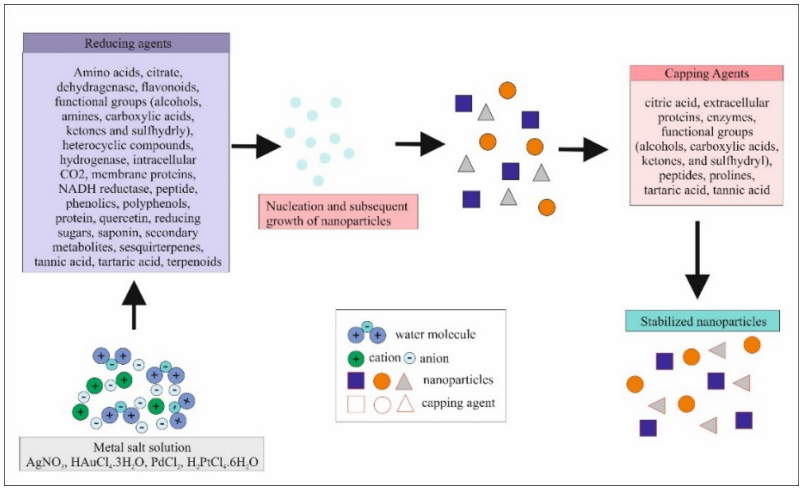

Figure 2. Green synthesis of metal NPs

A summary of green synthesis of GNPs can be seen in Figure 2. Individual molecule or a combination of molecules can be involved in the reduction of gold. As reducing agents, capping agents can also vary since after the reaction a molecule can be changed.

1.3 Background of Plant Extracts

Plants have variety of molecules such as; amino acids, citrate, dehydrogenase, functional groups (alcohols, amines, carboxylic acids, ketones and sulfhydryl), heterocyclic compounds, hydrogenase, intracellular CO_2, membrane proteins, NADH reductase, peptide, phenolics, polyphenols, protein, quercetin, reducing sugars, tannic acid, tartaric acid, and secondary metabolites such as alkaloids, flavonoids, sesquiterpenes, saponin, and terpenoids[41-42] It is also well-known that the plants have high phenolic content[45] which plays an important role especially for reduction reactions.

Investigation of different molecules in a plant extract is an area that has been widely focused on. For example, anti-inflammatory effects of terpenoid from *Lepidozia reptans* have been investigated by Li et. al.[43] *Camellia oleifera*, *Quillaja saponaria* and *Chenopodium quinoa* have also been investigated for their toxicities based on the saponin content.[44]

1.3.1 Melissa officinalis

Lemon balm or melissa (*Melissa officinalis*) is a member of the Lamiaceae family. Other members of the Lamiaceae family involve dittany, mint, sage, siderites, and sweet marjoram. It is a perennial lemon-scented herb in the mint family native to the Mediterranean and to Southern Europe.[45] The plant has been used for centuries in various cultures internationally for treating melancholy and disorders of the nervous system.[46] Nowadays, herbalists recommend the leaves to treat migraines and stomach ailments, to improve memory and strengthen the heart.[47] Also, in Danish folk medicine, lemon balm is used to treat sleeplessness.[48] Lately, *Melissa officinalis* has also shown anxiolytic, mood and memory-enhancing effects[49], sedative[50], antioxidant, antimicrobial and anti-tumour actions.[51]

Figure 3. *Melissa officinalis* plant [61]

The known major components of melissa are; hydroxycinnamic acid derivatives, particularly rosmarinic acid, caffeic acids, chlorogenic acid, and metrilic acid[52];

tannins[53]; flavonoids, including luteolin, luteolin 7-O-beta-D-glucopyranoside, apigenin 7-O-beta-D-glucopyranoside, and luteolin 3-O-beta-D-glucuronopyranoside[54]; monoterpene glycosides[55]; sesquiterpenes, including β-caryophyllene and germacrene[55]; triterpenes[56]; and volatile oils, including citronellal, citral a (geranial), citral b (neral), methyl citronellate, ocimene, citronellol, geraniol, nerol, β-caryophyllene, β-caryophyllene oxide, linalool, and ethric oil.[57] The volatile oil comprises 0.5-0.1% of the plant by weight, and citronellal, geranial, and neral constitute about 50-70% of this oil.[58] Eugenylglycoside has been isolated from lemon balm leaves. The chemical composition of lemon balm tea yielded 10 mg/L of essential oil (74% citral) and large amounts of polyphenol compounds.[59] Steam distillates of lemon balm callus cultures yielded dehydroabietane and another diterpene hydrocarbon, with the relative proportion of those two compounds varying considerably during cultivation passage.[60]

1.3.2 Punica granatum

Figure 4. Different types of *Punica granatum* [63]

The pomegranate, *Punica granatum* L., is the predominant member of two species consisting the Punicaceae family. The genus name, Punica, was the Roman name for Carthage, where the best pomegranates were known to grow. It was mentioned in ancient times in the Old Testament of the Bible, the Jewish Torah, and the

Babylonian Talmud as a sacred fruit giving powers like fertility, abundance, and good luck. The pomegranate tree typically grows 3-4 meters, has many spiny branches, and can be extremely long lived, as evidenced by trees at Versailles, France, which are considered to be over 200 years old.

The pomegranate is native, from the Himalayas in northern India to Iran but has been farmed and naturalized since ancient times over the entire Mediterranean area. It is also found in India and more desiccated regions of Southeast Asia, the East Indies, and tropical Africa. The tree is also farmed for its fruit in the drier regions of California and Arizona.[62]

Products from all parts of the pomegranate tree, including the fruit, flowers, roots, bark, and leaves, were used for medicinal treatments of a wide list of diseases and ailments of humans. Disease targets of pomegranates include coronary heart diseases, cancer (skin, breast, prostate, and colon), inflammation, hyperlipidaemia, diabetes, cardiac disorders, hypoxia, ischemia, aging, brain disorders, and AIDS.[63] The molecules in different pomegranate extracts are given in Table 5.

1.3.3 Salvia officinalis

Salvia officinalis (sage, also called as garden sage, common sage, or culinary sage) is a perennial, evergreen subshrub, with woody stems, greyish leaves, and blue to purplish flowers. It is a member of the mint family Lamiaceae and native to the Mediterranean region. It has a long history of medicinal and culinary use, and in modern times as an ornamental garden plant. In folk medicine, *S. officinalis* has been used for different kinds of disorders such as; seizure, ulcers, gout, rheumatism, inflammation, dizziness, tremor, paralysis, diarrhoea, and hyperglycaemia. Today, there has been an intense study to document the traditional use of this plant and to find new biological effects.

The main phenolic compound in the methanolic extract for *S. officinalis* is rosmarinic acid, while the main compounds in the aqueous extract is rosmarinic acid and luteolin-7-glucoside. The methanolic extract has a higher content of phenolic compounds and a higher antiradical efficiency than the aqueous extract. Additionally, essential oil of *S. officinalis* consists of (1r)-(+)-α- pinene, (-)- camphene, β – pinene, sabinene, β- myrcen, α- terpinene, (r)-(+) limonene, 1,8- cineole, γ- terpinene, p-

cymene, terpinolene, (-)-α- thujone, β- thujone, camphor, (-)- linalool, linalyl acetate, (-)-trans- caryophyllene, monoterpene, (+)- menthol, borneol, α- terpineol, geranyl acetate, geraniol, phyto, thymol, carvacrol, farnesol, trans-trans-farnesol.[64]

Table 5. Components of *Punica granatum*

PLANT COMPONENT	CONSTITUENTS
Pomegranate juice	anthocyanins[65]; glucose, ascorbic acid; ellagic acid, gallic acid, caffeic acid[66]; catechin, EGCG[67]; quercetin, rutin[68]; numerous minerals, particularly iron[69]; amino acids[70]
Pomegranate seed oil	95% punicic acid[71]; other constituents, including ellagic acid[68]; other fatty acids[71]; sterols[72]
Pomegranate pericarp (peel, rind)	phenolic punicalagins; gallic acid and other fatty acids[68]; catechin, EGCG[67]; quercetin, rutin, and other flavonols[68]; flavones, flavonones[72]; anthocyanidins[73]
Pomegranate leaves	tannins (punicalin and punicafolin); and flavone glycosides, including luteolin and apigenin[72]
Pomegranate flower	gallic acid, ursolic acid[74]; triterpenoids, including maslinic and asiatic acid; other unidentified constituents
Pomegranate roots and bark	ellagitannins, including punicalin and punicalagin[70]; numerous piperidine alkaloids[72]

1.4 Water Pollution

Water is an essential resource for human health, prosperity, security and the preservation of ecosystem. Water pollution is one of the major global environmental problems of the 21st century caused by the discharge of toxic substances from anthropogenic activities.[75] Lack of access to good quality drinking water remains one of the major worldwide health problems, mostly in under-developed and rural countries. Thus, there is a great demand on this area due to the need of fresh water and proper screening of water quality is required.

In general, pollution sources are divided into two main groups; point sources and non-point sources. Point sources are definable sources of pollutants such as power plants, refineries, mines, factories, wastewater treatment plants, etc. Non-point sources are, those spread over a large geographical area such as the basin.[76] Rare sources may

also include mobile sources such as cars, buses and trains. Although they are all a point source, since they are moving, so, they spread cumulative effects over a large geographical area. A distinct pollution source, can be an urban stream where the pollutant cargo can be the collection of huge amounts of small point sources in the basin.[77] Main pollutants in waters are shown in Table 6, with the probable sources.

Figure 5. The plant *Salvia officinalis*

1.4.1 Cyanide as a Pollutant

Cyanide ion (CN^-) is one of the main pollutants in water that causes harm to both human and animal health worldwide. CN^- can be classified as ecosystem effecting point source that is highly reactive with some biological components containing ferric ion, which causes harm to respiratory and central nervous systems in mammals when swallowed.[78-80]

CN^- rapidly converts into thiocyanide in case of swallowing, which causes acute and chronic illnesses.[81] HCN or HNC is considered to be toxic above 1 ppm concentration[82], though it is also the easiest way of obtaining CN^-. CN^- is used in many areas such as polymer synthesis[6], pest control[8], noble metal mining[7], medicine[83], and in the manufacture of plastics, paints and synthetic fibres.

Maximum concentration value of CN^- that has been set by the governmental regulations is 0.2 mg/L (200 µg/L) for free CN^- ion in drinking water. In short-term

exposure, EPA[84] has found CN^- to potentially induce the following health problems: rapid breathing, tremors and other neurological effects. In long-term exposure, CN^- has the potential to result in the following effects: weight loss, thyroid problems, nerve damage.

Table 6. Main pollutants of waters

Category	Examples	Sources
1. Health Affecting		
Infectious agents	Bacteria, viruses, and parasites	Sewage, human and animal excreta
Organic chemicals	Pesticides, plastics, detergents, oil	Agricultural, industrial, and domestic wastes
Inorganic Chemicals	Acids, caustics, salts	Industrial and domestic effluents
Radioactive	Uranium, thorium, radon	Mining, power plants, natural sources
2. Ecosystem Affecting		
Plant nutrients	Nitrates, phosphates	Chemical fertilisers, sewage, manure
Sediments	Silt, soil	Soil erosion
Thermal	Heat	Industries, power plants
Oxygen demanding	Agricultural wastes, manure	Sewage, agricultural runoff

However, fatal oral doses for CN^- can range from 50 to 200 mg CN [0.7 to 2.9 mg/kg bodyweight (bw)]; which is built on the poisonings.[85, 86] While low exposure through long time periods can cause neural damage, high exposure causes death within one hour.[87] As an advantage; low exposures can be cured by effective detoxification methods without permanent damage.[7]

1.4.2 Cyanide Detection Methods

In the recent years, CN^- detection in ground and drinking water became significantly important. Several methods have been elaborated on detection of CN^- in water resources to avoid any intoxication as shown in Table 7. Mostly, naked eye detection of CN^- has been investigated, since pollution of water resources are the main problem in under developed countries.

Some screening techniques that is used for CN^- detection utilize harsh chemicals such as indanedione-derivatives[88] and heterocyclic imidazo-anthraquinones.[89] The number of studies, have also described new CN^- receptors such as an acylhydrazone, gluco-conjugated o-(carboxamido) aldehyde hydrazine linked azo dye[90], which was used to detect CN^- in water. In another study, 4,4_ -bis-[3-(4-nitrophenyl) thiourea] diphenyl methane (or ether)[91] complex was used to determine the concentration of both CN^- and fluorine in an aqueous media. Li et. al used dual-modal probes based on coumarin and a malonyl urea derivatives dyes[9] for biological application. Electron transfer based CN^- detection was done with 7,7,8,8-tetracyanoquinodimethane.[92] Alternatively, near-infrared chemodosimeters based on 5,10-dihexyl-5,10-dihydrophenazine[93] was used for a novel CN^- detection probe.

Although numbers of assays are available for cyanide detection in aqueous media, they lack in situ options requiring laboratory facilities and trained personal.

1.4.3 Cyanide Detection Methods via GNPs

GNPs undergo an oxidation reaction when faced to a CN^- source, which cause the naturally occurring color to disappear. Gold NPs has been used as colorimetric sensors for CN^- sensing, since they rapidly generate Au-CN complex in the presence of oxygen (Eqn. 1.4).[94]

Fluorescent detection of cyanide ion via GNPs or silver nanoparticles (SNPs) was reported in recent studies[101-103]. In another study, bimetallic core-shell NPs were used for the sensing of cyanide ion with high selectivity and sensitivity.[104]

Wei et. al developed two fluorescent nanosensors, both featuring bovine serum albumin labelled with fluorescein isothiocyanate (FITC))-capped GNPs (FITC-BSA-Au

NPs), for the selective sensing of CN^- and iodine (I^-) ions in high-salinity solutions and edible salt samples.[10]

Table 7. Standard cyanide detection methods from EPA[95]

Methodology	Detection limit (mg/l)	Method*
Distillation, Spectrophotometric	0.02	ASTM D2036-98 A
Distillation, Spectrophotometric	0.02	SM 4500-CN− A, C, E
Distillation, Spectrophotometric	0.02	USGS I-3300-8
Distillation, Automated, Spectrophotometric	0.005	EPA 335.4
Distillation, Amenable, Spectrophotometric	0.02	ASTM D2036-98 A, B
Distillation, Amenable, Spectrophotometric	0.02	SM 4500-CN− A, C, G
Distillation, Selective Electrode	0.05	SM 4500-CN− A, C, F
UV, Distillation, Spectrophotometric	0.0005	Kelada-01
Micro Distillation, Flow Injection, Spectrophotometric	0.0006	QuikChem 10-204-00- 1-X
Ligand Exchange with Amperometry	0.0005	ASTM D6888-04
Ligand Exchange with Amperometry	0.0005	OIA-1677, DW

*Methods are standardized techniques by several institutions.

Although these studies are successful, all of which are using another harsh chemical or utilize heavy chemical synthesis processes for the detection of a toxic material (CN^-). Therefore there is an unmet need in this field that utilize green synthesis approach or environmentally friendly materials for the screening of toxic cyanide ion.

$$\underset{\text{Pink-Purple Colored Solution}}{Au^0} + 4NaCN + O_2 + 2H_2O \longrightarrow \underset{\text{Colorless Solution}}{2Na[Au(CN)_2]} + 2NaOH + H_2O_2 \quad (1.4)$$

CHAPTER 2

MATERIALS & METHODS

2.1 Materials

Gold(III) chloride hydrate (99.999% trace metal basis) and poly-L-lysine hydrobromide (PLL, 0.05 mg/mL) (MW 70.000 – 150.000) was purchased from Sigma-Aldrich Company (St. Louis, MO, USA). Cyanide source (KCN, 500 mg) was purchased from Alfa Aeser Co. (Germany). All the solvents were purchased from Merck Company. Poly-methyl methacrylate (PMMA) sheets (300 mm x 400 mm) were purchased from Net Plexi (Ankara, TR) for the purpose of Scanning Electron Microscopy platforms. Ultrapure water (Sartorius Water Purification Systems - Arium Pro Ultrapure Water System) was used throughout the experiment. Dry melissa and sage leaves and pomegranate fruit were purchased from a local market.

2.2 Methods

2.2.1 Preparation of the Plant Extracts

Dry melissa leaves were weighed as 4.0 g and rinsed with ultrapure water (UPW). The leaves were chopped in blender with 30 mL of UPW, until a homogeneous liquid was obtained. After the dicing, volume of the extract was topped up to 50 mL. The liquid is filtered through 120 mm filter paper to remove unchopped solids. Afterwards, remaining content was filtered through 0.2 µm filter paper, to remove any other particles. The extract was aliquoted into 0.5 mL solutions and stored at -20 ºC up to 10 months.

Pomegranate fruits were weighed as 20 g and rinsed once with tap water then rinsed with UPW. The fruits were chopped in blender with 30 mL UPW until a homogeneous liquid was obtained. Then the volume was topped to 50 mL with UPW. The obtained liquid was first filtered through 120 mm filter paper, then 0.2 µm filter

paper to remove any remaining solid particles. The extract was aliquoted into 0.5 mL solutions and stored at -20 ºC up to 10 months.

Dry sage leaves were weighed as 4.0 g and cleaned as same as melissa leaves using UPW. Leaves were chopped in blender with 30 mL UPW and volume is completed to 50 mL. The liquid was first filtered through 120 mm filter paper, then 0.2 µm filter paper to remove any remaining solid particles. The extract was aliquoted into 0.5 mL solutions and stored at -20 ºC up to 10 months.

2.2.2 Green Synthesis of GNPs

0.01 g of solid $HAuCl_4$ was dissolved in a 100 mL volumetric flask using UPW to get final concentration of 0.1 g/L. The solution stored at 4 ºC and covered with aluminium foil to prevent interaction with light.

Either 375 µL of melissa extract; or 375 µL of pomegranate extract; or 375 µL of sage extract was separately mixed with 5 mL of $HAuCl_4$ solution in glass vials. Green synthesis of GNPs was carried out to optimize the reaction conditions at different temperatures (4 ºC, RT, 30 ºC, 40 ºC, 50 ºC, 60 ºC) and varying time scales (6 hours, 1 day).

2.2.3 Characterization of the Green Synthesized GNPs

2.2.3.1 Spectrophotometric Analysis of the Green Synthesized GNPs

The absorbance spectrum of both the plant extracts and GNP solutions was obtained with Thermo Scientific Multiscan GO Microplate Reader (Thermo-Fisher Scientific Inc., MA, USA).

Ultraviolet-Visible Spectrophotometry (UV-Vis) is a technique that measures the absorbance of materials in UV-Vis region, which is between 180-750 nm. When divided as UV and visible region, UV region is between 180-400 nm, while visible region is between 400-750 nm.

Absorbance analysis was used periodically to qualify and quantify the reaction efficiency. UV spectrum of 100 µL of each solutions (different extracts and different

temperature GNP solutions) was measured in a 96-well plate format as six repeats and the average data was calculated and normalized for evaluation.

2.2.3.2 Size Analysis of the Green Synthesized GNPs

Sizes of the green synthesized GNPs were measured by NanoPlus DLS Nano Particle Size and Zeta Potential Analyzer (Micromeritics Instrument Corp.,USA).

The Z-average can be described as an intensity-based harmonic mean (Eqn. 2.1). The equation for this description is shown below:

$$Dz = \frac{\sum Si}{\sum(\frac{Si}{Di})} \quad (2.1)$$

Here, S_i is the scattered intensity from particle *i* and D_i is the diameter of particle *i*. Note that the result is in the form of a harmonic mean. Since this mean is calculated from the intensity weighted distribution, leading to the statement that the Z-average size is the intensity weighted harmonic mean size. Size analysis was accomplished prior to green synthesis without further treatment. 2-3 mL of sample were put into plastic cuvette specific to the instrument to avoid any noise. Three separate measurements were obtained and mean values were calculated accordingly.

2.2.3.3 Zeta Potential Analysis of the Green Synthesized GNPs

Zeta potential of the green synthesized GNPs has been measured by NanoPlus DLS Nano Particle Size and Zeta Potential Analyzer (Micromeritics Instrument Corp., USA). Zeta potential means the electrokinetic potential energy in a colloidal dispersion.[96] Zeta potential originates from the net electric charge in the region limited by the shear plane and also influenced by the position of that plane. The samples are put into the fluid pipe in between the electrodes, when the electrical field is applied to the solution, according to the behaviour of charges in solution; surface charge of the particles is determined.

Green synthesized GNP samples were measured prior to synthesis without further treatment. 2-3 µL of solution was put inside the fluid pipe and three consecutive measurements were taken.

2.2.3.4 Fourier Transform Infra-Red (FTIR) Spectroscopy Analysis of the Green Synthesized GNPs

Fourier Transform Infra-Red (FTIR) Spectroscopy analysis was done by Perkin Elmer Spectrum 100 FT-IR Spectrometer (Perkin Elmer Inc., USA). FTIR Spectroscopy measures the vibrational modes revealing the functional group of the sample. Vibrational modes are shown in Table 8.

Table 8. Vibrational modes

Direction	**Symmetric**	**Asymmetric**
Radial	Symmetric stretching	Asymmetric stretching
Latitudinal	Scissoring	Rocking
Longitudal	Wagging	Twisting

Both the plant extracts and green synthesized GNP solution was frozen at -20 ºC and then lyophilized overnight to obtain powder form. KBr pellet was used as a control over the plant extracts and GNPs. Lyophilized solids were mixed with KBr pellets separately to measure FT-IR spectra. Further analysis was done by using proper guidelines for the post-processing of FTIR signal.

2.2.3.5 Atomic Force Microscopy (AFM) Analysis of the Green Synthesized GNPs

Atomic Force Microscopy (AFM) measurements for topographical analysis was undertaken with Multimode 8-HR AFM (Bruker Corp., MA). AFM is a high-resolution surface characterization technique that measures the topographical properties depending on the physical interaction of the AFM tip and corresponding surface.

For AFM measurements, green synthesized GNPs were immobilized onto PLL coated gold slides. AFM was used in contact mode to overview the surface properly.

2.2.3.6 Scanning Electron Microscopy (SEM) Analysis of the Green Synthesized GNPs

Scanning Electron Microscopy (SEM) analysis was done by Quanta SEM FEI (Thermo-Fisher Scientific Inc., MA, USA). SEM is a high-resolution electron microscope that generates images of scanned surface via focused beam of electrons.

SEM samples of green synthesized GNPs were prepared by using 1x1 cm PMMA sheets covered with aluminium foil, and then 100 µL PLL was incubated for 24 hours. After rinsing twice with UPW, the surface was incubated with 100 µL green synthesized GNP solution for 24 hours, then it was rinsed with UPW twice and dried under N_2 flow and proceeded with SEM analysis.

2.2.3.7 Energy Disperse X-Ray (EDX) Diffraction Analysis of the Green Synthesized GNPs

EDX analysis was done by SEM equipment with EDX detector and corresponding software (Oxford Azteck). Analysis was done at 50000x magnification and the analysis area was selected from the densest area of visualized GNPs.

2.2.4 Cyanide Detection via the Green Synthesized GNPs

2.2.4.1 Cyanide Solution Preparation

Different concentrations of CN^- were prepared from KCN. A main stock solution was prepared as follows; 1.63 g of KCN was dissolved in 250 mL UPW to obtain 10^{-1} M concentration. Dilution series were prepared from 10^{-1} M to 10^{-15} M as given in Table 9.

2.2.4.2 Cyanide Detection

CN^- detection was done in 96 well plates. For both melissa-based GNPs and pomegranate-based GNPs four well plates was functionalized with PLL and then GNPs.

Initially, 100 µL 0.05 mg/mL PLL was incubated in well plates for 24 hours (Figure 6). To remove excess PLL from the surface, well plates were rinsed with 100 µL of UPW, twice. After rinsing procedure, the UV-Vis spectrum data was obtained from PLL immobilized plates by using plate reader. For the next step, 100 µL GNPs of both melissa and pomegranate, which synthesized at different temperatures, were incubated on 96 well plates for 24 hours. To remove the excess GNP solution, well plates were rinsed twice with 100 µL UPW, and their UV-Vis spectrum was analysed.

Table 9. Dilution series for cyanide solutions

Molarity (M)	**Stock Solution Used (M)**	**Volume Needed**
10^{-1} (250 mL)	-	-
10^{-2}	10^{-1}	1.5 mL
10^{-3}	10^{-1}	150 µL
10^{-4}	10^{-1}	15 µL
10^{-5} (250 mL)	10^{-1}	25 µL
10^{-6}	10^{-5}	1.5 mL
10^{-7}	10^{-5}	150 µL
10^{-8}	10^{-5}	15 µL
10^{-9}	10^{-5}	1.5 µL
10^{-10} (250 mL)	10^{-1}	2.5 µL
10^{-11}	10^{-10}	1.5 mL
10^{-12}	10^{-10}	150 µL
10^{-13}	10^{-10}	15 µL
10^{-14}	10^{-10}	1.5 µL
10^{-15}	10^{-14}	1.5 mL

Last step of the CN^- detection was the addition of the varied concentration of CN^- solutions. Each concentration is added to GNP functionalized wells, according to the pattern shown in Figure 6, to see colour change. Periodical absorbance measurements were taken to observe the oxidation reaction. Data was analysed according to temperature and concentration parameters.

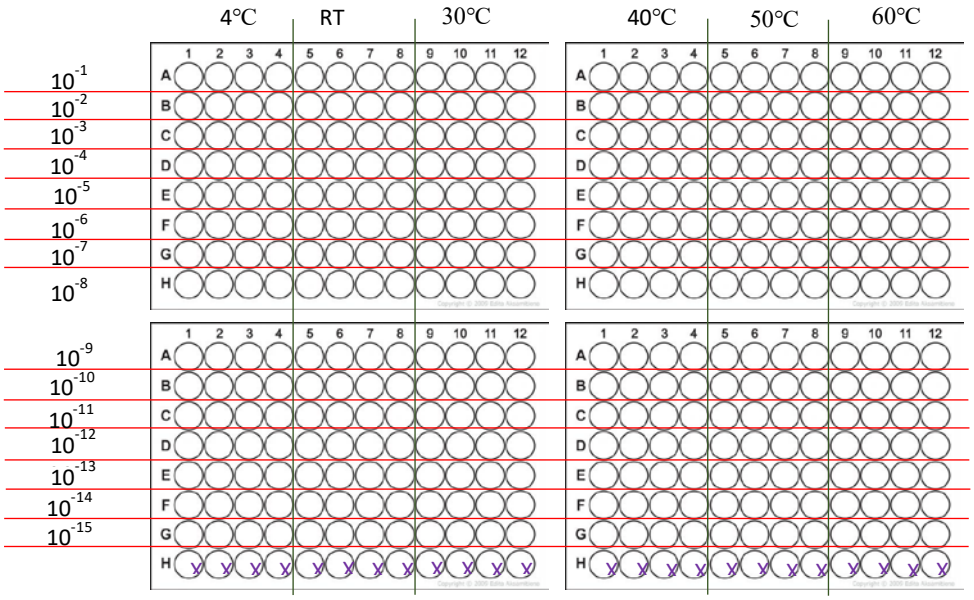

Figure 6. Well plate pattern for CN^- Detection

CHAPTER 3

RESULTS & DISCUSSION

3.1 Extract Analysis

UV-Vis spectrophotometric analyses of the plant extracts were done to establish a baseline for GNP synthesis. FTIR analysis was done to observe the functional groups in the plant extracts, and also to differentiate the FTIR spectrum of the extracts from the green synthesized GNPs.

3.1.1 Spectrophotometric Analysis of the Plant Extracts

Three different plants; *Melissa officinalis* (melissa or lemon balm), *Punica granatum* (pomegranate), and S*alvia officinalis* (sage), were used as mild reducing agents for green synthesis of GNPs.

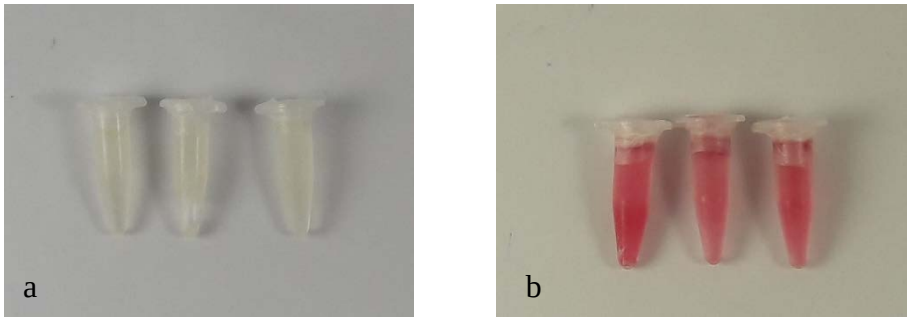

Figure 7. Aliquots of the extracts frozen at -20 °C; a) *Melissa officinalis*, b) *Punica granatum*

As observed by naked-eye, melissa is yellow-colored while pomegranate is pink-purple colored as shown in Figure 7. As shown in Figure 8, melissa and

pomegranate had unique absorbance characteristics at UV-Vis region. We observed a λ_{max} at 325 nm for melissa, while for pomegranate λ_{max} was 515 nm, both correlates well with the visual observation.

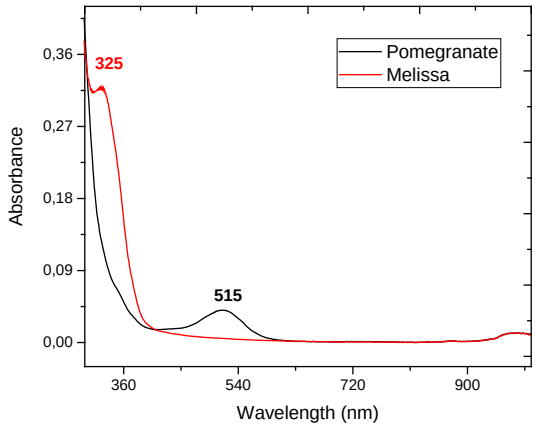

Figure 8. Absorbance spectrum of the extracts; red (*Melissa officinalis*), black (*Punica granatum*)

3.1.2 FTIR Analysis of the Plant Extracts

Melissa and sage are from the same genus as mentioned before in Chapter I. Accordingly, it is expected that their chemical content can be very similar. Therefore, obtained FTIR spectrum for each extract is quite similar however the intensity of the peaks is different which indicates the varying concentration of the components for each extract.

As given in Figure 9, melissa extract show O-H stretching at 3277 cm^{-1}, C-H stretching at 2924 cm^{-1}, and C-H bending for sp^3 hybridized carbon at 1404 cm^{-1}. Differently, melissa extract shows the distinct signal for acyl groups at 1574 and 1255 cm^{-1}. And finally, at 1042 cm^{-1}, C-O alkoxy stretching is observed.

Pomegranate spectra shows peaks at 3295, 2924, 1717, 1414, 1027 and 774 cm^{-1}, which are O-H , C-H, 6 atom ring ketone stretching, sp^3 C-H bending, C-H alkoxy stretching and ortho substituted aromatic sp^2 C-H bending peaks, respectively. It also shows N-H bending at 1600 cm^{-1}, C-O alkoxy stretching at both 1341 and 1235 cm^{-1},

meta substituted aromatic sp^2 C-H bending at 864 cm^{-1}, para substituted aromatic sp^2 C-H bending at 819 cm^{-1}.

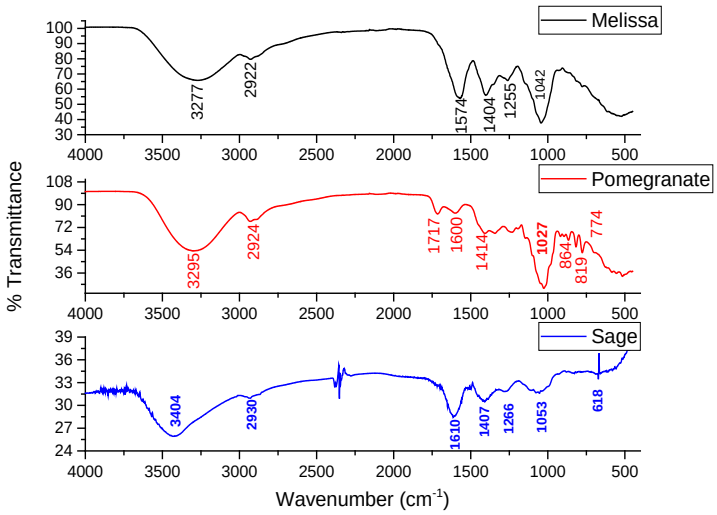

Figure 9. FTIR spectrum of the extracts; *Melissa officinalis, Punica granatum, Salvia officinalis*

FTIR spectra of sage is also given in Figure 9. It is observed that O-H stretching at 3404 cm^{-1} exists. Also, the signal around 1700 cm^{-1} indicates that sample have carbonyl groups. At 1610 cm^{-1}, N-H bending was observed, which supports amine group existence. Sage extract peak at 1407 cm^{-1} indicates C-H bending for sp^3 hybridized carbon . The peak at 1053 cm^{-1} represents the alkoxy (C-O) stretching signals. Also at 618.04 cm^{-1} the same characteristic peak was obtained for aromatic sp^2 C-H bending.

As known from the literature, melissa mainly consists of rosmarinic acid and caffeic acid, which contain several branches of hydroxyl groups and aromatic rings.[53] They also contain carboxylic groups in their structures. From FTIR data, the main components of the melissa extract can be confirmed such as; O-H, C-H stretching and C-O alkoxy stretching. Pomegranate, on the other hand, mainly consists of ellagic acid and gallic acid.[65] Ellagic acid is a fused four ring polyphenol that contains aromatic rings and several carboxyl and hydroxyl groups, while gallic acid is a simpler compound that contains only one aromatic ring decorated by hydroxyl groups and one carboxyl functional group. This confirms the existence of several FTIR data such as; C-

H bending for sp^3 hybridized carbon and alkoxy (C-O) stretching. Furthermore, sage consists of rosmarinic acid as melissa. Differently one of the main components of sage is luteolin.[64] These two molecules are very similar structurally, therefore confirming the FTIR output.

3.2 Characterization of the Green Synthesized Gold Nanoparticles

3.2.1 Spectrophotometric Analysis of the Green Synthesized GNPs

Initially for the purpose of creating a baseline, $HAuCl_4$ solution (gold salt) absorbance was measured. UV-Vis spectrum did not show any absorbance peak, even though the solution is slightly yellow coloured (Figure 10).

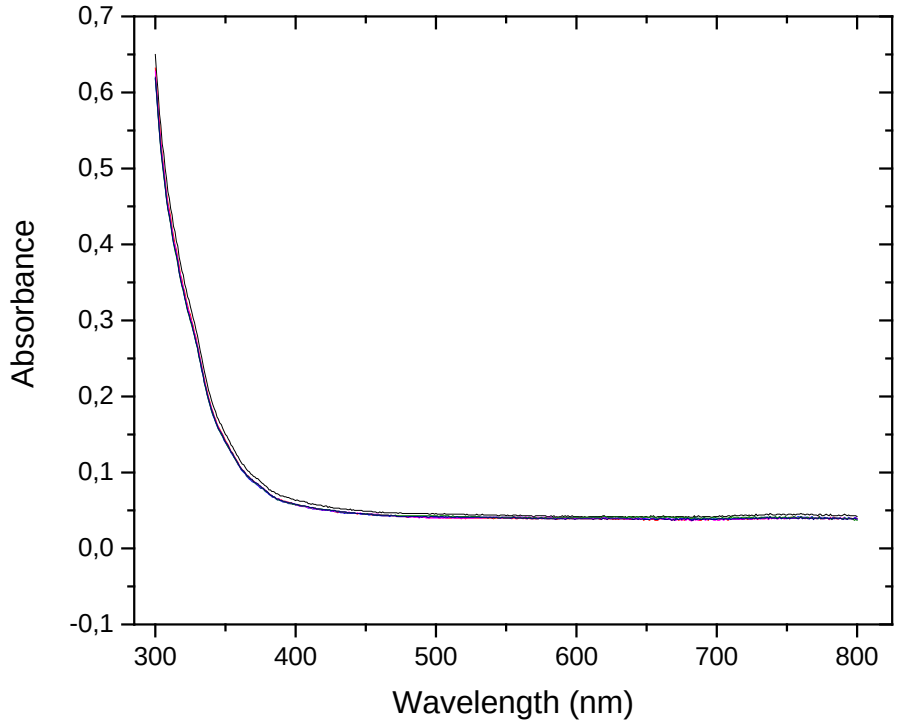

Figure 10. UV-Vis spectrum of $HAuCl_4$ solution

GNP synthesis was performed at room temperature (RT) for initial trials to optimize the reaction parameters. Absorbance measurements were done at different time scales to observe the reaction kinetics, and also reducing potential of plant extracts since they are considered as mild reducing agents. Analysis of green synthesized GNPs from melissa, pomegranate and sage extracts were done at ½, 24, 48, 72, and 96 h time intervals. Initial results showed that, at RT, GNPs are stable for each extract at least for 96 hours as shown in Figure 11. GNPs synthesized by the reduction of the melissa extract have λ_{max} at 540 nm. According to the literature[97], absorbance max value also indicates the size of the GNPs. In this case we expect the GNPs synthesized by the reduction of the melissa extract have around 60 nm sizes. While for GNPs synthesized by the reduction of the sage extract, λ_{max} is at 537 having similar size to melissa. UV-Vis spectra of GNPs synthesized by the reduction of the pomegranate extract shows two peaks at 528 and 675 nm that can be related to nanoplate generation, one of which is at ~ 500 nm and the other is at ~ 650 nm.[98] A study suggest that, if there are two peaks in a spectra of GNP solution, it is related to nanoplates and one signal indicates the size in x-axis while the other one indicates the size in y-axis.[17]

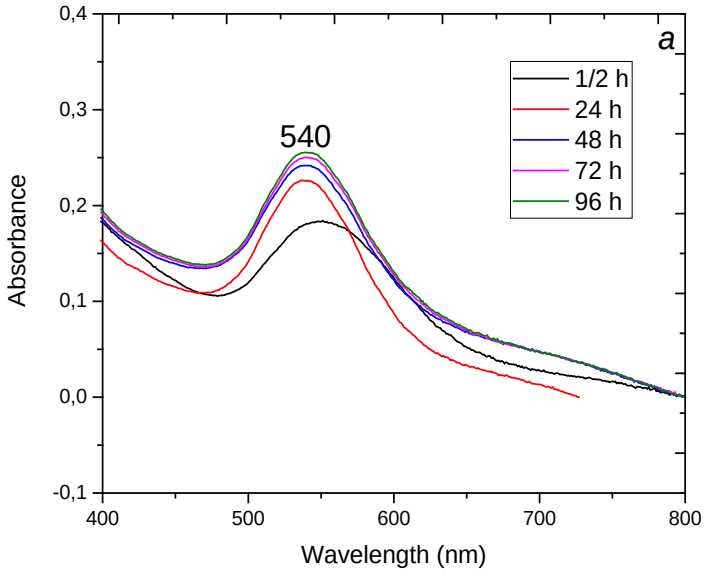

Figure 11. UV-Vis spectra of GNPs synthesized from melissa (a), pomegranate (b) and sage (c)

(Cont. on next page)

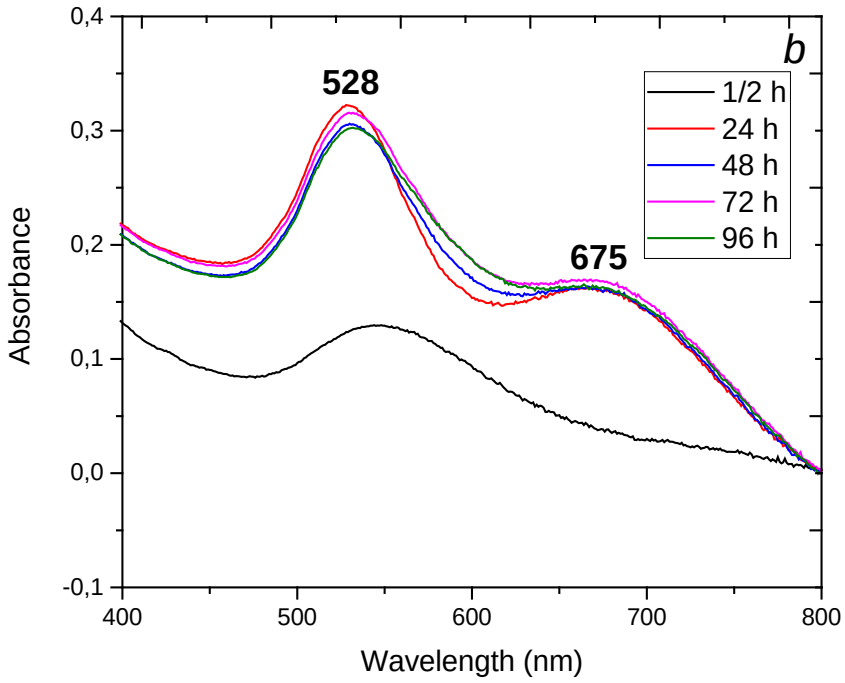

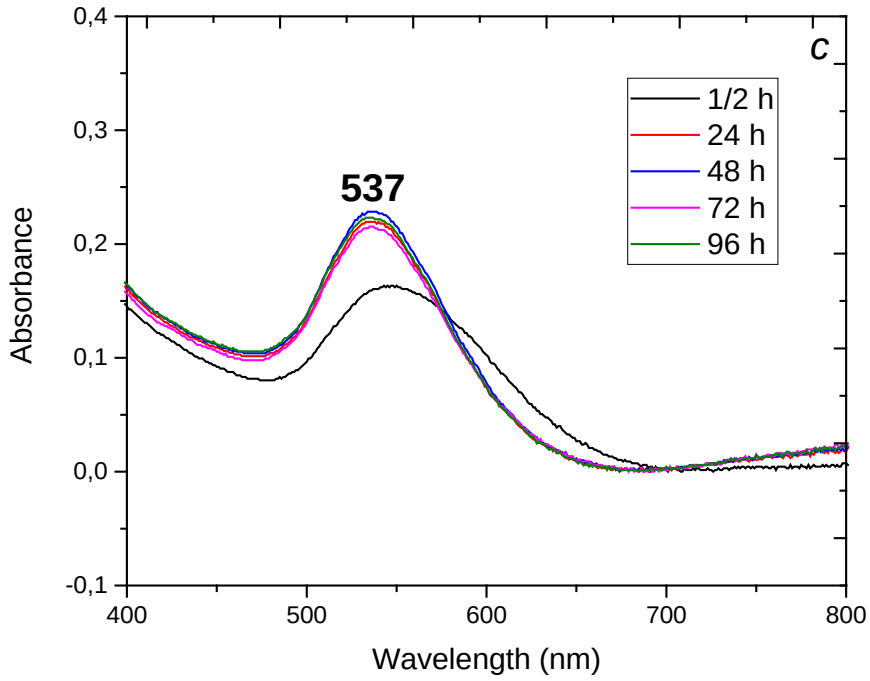

Figure 12. (Cont.)

The effect of the varied temperatures; 4 ℃, RT, 40 ℃ and 60 ℃, on GNP synthesis was observed via absorbance behaviours of GNP solutions. Initially, the frozen extracts were removed from the freezer, and $HAuCl_4$ solution was removed from 4 ℃. They were kept in water bath for stabilizing the corresponding temperature, except 4 ℃ samples, which are placed in 4 ℃. After mixing the components, the samples were left for the incubation at the corresponding temperatures. In order to observe the effect of varied temperatures on green synthesis of GNPs, UV-Vis measurements were collected at the same time. Based on the data collected from these trials, it was observed that the temperature affects the kinetics of the reaction, while changing physical and chemical properties of GNPs. Lack of heat through the course of the reaction causes slow nucleation. Equation 1.2 (second-step) is the key step toward NP or nanoplate generation, which can be manipulated by heat.

Advanced analysis was done by using six different temperature; 4 ℃, RT, 30 ℃, 40 ℃, 50 ℃ and 60 ℃. Temperatures higher than 60 ℃ are not preferred, because the plant extracts can decompose. It is well known that flavonoids and phenolic compounds in plants are highly responsive to high temperatures. However, the results obtained from sage GNPs was not satisfactory, and from that point, only melissa and pomegranate extracts were used as reducing agents. At the same temperatures, plant extracts show different reduction potential as shown with UV-Vis analysis. The difference between the extracts is probably caused by the content of the plant extracts and molecules responsible for the reduction of gold. The melissa extract may have less molecules involved in the reduction or the activation energy required for the reaction is higher than of pomegranate.

Figure 14 shows that melissa extract reacts very slow at 4 ℃ while pomegranate extract reacts partially slow. GNPs synthesized from the melissa extracts had λ_{max} at around 680 nm, while GNPs from the pomegranate extracts had λ_{max} at around 525 nm and 970 nm. At RT as shown in Figure 15, the melissa samples have λ_{max} at around 550 nm and 960 nm, and the pomegranate samples had λ_{max} at around 550 nm and 970 nm. Both reactions occur moderately slow. Figure 16 illustrates the results at 30 ℃, and melissa GNPs had λ_{max} at around 565 nm and 970 nm, while pomegranate GNPs had λ_{max} at around 525 nm and 680 nm. However, in this case, the pomegranate samples have blue shift from 680 nm to 670 nm after 1 day. This may be caused by the slight dimension change of NPs. Similarly, 40 ℃ samples of both extracts showed almost

identical spectra. In this case, the reactions occurs fast, and λ_{max} for melissa was around 500 nm and 750 nm, while λ_{max} for pomegranate was around 525 nm and 665 nm. As also seen from Figure 17, a slight blue shift occurs in the spectrum, as well. At 50 ℃, reactions occur fast and λ_{max} values are similar to 40℃ samples (Figure 18). In this case the pomegranate samples lost the blue shift occurrence in the spectrum. This can be explained that the active molecules at lower temperatures may lost their activities with increasing temperatures. At 60 ℃ very fast reaction was observed for both of the extracts as represented in Figure 19. The melissa samples had λ_{max} at around 540 nm and 665 nm, and the pomegranate samples had λ_{max} at around 535 nm and 630 nm without blue shift.

As mentioned before in Chapter I, nanoparticle and nanoplate signals can be differenciated in an UV-Vis spectrum.[98] Nanoplates have two dimensional (2D) structures contributing the UV-Vis analysis; one of which is the thickness and the other one is the exact shape (hexagonal, triangular, square, etc.). The signal for NPs are specific to their size and only one peak is observed. While nanoplate spectrum had two different peaks; one of which is at ~530 nm and the other one is at ~630 nm. In this case, the experimental results proves the nanoplaate existance in GNP solutions reduced by the plant extracts.

From the Figures 20 and 21, the different behaviour of GNPs, depending on both temperature and reducing agent can be seen. Color scale of GNPs, changes from light purple to dark purple. The color change occurs when the size and shape of the GNPs are different. Since all the samples were synthesized at different temperatures, it can be said that the size and the shape difference can be observed visually, as well. The bigger the size of GNPs, the colour darkens toward purple from pale violet.

3.2.2 Size Analysis of the Green Synthesized GNPs

Another important method to characterize the green synthesized GNPs is the size measurement. The size of the GNPs affects their physical and chemical properties. Their surface/volume ratio is an important property of the GNPs that is related to functionalization conditions as well. First results obtained 2 hours after green synthesis of the GNPs and the rate of agglomeration was controlled weekly. Size data, also,

indicates the shelf life of the solutions, which means how long they can be used efficiently.

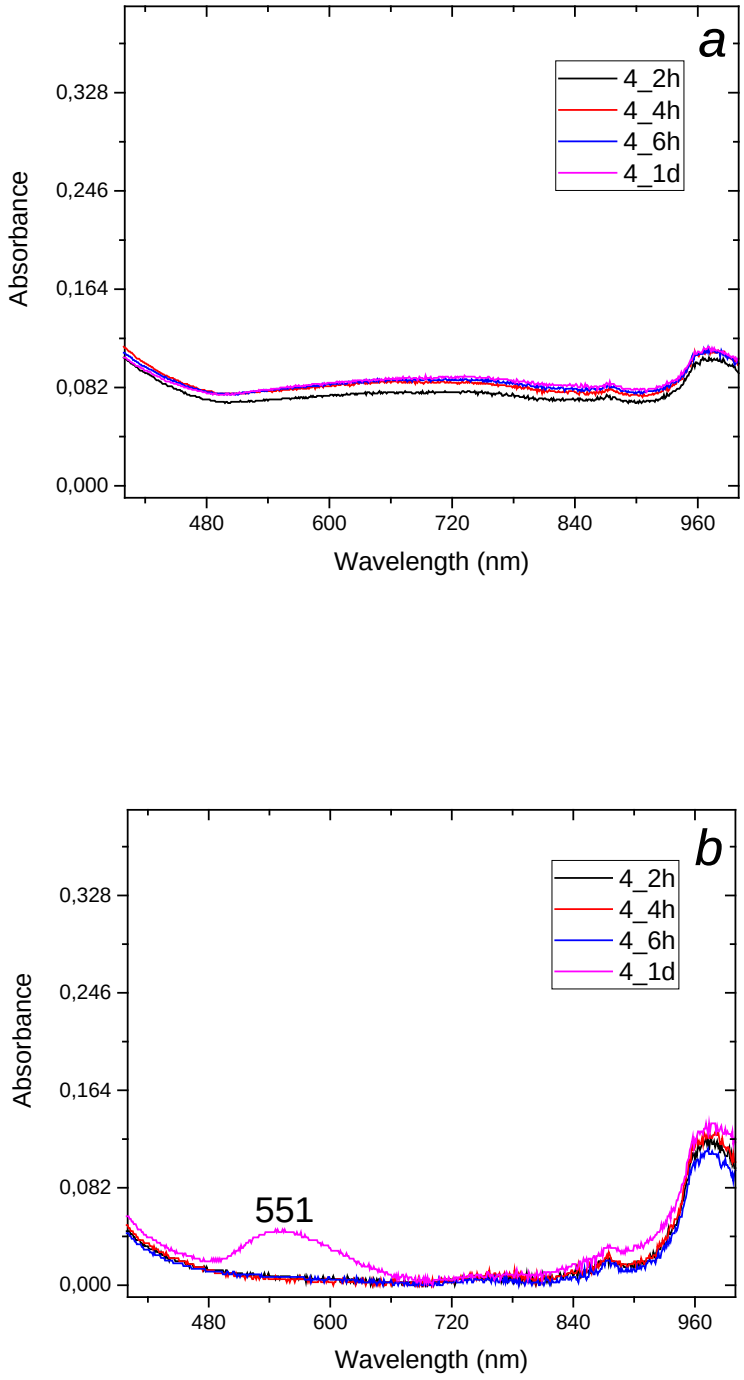

Figure 13. UV-Vis spectrum of the GNPs reduced by a) melissa, b) pomegranate at 4 ℃

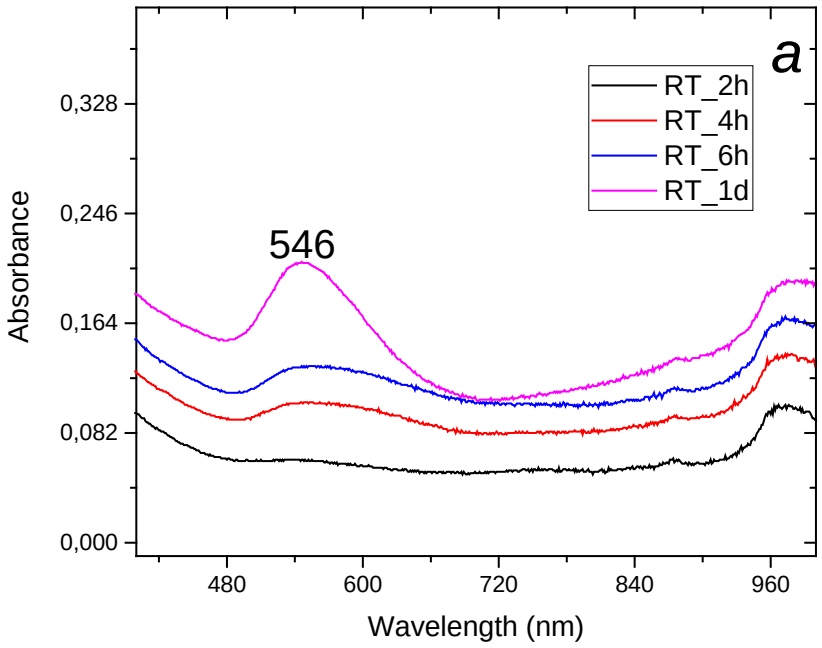

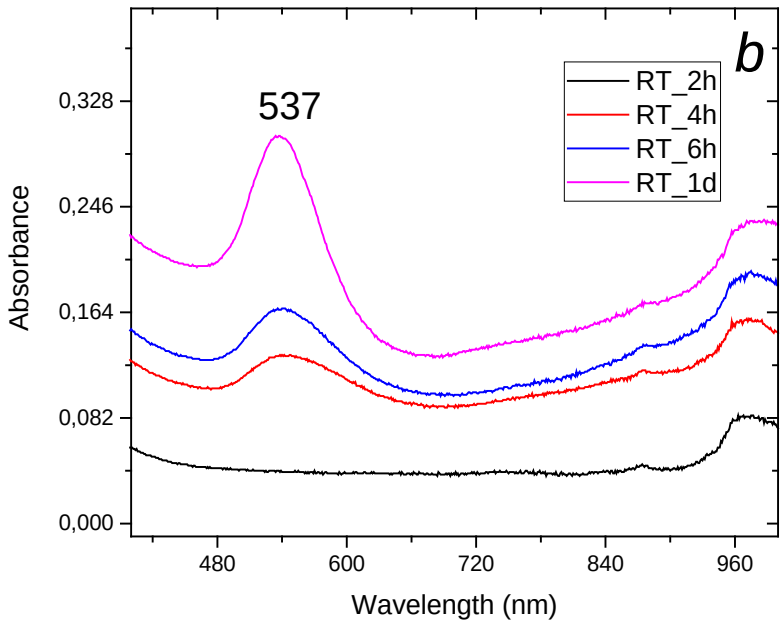

Figure 14. UV-Vis spectrum of the GNPs reduced by a) melissa, b) pomegranate at RT

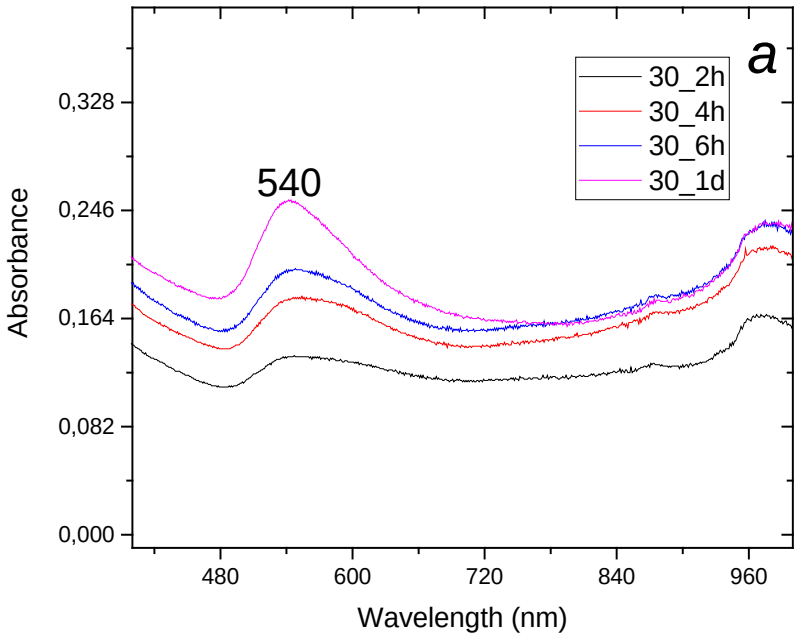

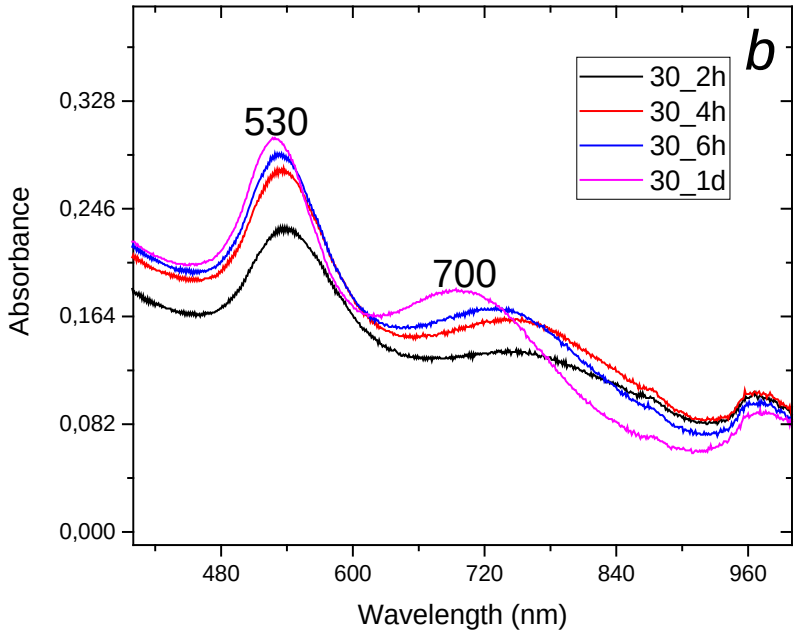

Figure 15. UV-Vis spectrum of the GNPs reduced by a) melissa, b) pomegranate at 30 ℃

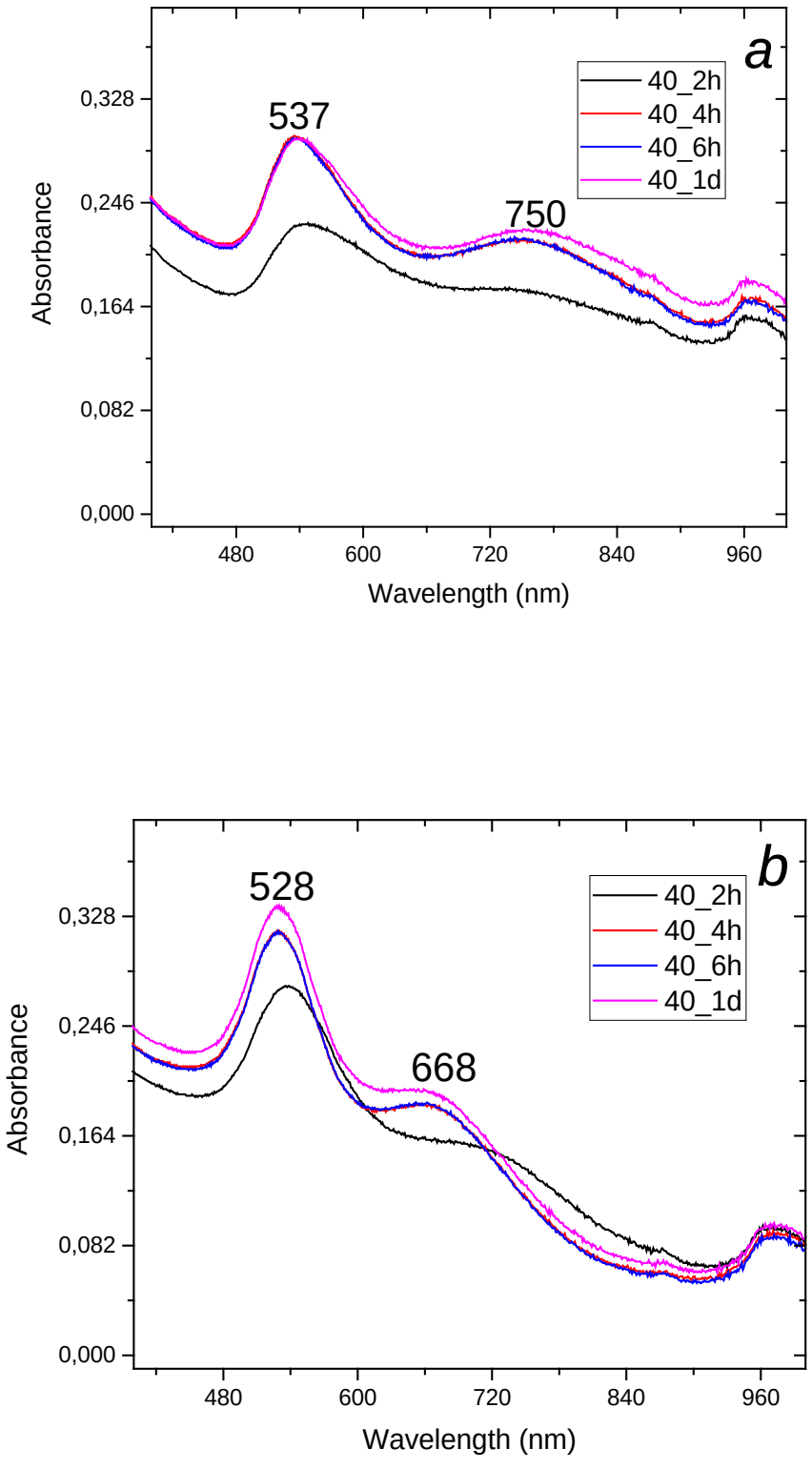

Figure 16. UV-Vis spectrum of the GNPs reduced by a) melissa, b) pomegranate at 40 ℃

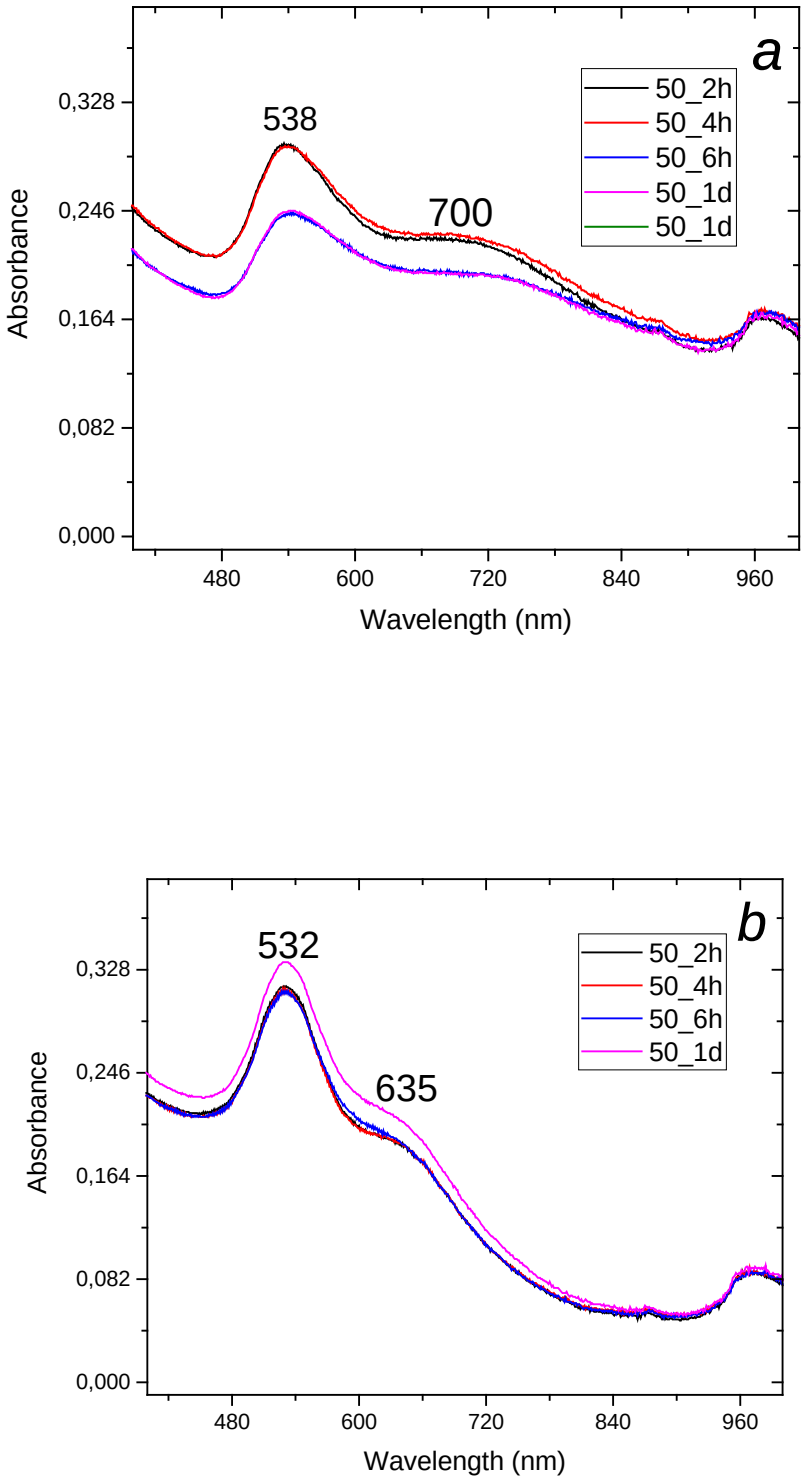

Figure 17. UV-Vis spectrum of the GNPs reduced by a) melissa, b) pomegranate at 50 ℃

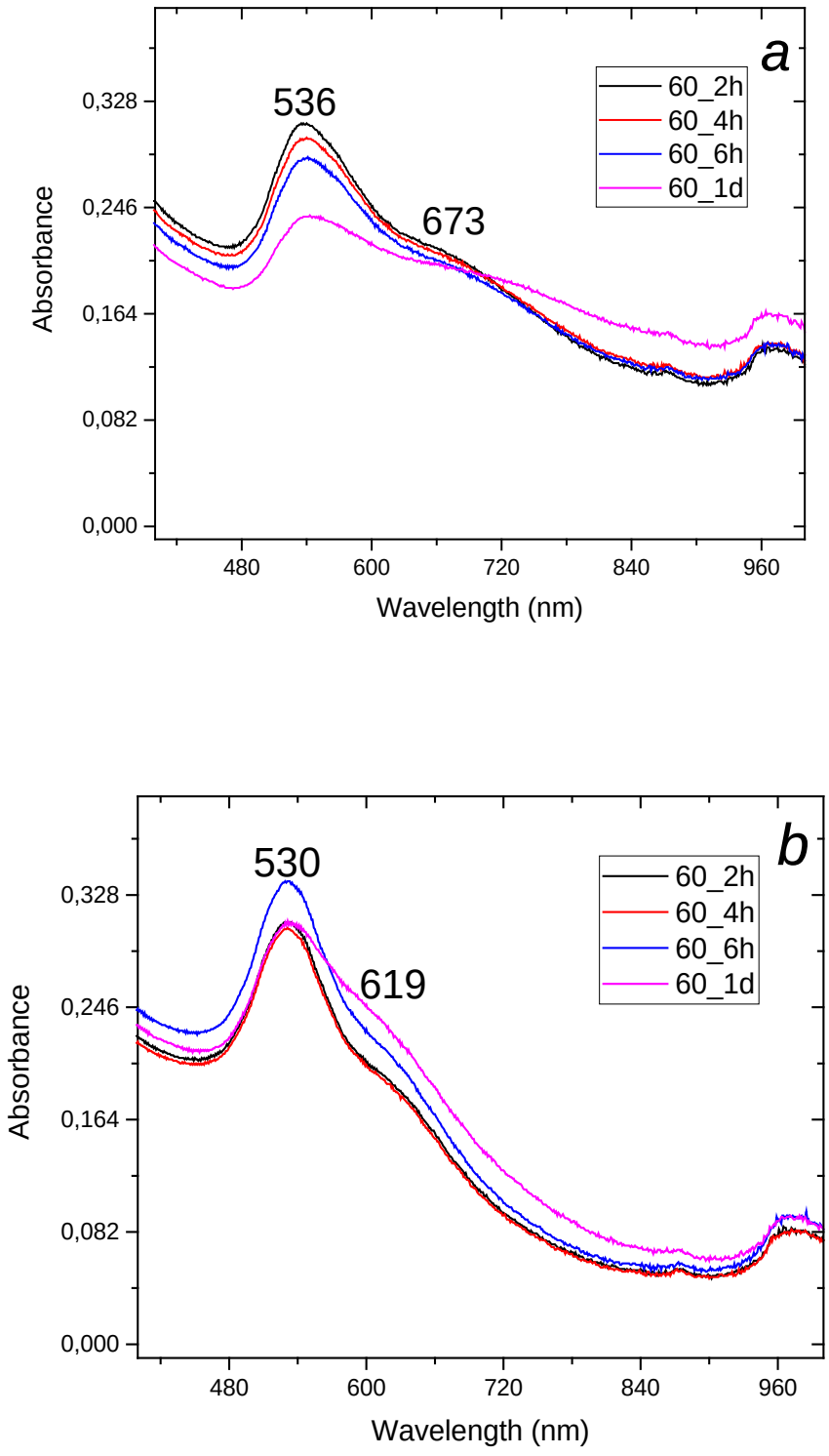

Figure 18. UV-Vis spectrum of the GNPs reduced by a) melissa, b) pomegranate at 60 ℃

Figure 19. GNPs synthesized from the melissa extract at different temperatures: 4 ℃, RT, 30 ℃, 40 ℃, 50 ℃, 60 ℃ (from left to right, respectively)

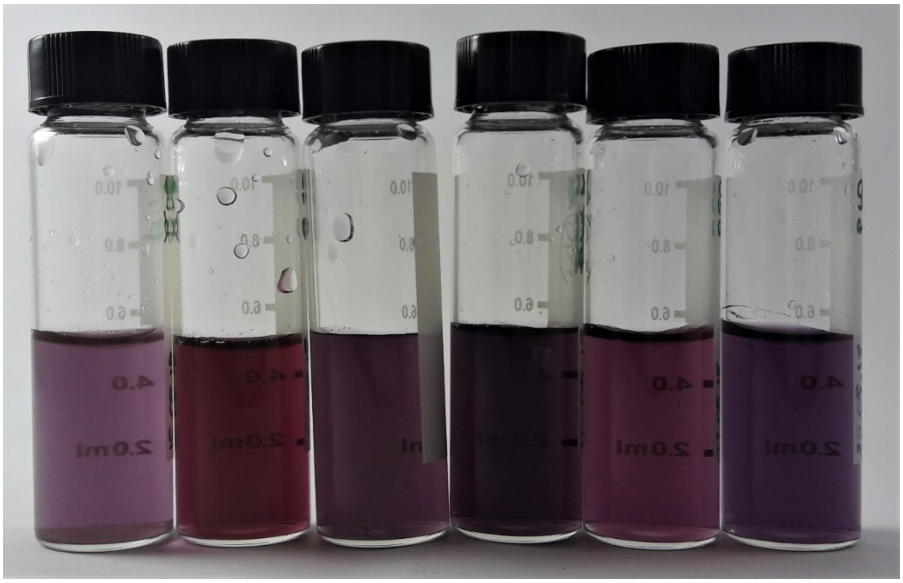

Figure 20. GNPs synthesized from the pomegranate extract at different temperatures: 4 ℃, RT, 30 ℃, 40 ℃, 50 ℃, 60 ℃ (from left to right, respectively)

Based on the size analysis data, generally melissa and sage reduced GNP solutions showed similar behaviour while pomegranate was quite different. From Figure 21, it can be seen that the size change is not significant for both melissa and sage

reduced GNPs, and therefore GNPs are stable through 4 weeks of time. For pomegranate reduced GNPs slight agglomeration occurs when solutions were analysed through 4 weeks. When compared with the UV-Vis spectrum data, it can be said that the expected results were obtained.

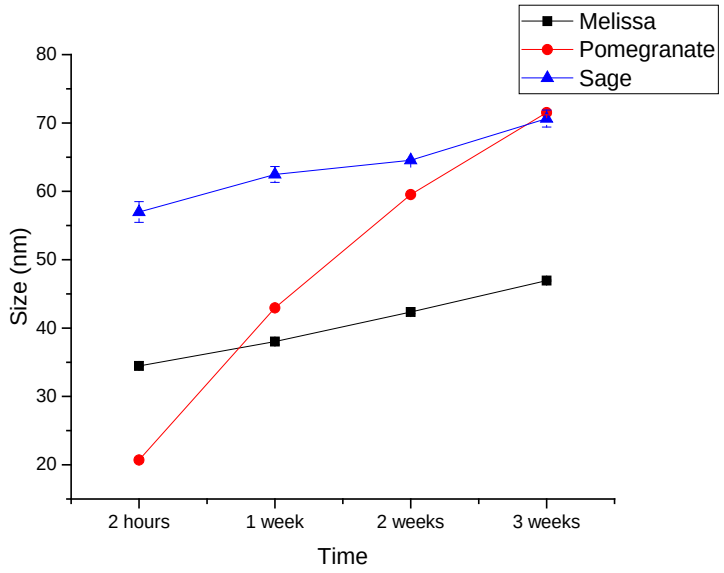

Figure 21. Size change of GNPs synthesized from melissa (black), pomegranate (red), sage (blue) through four weeks

3.2.3 Surface Charge Analysis of the Green Synthesized GNPs

Surface charge of GNPs affects the binding mechanism to another substance. Surface charge and capping of GNPs may change according to the capping agent; which is mostly a component or components of reducing agent. The reaction between plant extracts and gold salt solution might result in positively charged or negatively charged GNPs.

Surface charge of the green synthesized GNPs were analysed via Zeta Potential at 24th hour prior to reaction completion. Figure 23 and 24 shows the surface charge of the GNPs synthesized by using the melissa and pomegranate extracts respectively. The data shows that, GNPs synthesized from both plant extracts are negatively charged. Hence, the amplitude of the charge changes with temperature and reducing plant

extracts. It can be concluded that the surface charge is an important parameter and the intensity is decreasing when the nanoparticle size moves more towards spherical shapes.

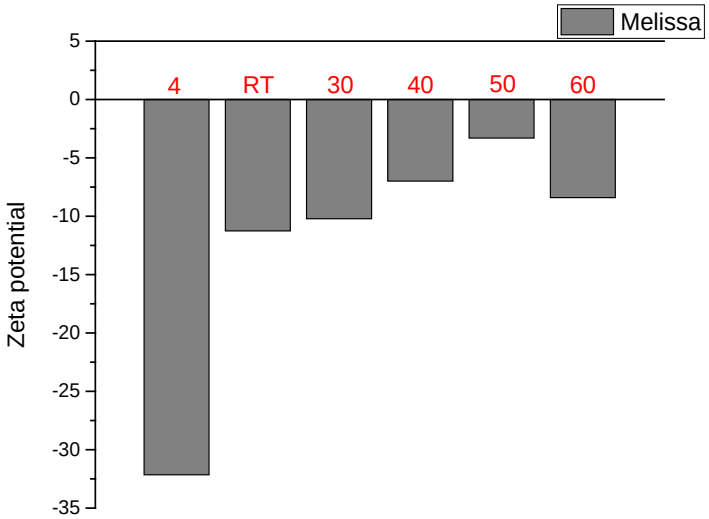

Figure 22. Zeta potential graph of melissa reduced GNPs

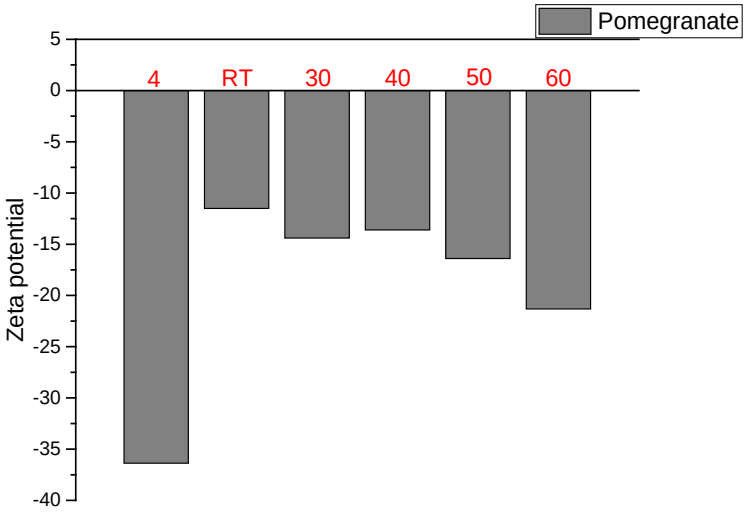

Figure 23. Zeta potential graph of pomegranate extract reduced GNPs

3.2.4 FTIR Analysis of the Green Synthesized GNPs

Fourier-Transform Infra-Red Spectroscopy (FTIR) is a method of determining the content and structure of molecules with their characteristic infrared radiation absorption. Each bond vibrate differently when exposed to IR radiation. These vibrational modes are separated in two main groups; bending and stretching. Bending vibrations can be symmetrical or non-symmetrical. Stretching vibrations are twisting, scissoring, rocking and wagging. Each mode has different IR absorption within different molecules. This phenomenon enables to identify radical groups in a sample.

FTIR analysis of both plant extracts and plant extract-reduced GNPs were obtained as shown in Figure 25, Figure 26, and Figure 27. The distinctions in spectrum were caused by the different content of the extracts. All GNPs has different chemical, physical and surface properties due to the different molecules in the extracts, which are mainly the reducing agents utilized for the GNP synthesis.

Figure 25 shows FTIR spectra for melissa. Both samples show O-H stretching at 3277 cm^{-1}, C-H stretching at 2922 and 2936 cm^{-1}, and C-H bending for sp^3 hybridized carbon at 1404 and 1410 cm^{-1}. Different from each other, melissa extract shows the distinct signal for acyl groups at 1574 and 1255 cm^{-1}, which disappears from the spectrum of the GNPs. Finally, at 1042 cm^{-1}, C-O alkoxy stretching is observed. On the other hand, GNP spectra has saturated aldehyde stretching, seen at 1723 cm^{-1}, and N-H bending at 1638 cm^{-1}. At 1227 cm^{-1}, spectrum shows a peak that is C-O stretching for both acyl and phenol radicals.

The difference between FTIR spectrum indicates the groups involving in reduction of gold to GNPs. Acyl group involving phenolic compounds can be identified as reducing agents. In this case, rosmarinic acid and caffeic acid can be suggested for possible reducing agents.

FTIR spectrum of pomegranate is shown in Figure 26. Spectrum shows similar peaks at 3295, 2924, 1717, 1414 (1403), 1029 (1027) and 774 cm^{-1}, which are O-H , C-H, 6 atom ring ketone stretching, sp^3 C-H bending, C-H alkoxy stretching and ortho substituted aromatic sp^2 C-H bending peaks, respectively. Extract sample, also, shows N-H bending at 1600 cm^{-1}, C-O alkoxy stretching at both 1341 and 1235 cm^{-1}, meta substituted aromatic sp^2 C-H bending at 864 cm^{-1}, para substituted aromatic sp^2 C-H bending at 819 cm^{-1}. Differently, GNP samples show saturated amide peak at 1645 cm^{-}

[1], C-H alkoxy stretching at 1336 and 1235 cm^{-1}, terminal sp^2 alkene C-H bending at 915 cm^{-1} and tri substituted sp^2 alkene C-H bending at 813 cm^{-1}.

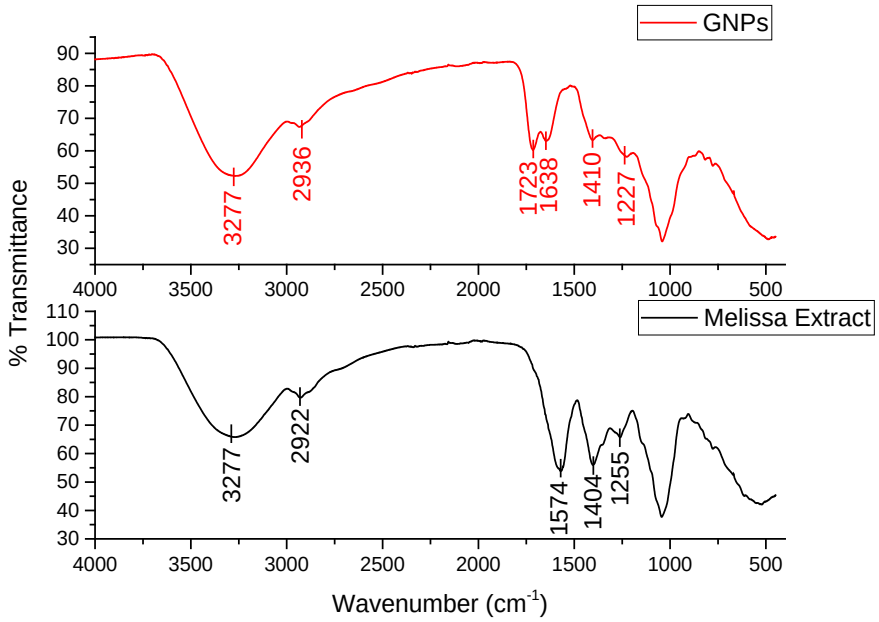

Figure 24. FTIR spectrum of melissa (black) and GNPs (red) synthesized from melissa extract

Several aromatic peaks are observed from the FTIR spectra of pomegranate extract, which are absent from the GNP spectra. This difference suggest possible molecules that are involved in GNP synthesis. Alkoxy and amine groups can be considered as reducing agents, therefore ellagic acid can be considered as main molecule in the reaction medium.

A FTIR spectra of sage is given in Figure 27. Both sage extract and GNP solution has O-H stretching at 3404.32 and 3423.19 respectively. Also, between 3300-3500 cm^{-1} the peak can be related to 2º amine groups. Generally, between 3000-2800 cm^{-1}, we observe two peaks that is specific to self-assembly, which are at 2850 and 2918 cm^{-1}. A finger print signal was observed at 2850.65, 2867.99, 2930.97 cm^{-1}, which is an indication of self-assembled structures and capping around GNPs. Also, the signal around 1700 cm^{-1} shows that both samples have carbonyl groups. At 1610.71 and 1632.79, N-H bending was observed for both sage extract and GNP solution, which supports amine group existence. The only difference in the spectrum between sage

extract and GNP solution is the sage extract peak at 1407.52 cm^{-1} that disappears from the GNP spectra. This peak shows the acyl group stretching. At 1268 cm^{-1}, we observe phenolic acyl groups. The peaks at 1053.10 and 1108.20 cm^{-1} represent the alkoxy (C-O) stretching signals. Also at 618.04 and 656.10 cm^{-1}, the same characteristic peaks were obtained for aromatic sp^2 C-H bending.

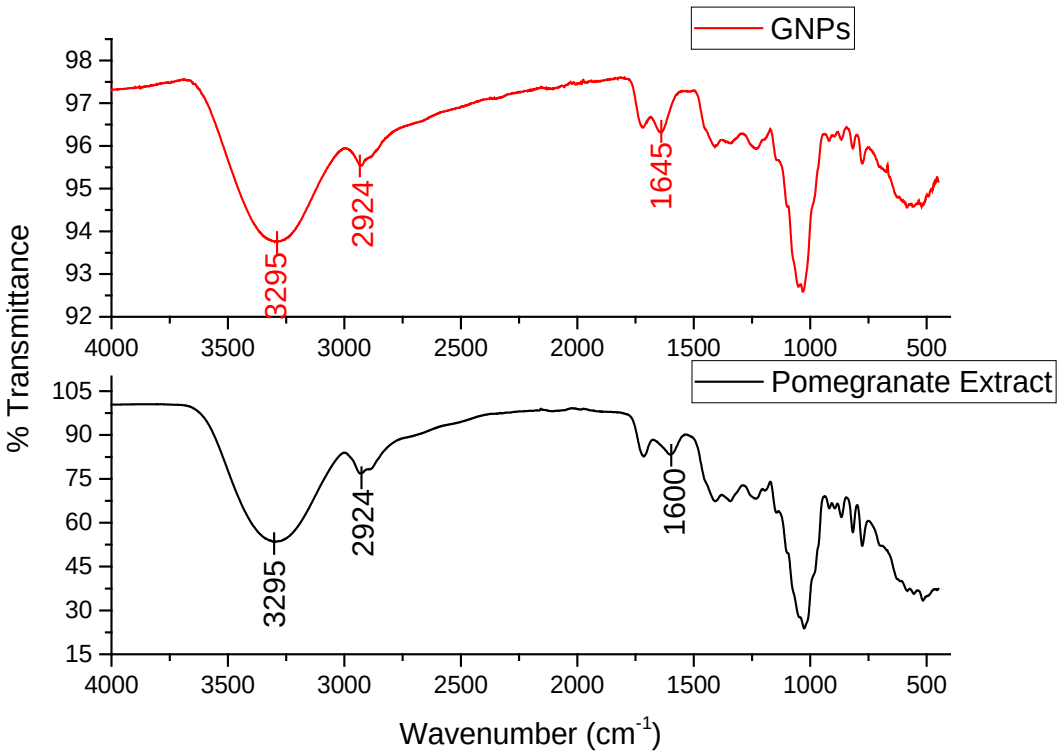

Figure 25. FTIR spectrum of pomegranate (black) and GNPs (red) synthesized from pomegranate extract

In case of sage, acyl groups involving structures are responsible for the reduction of GNPs. As mentioned before in Chapter I, luteolin is the most abundant molecule in sage extracts. The structure of luteolin confirms the participation of acyl groups in the reduction reaction.

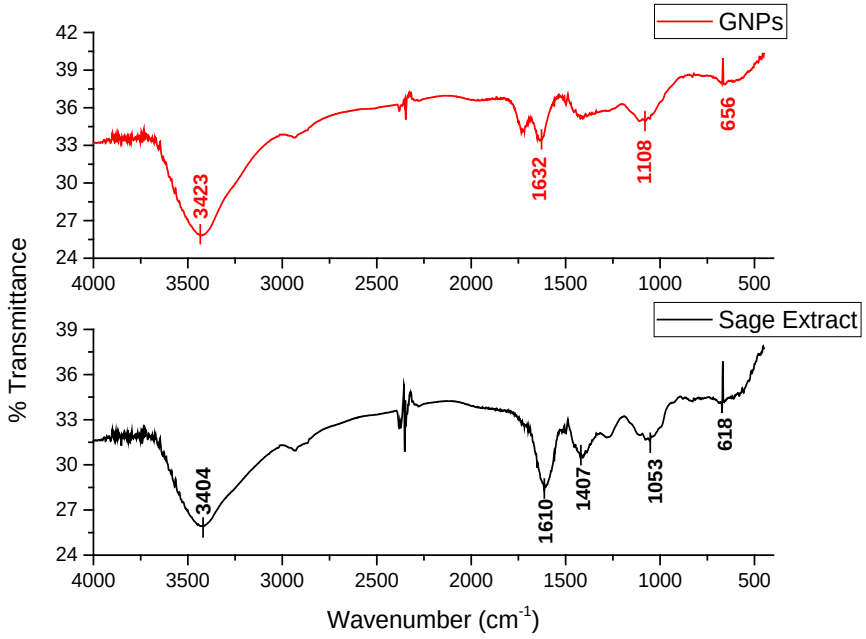

Figure 26. FTIR spectrum of sage (red) and GNPs (black) synthesized from sage extract

3.2.5 Atomic Force Microscopy (AFM) Analysis of the Green Synthesized GNPs

AFM analysis was done with gold slides due to easy immobilization procedure for AFM measurements. AFM analysis for melissa extract (Figure 28) indicates that the binding of green synthesized GNPs on a gold slide functionalized with PLL is successfully achieved. From 2D images, it is observed that the GNPs are attached to the surface with slight agglomerations. Surface profiles and 3D images, also contributes to those findings. Magnitudes of the obtained images correspond to 25 nm, which is also supported by the data found in size measurements.

As AFM findings indicate pomegranate extract reduced GNPs (Figure 29) have higher adsorption to the surface than the others. The magnitude is around 35 nm showing the nanoparticle diameter is consistent with size measurements.

Sage reduced GNPs and the even distribution of GNPs on solid surface is analysed by AFM results as given in Figure 30. Similarly, 3D images support the even distribution of the GNPs.

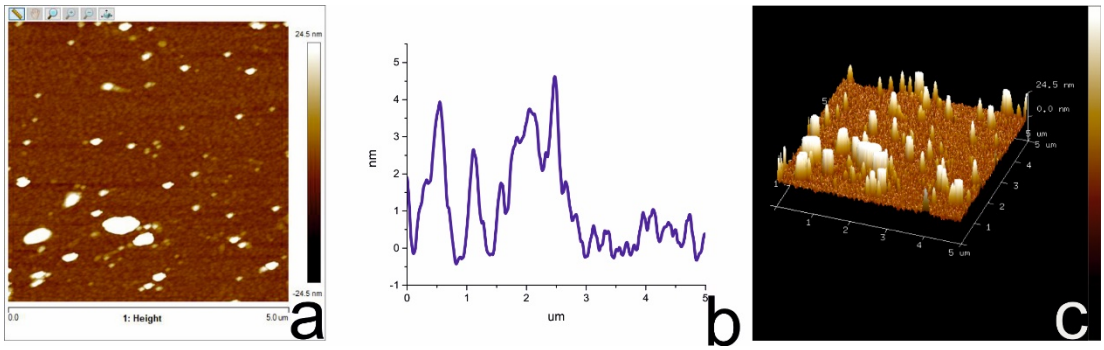

Figure 27. AFM images of the melissa extract reduced GNPs on solid surface; 2D images of surface (a) surface profile (b), and 3D images of surface (c)

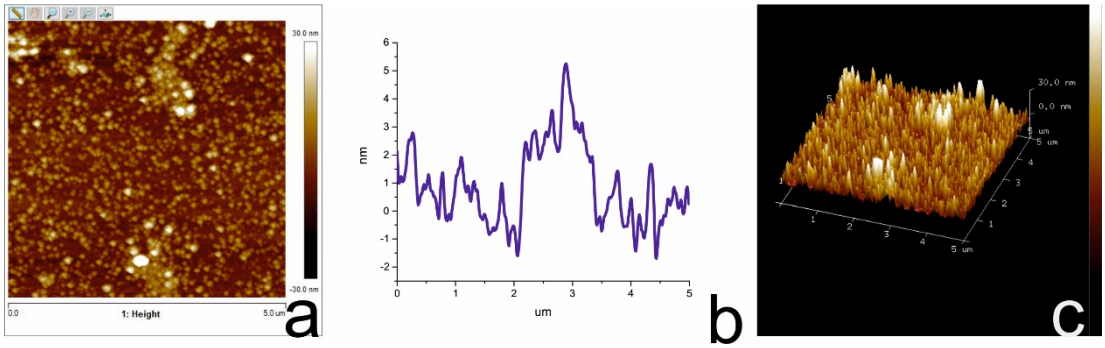

Figure 28. AFM images of the pomegranate extract reduced GNPs on solid surface; 2D images of surface (a) surface profile (b), and 3D images of surface (c)

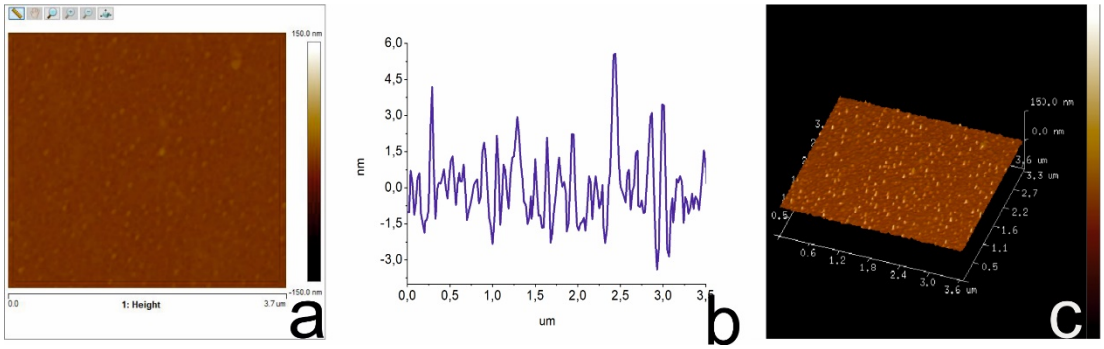

Figure 29. AFM images of the sage extract reduced GNPs on solid surface; 2D images of surface (a) surface profile (b), and 3D images of surface (c)

3.2.6 Scanning Electron Microscopy (SEM) Analysis of the Green Synthesized GNPs

Imaging of a nano-sized material is one of the most important steps of characterization. SEM captures the images of a surface, giving an idea about the surface topography, crystalline structure, electrical behaviour or chemical composition.[99] The analyses were done under several voltages, pressure, and magnification to obtain the best results and backscattered electron detector (BSED) was used. Both melissa and pomegranate reduced GNPs for varied synthesis temperatures were immobilized on PLL functionalized aluminium surface.

SEM images; from Figure 31 to Figure 36, indicate that the melissa extract reduced GNP solutions contains both NPs and nanoplates shaped as triangular, hexagonal, and truncated triangular. Size of the nanoplates varies from 6 to 50 nm with varying temperature. Previously, it was mentioned that the external energy applied to the system (temperature) was leading to extinction of nanoplates. In the latest experiments, absorbance data was showing two peaks at different wavelength, indicating different shape existence. According to the Figures 31-36, it can be seen that nanoplates are exist in the GNP solution, however the size of the nanoplates gets smaller and smaller with increasing temperature as expected from the reaction kinetics. At higher temperatures, the reaction occurs faster than of lower temperatures, therefore nucleation and growing occurs slowly and slower reaction rates provide longer time for nanoplate formation.

Similar trend was also observed for pomegranate reduced GNP solutions. SEM images; from Figure 37 to Figure 42, indicate that the pomegranate extract reduced GNP solutions also contains both NPs and nanoplates shaped as triangular, hexagonal, and truncated triangular. Size of the nanoplates varies from 10 to 60 nm with varying temperature., since nucleation step is temperature dependent. Compared to melissa reduced GNPs, pomegranate reduced GNPs have higher monodispersity and the size of the GNPs (10-60 nm) are even. Similarly, nanoplates are observed with the pomegranate induced solutions, confirming absorbance data.

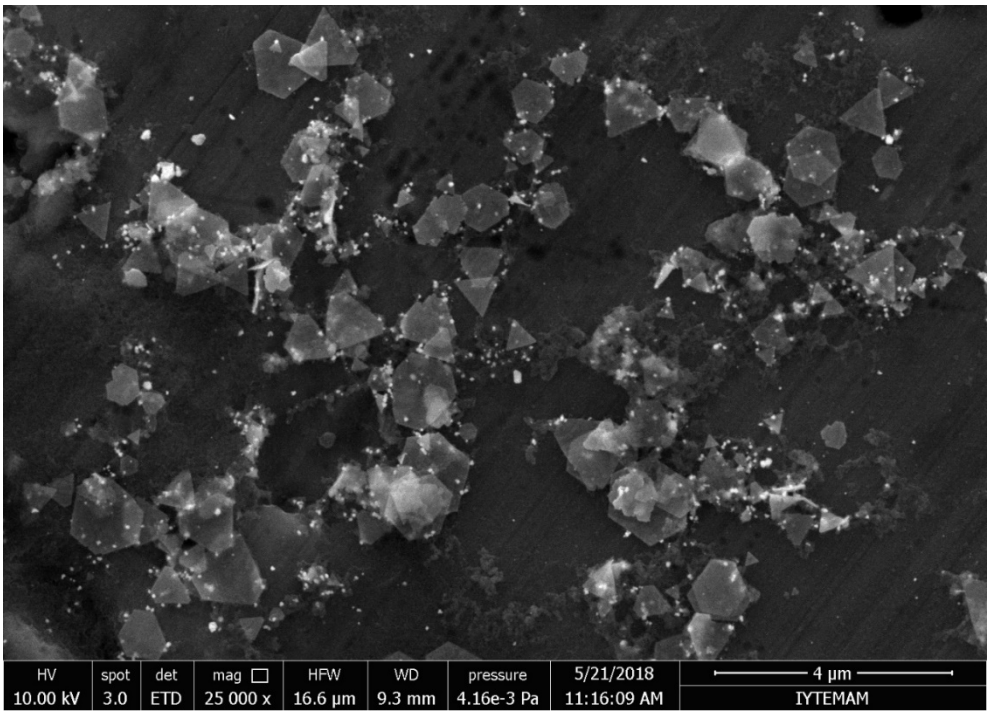

Figure 30. SEM image of GNPs reduced by the melissa extract at 4 ℃

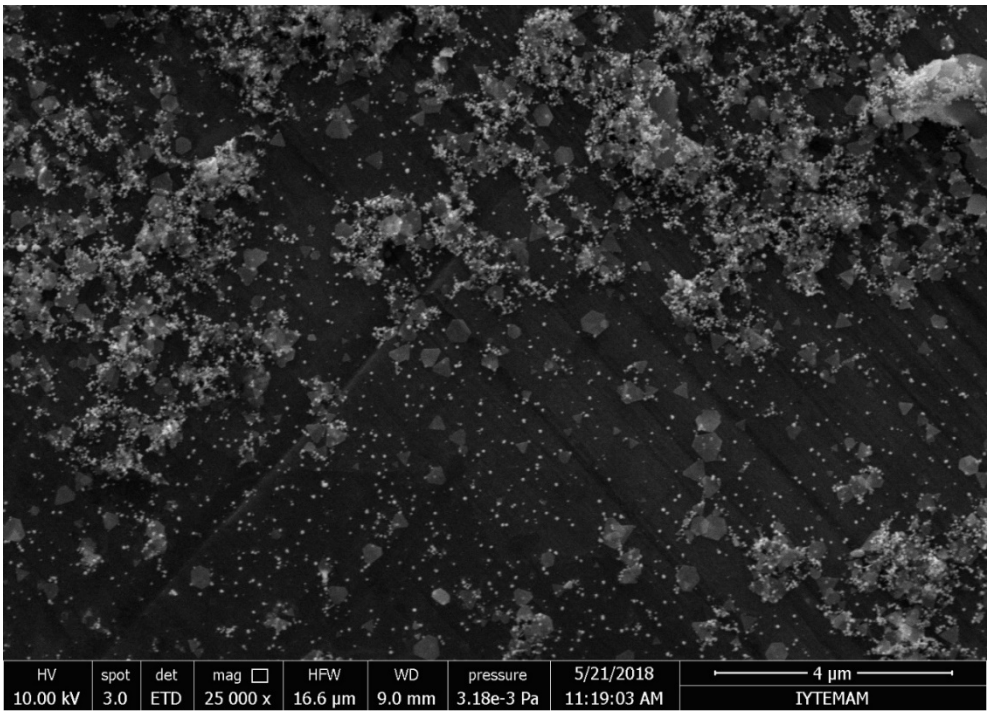

Figure 31. SEM image of GNPs reduced by the melissa extract at RT

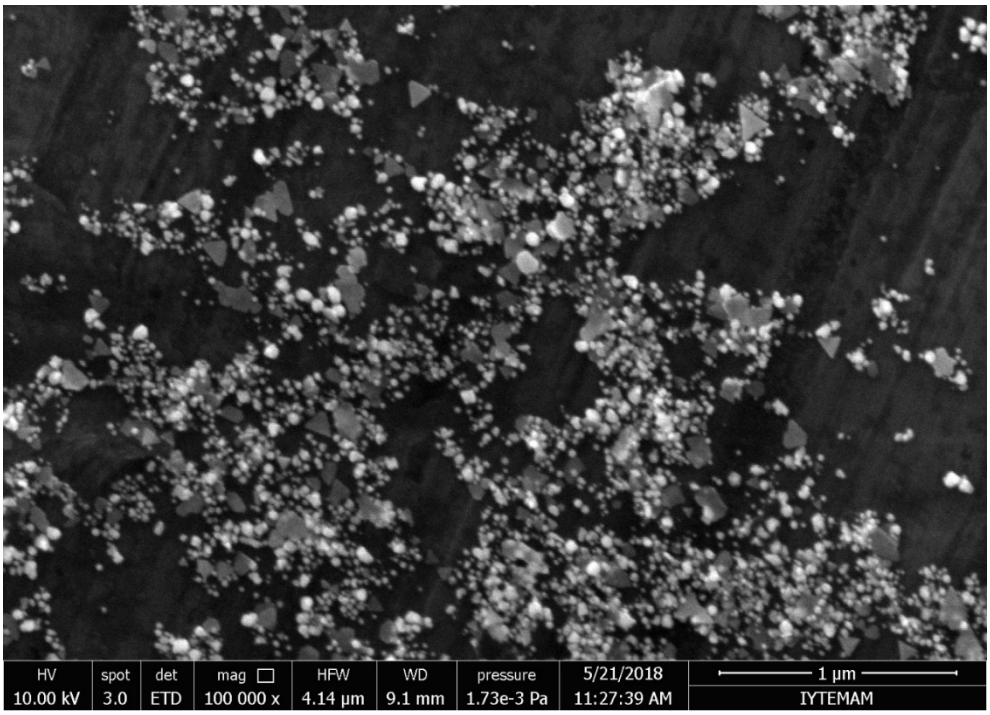

Figure 32. SEM image of GNPs reduced by the melissa extract at 30 ℃

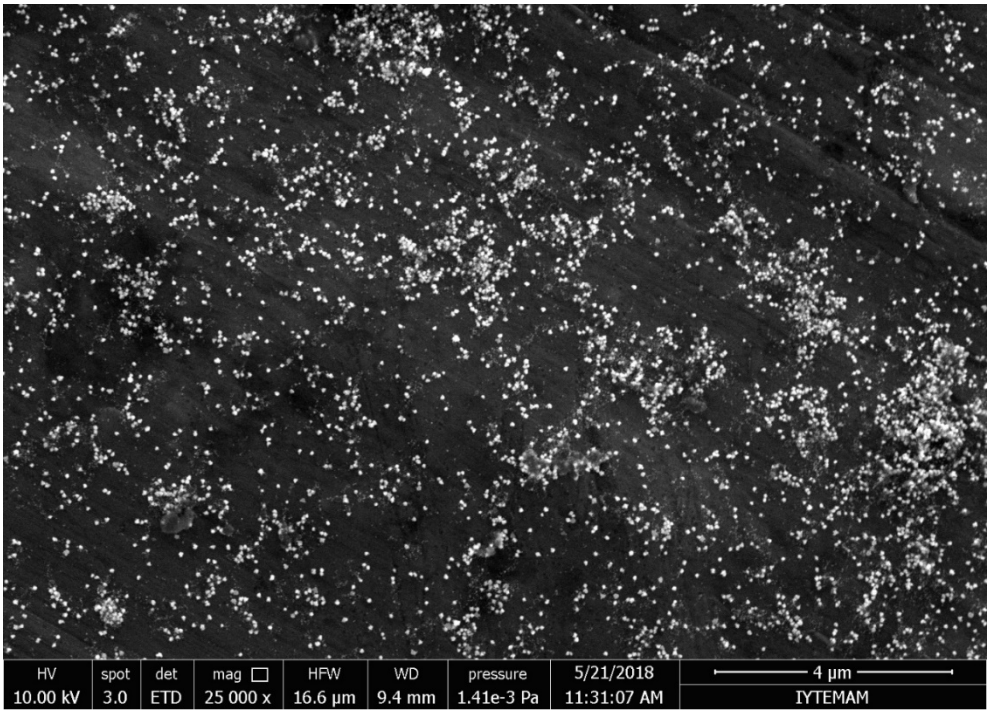

Figure 33. SEM image of GNPs reduced by the melissa extract at 40 ℃

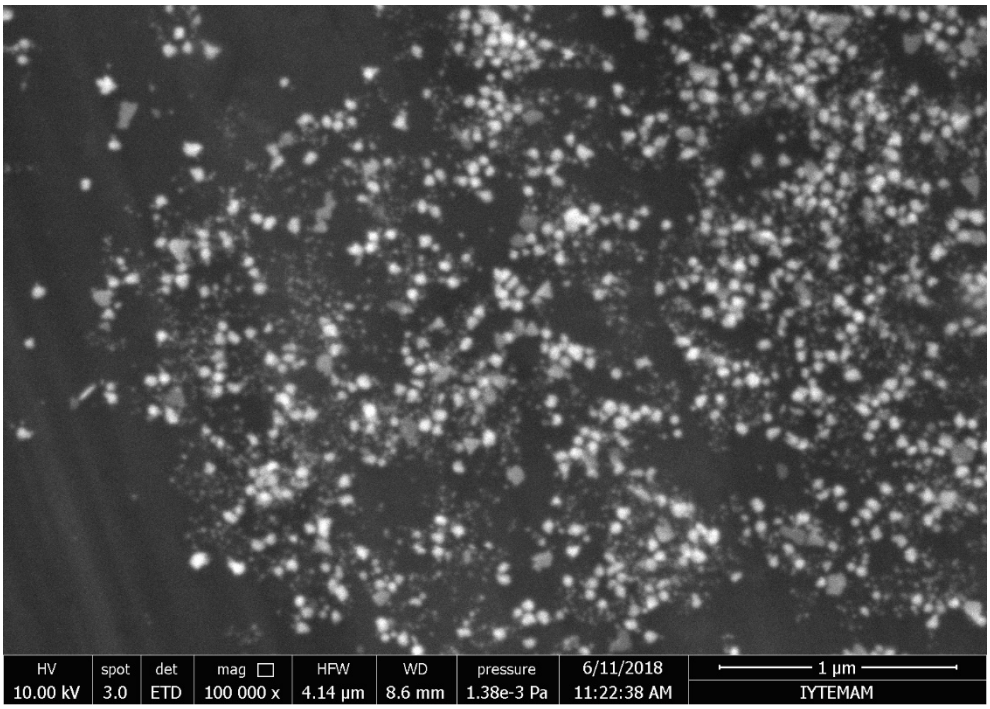

Figure 34. SEM image of GNPs reduced by the melissa extract at 50 ℃

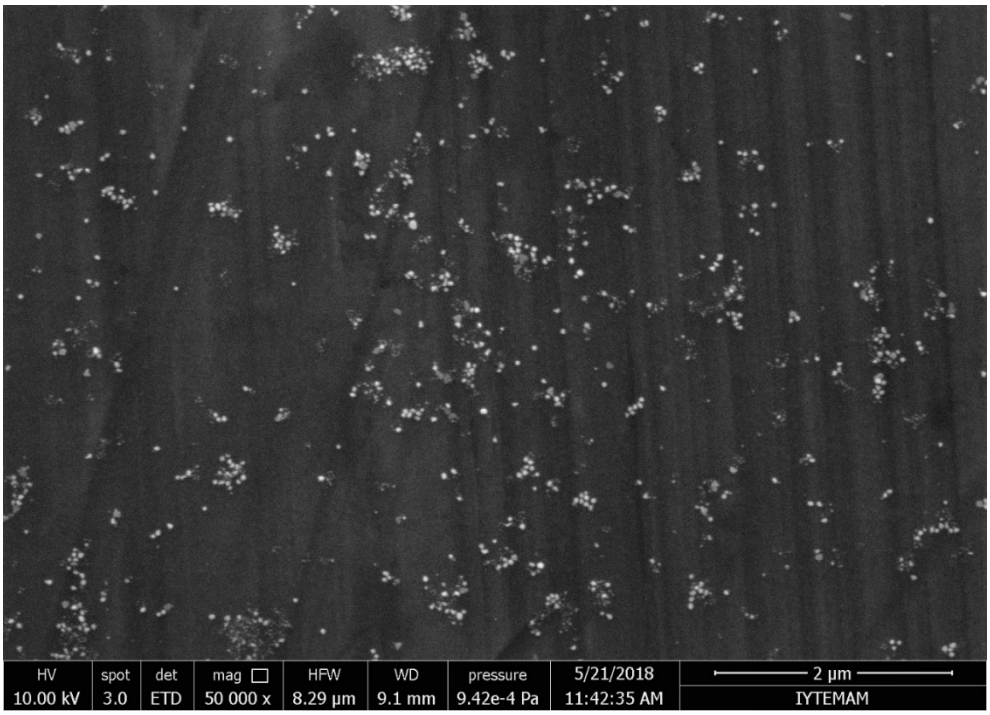

Figure 35. SEM image of GNPs reduced by the melissa extract at 60 ℃

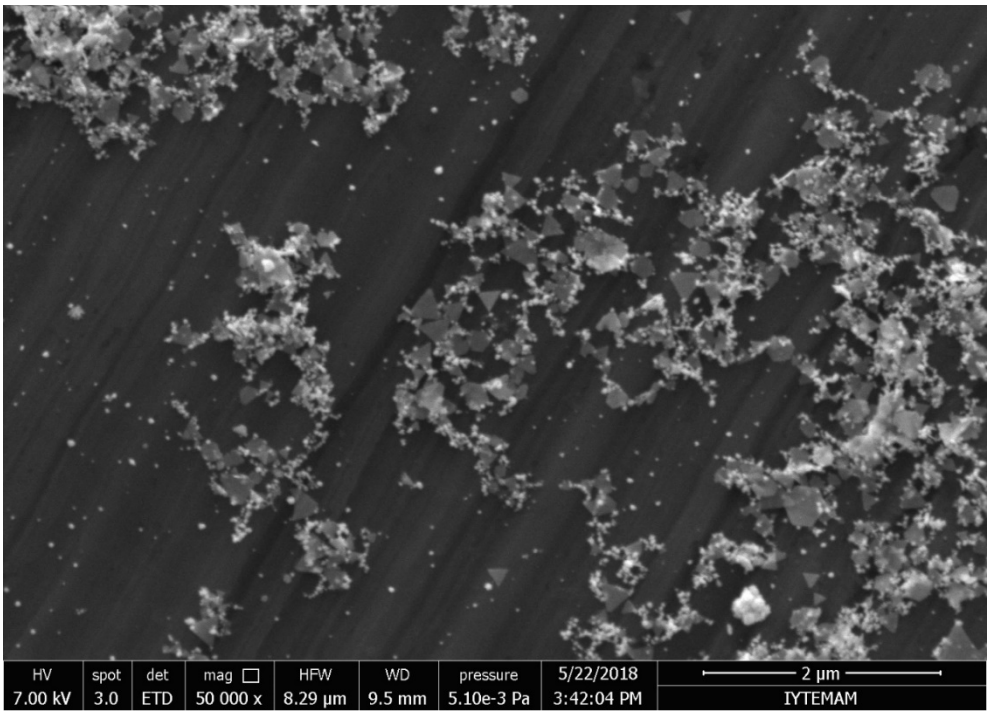

Figure 36. SEM image of GNPs reduced by the pomegranate extract at 4 ℃

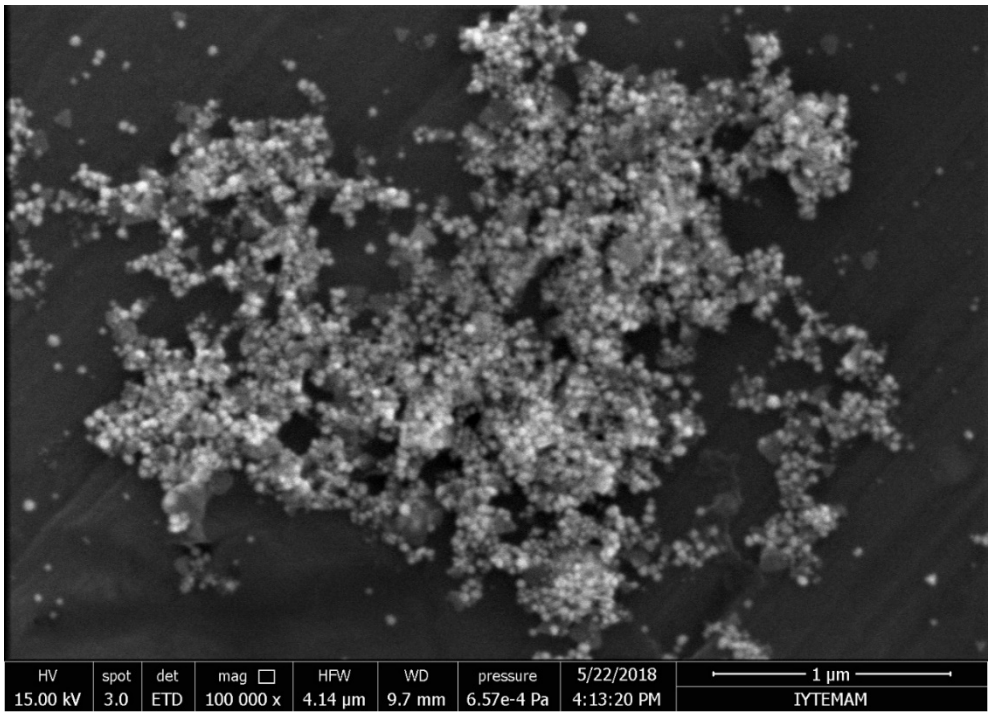

Figure 37. SEM image of GNPs reduced by the pomegranate extract at RT

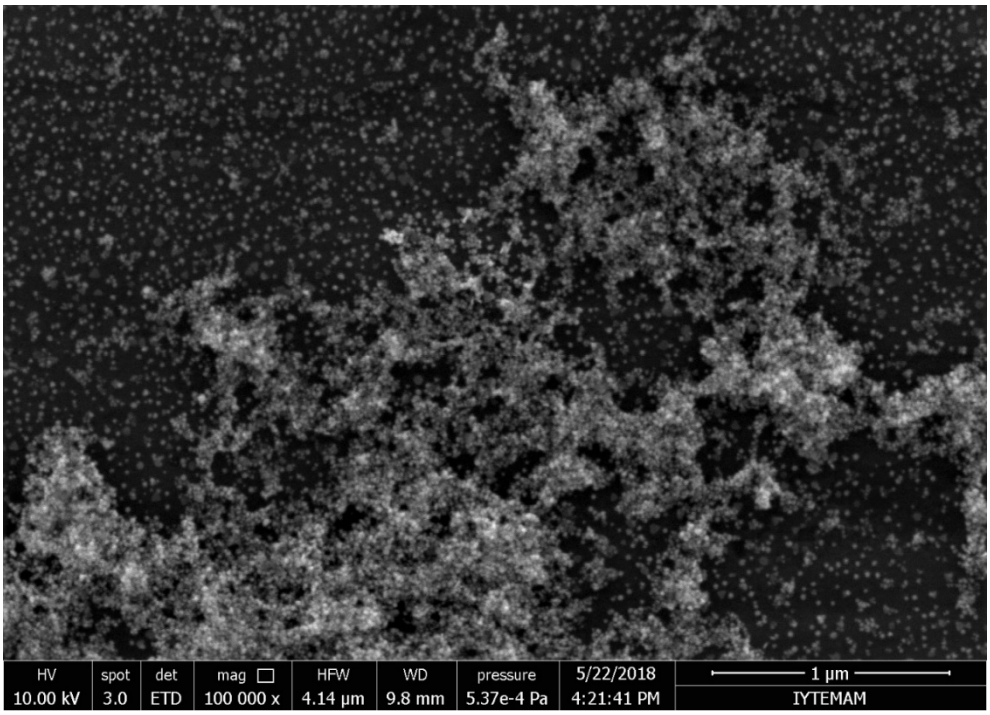

Figure 38. SEM image of GNPs reduced by the pomegranate extract at 30 ℃

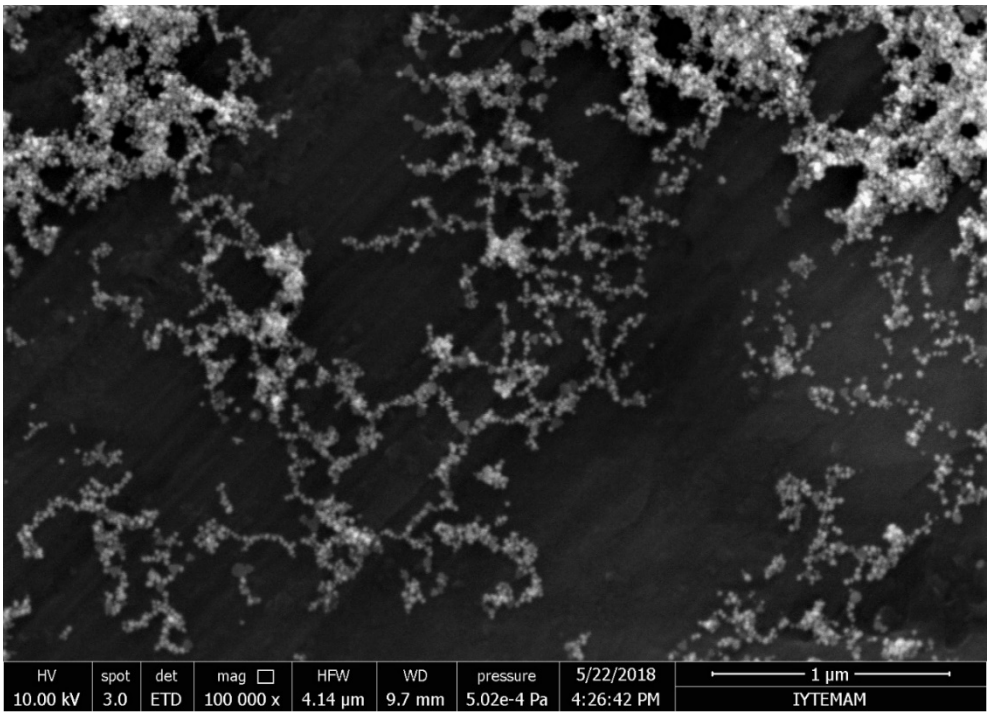

Figure 39. SEM image of GNPs reduced by the pomegranate extract at 40 ℃

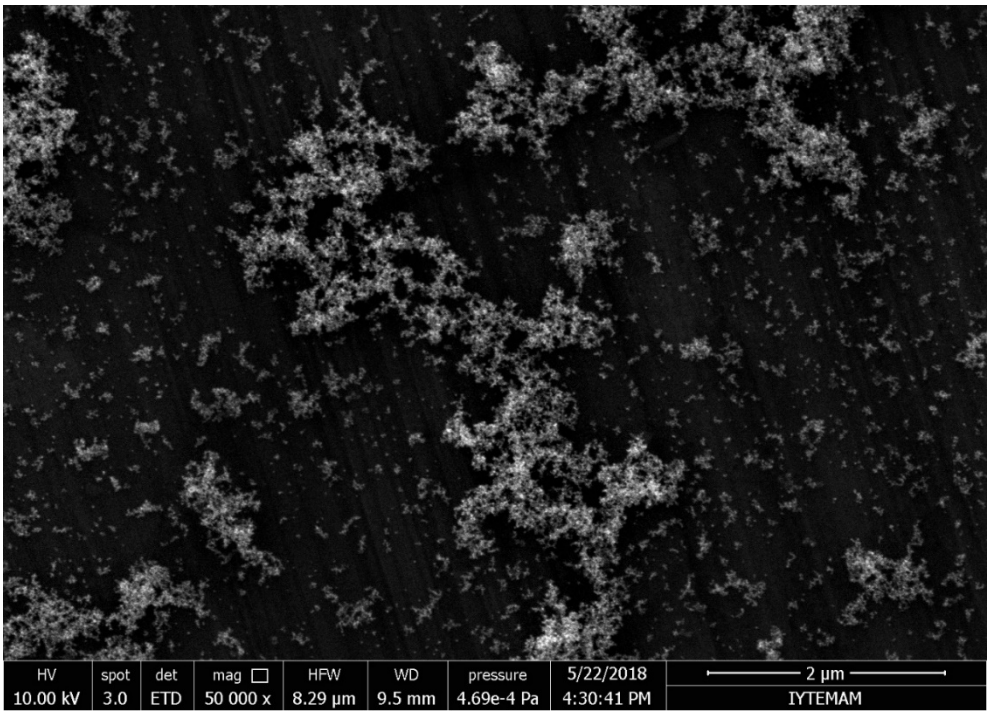

Figure 40. SEM image of GNPs reduced by the pomegranate extract at 50 °C

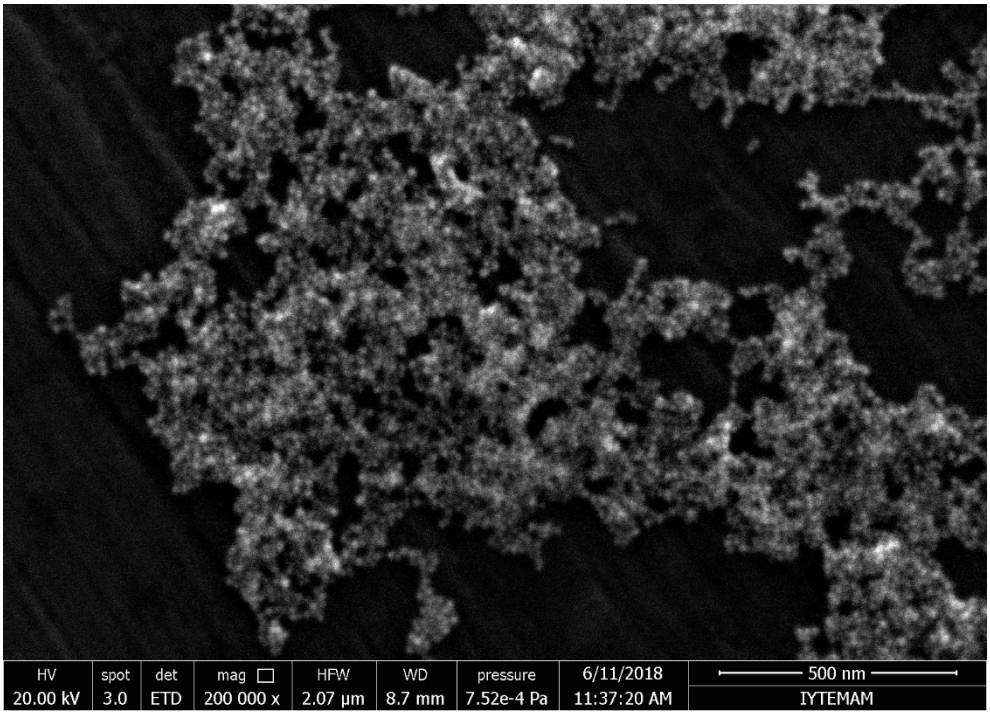

Figure 41. SEM image of GNPs reduced by the pomegranate extract at 60 °C

3.2.7 Energy Disperse X-Ray (EDX) Diffraction Analysis of the Green Synthesized GNPs

From the EDX data, gold (Au) is observed as the abundant element for both melissa and pomegranate reduced GNP solutions. Also carbon (C) and oxygen (O) content was observed in GNP solutions that indicate the presence of organic compounds originating from the plant extracts. In addition to Au, C and O is observed, which are thought to be caused by the extract content.

Table 10. Abundance of elements in GNP solutions

Melissa						
Elements	**C**		**O**		**Au**	
Tempratures	Wt%	Atomic %	Wt%	Atomic %	Wt%	Atomic %
4 ℃	12,87	30.54	34.73	61.88	52.40	7,58
RT	15,75	61,36	6,93	20,27	77,32	18,37
30 ℃	13,55	59,95	11,14	22,52	75,31	17,53
40 ℃	24,25	68,64	9,37	19,91	66,38	11,45
50 ℃	21,63	35,41	29,86	29,95	48,51	34,64
60 ℃	42,43	66,33	26,14	30,68	31,44	3,00
Pomegranate						
Elements	**C**		**O**		**Au**	
Tempratures	Wt%	Atomic %	Wt%	Atomic %	Wt%	Atomic %
4 ℃	12,65	35,36	25,81	54,15	61,54	10,49
RT	14,51	57,80	7,80	23,33	77,69	18,87
30 ℃	16,25	61,86	7,11	20,34	76,64	17,80
40 ℃	14,50	63,74	4,39	14,51	81,11	21,75
50 ℃	30,70	74,64	9,00	16,42	60,30	8,94
60 ℃	44,69	72,39	19,81	24,10	35,50	3,51

3.3 Cyanide Detection via Green Synthesized GNPs

As GNPs undergo an oxidation reaction (Eqn. 1.4) in the presence of CN^-, the color of the GNP solution turns to colourless from pink-purple color. Therefore, oxidation reaction between GNPs and CN^- can be observed visually, as well as from absorbance measurements. Here a plasmonic platform was utilized for the analysis of CN^- by immobilizing green synthesized GNPs on solid surface, namely well plate surface (Figure 43). An absorbance scan from 400 nm to 800 nm also verifies what is observed with naked eye for colorimetric detection. Spectrophotometric results from each extracts correlate that CN^-cause the oxidation of the GNPs from plant extracts, which result as a colour change.

3.3.1 Cyanide detection via *Melissa officinalis* reduced GNPs

The UV-Vis spectra of immobilized GNPs, which are synthesized at varied temperatures, are given in Figure 44. As it was observed previously, the size and the structure of GNPs are changing based on synthesis temperatures. Therefore absorbance intensity and also immobilization efficiency is correlating with it. According to Figure 44, absorbance intensity of the GNPs synthesized at different temperature via melissa extract is generally increasing with the increasing temperature which points out the higher amount of NPs and higher immobilization efficiency.

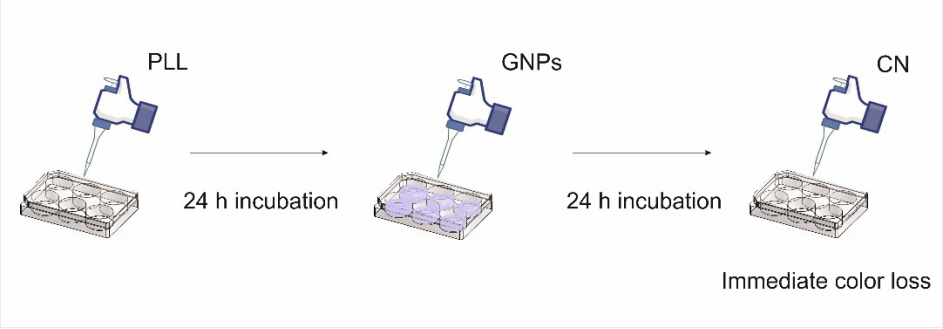

Figure 42. Schematic of GNP immobilized plasmonic platform preparation and cyanide detection in well plate format

Figures from 45 to 59, are showing the spectra of CN^- detection at varied cyanide concentrations (from 10^{-1} to 10^{-15} M) via melissa extract-reduced GNP oxidation. It is seen that at 10^{-1} and 10^{-2} M CN^- concentrations oxidation of GNPs were achieved completely. Starting from 10^{-3} M CN^- concentration, oxidation ability of cyanide is decreasing. However due to partial oxidation of GNPs both spectroscopic and colorimetric CN^- detection was done even at 10^{-15} M cyanide. Detection limit was as low as 10^{-15} M for CN^- detection via utilizing GNP immobilized plasmonic platform. Even though, all immobilized GNP samples undergo oxidizing reaction in the presence of CN^-no correlation is observed based on the properties and synthesis conditions of GNPs.

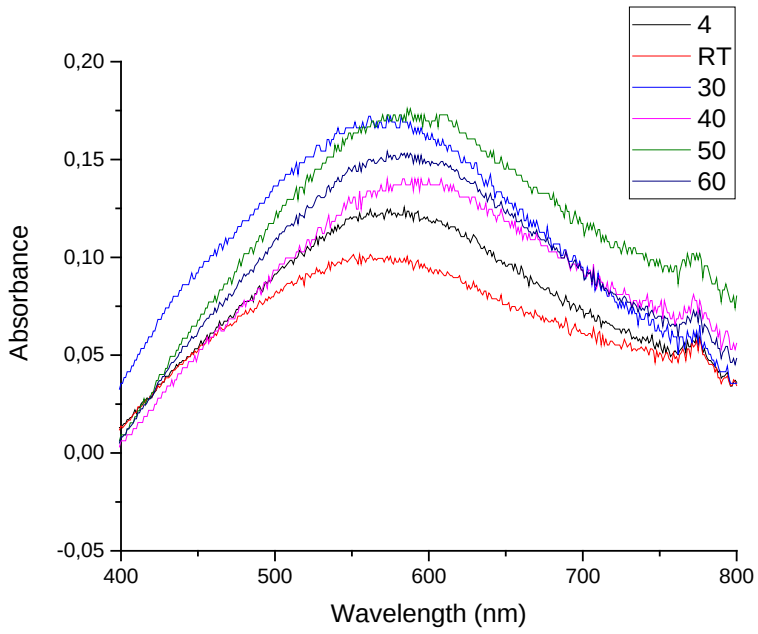

Figure 43. GNPs from the melissa extract immobilization on well plate

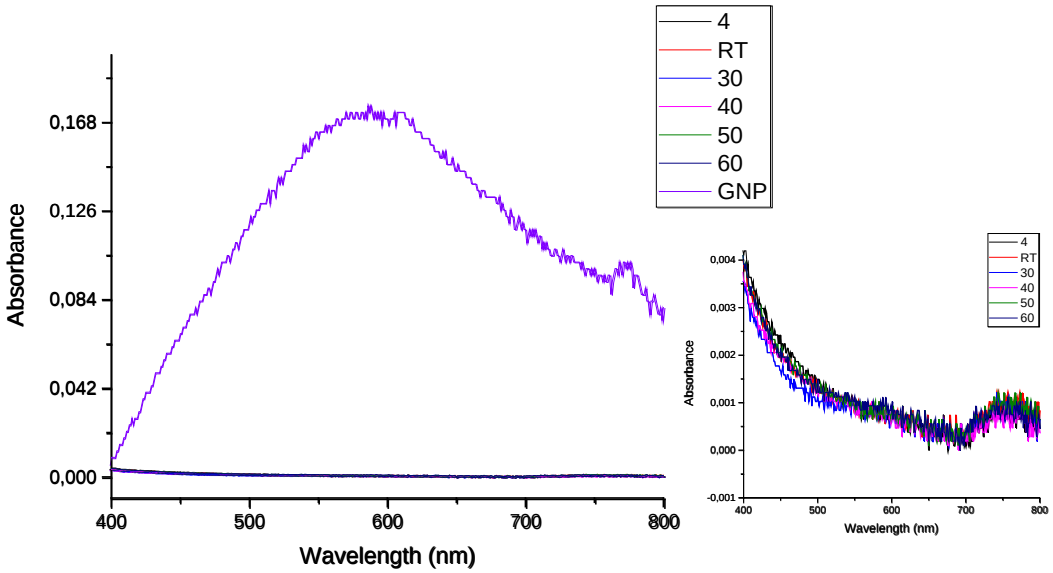

Figure 44. Oxidation spectrum of the melissa extract reduced GNPs for 10^{-1} M cyanide; inset shows the detailed view

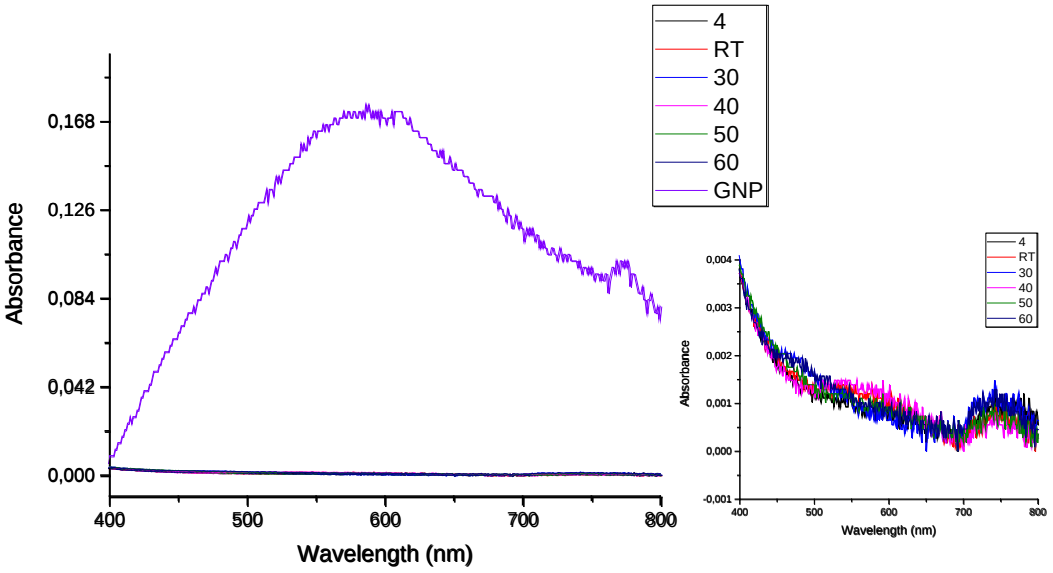

Figure 45. Oxidation spectrum of the melissa extract reduced GNPs for 10^{-2} M cyanide; inset shows the detailed view

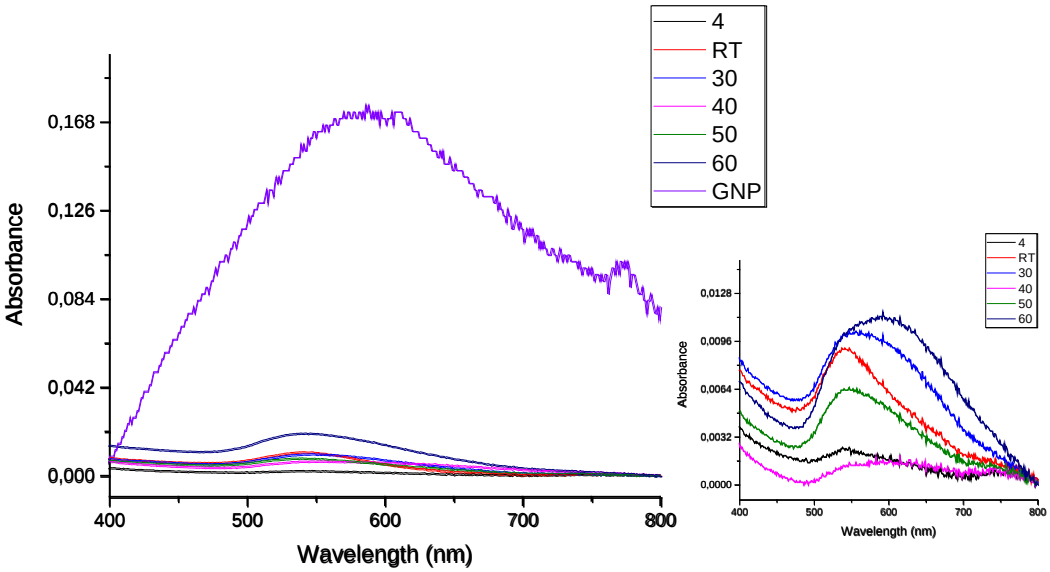

Figure 46. Oxidation spectrum of the melissa extract reduced GNPs for 10^{-3} M cyanide; inset shows the detailed view

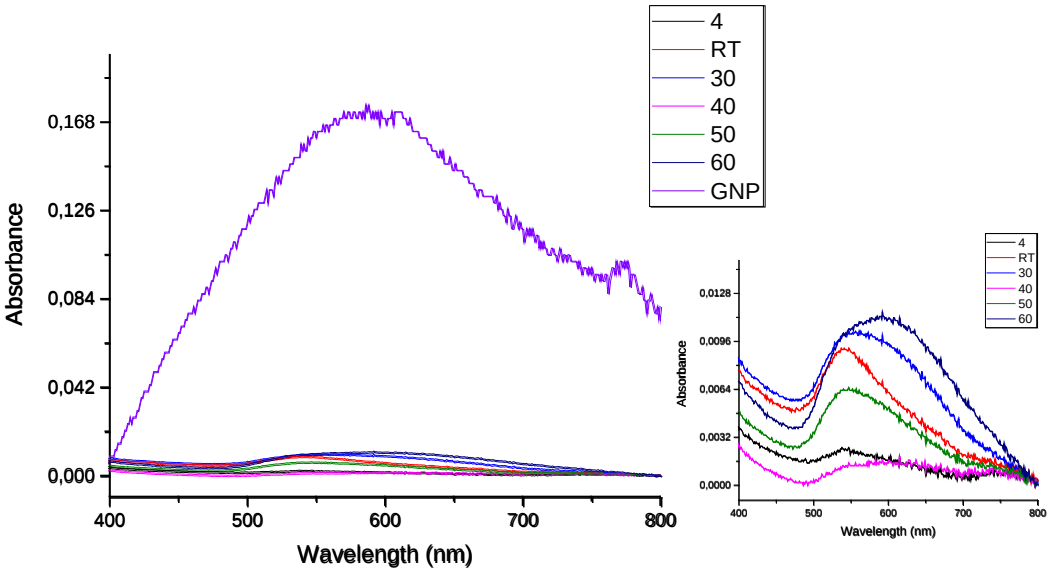

Figure 47. Oxidation spectrum of the melissa extract reduced GNPs for 10^{-4} M cyanide; inset shows the detailed view

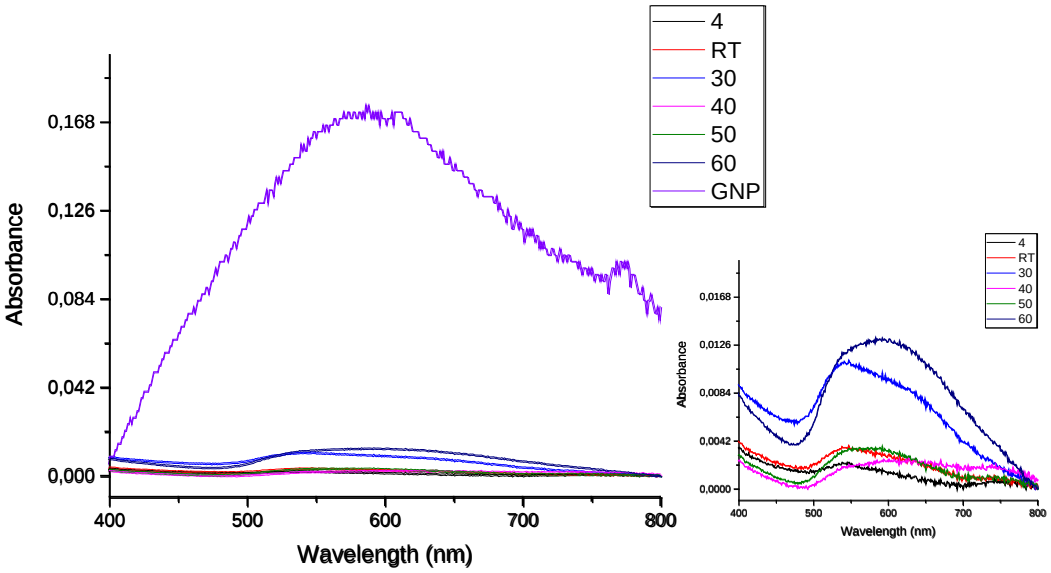

Figure 48. Oxidation spectrum of the melissa extract reduced GNPs for 10^{-5} M cyanide; inset shows the detailed view

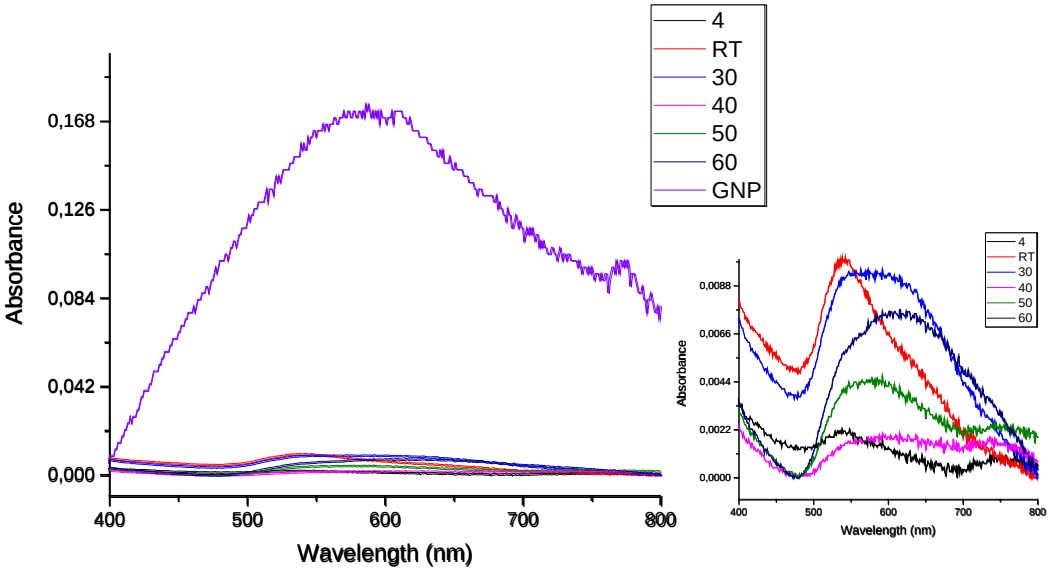

Figure 49. Oxidation spectrum of the melissa extract reduced GNPs for 10^{-6} M cyanide; inset shows the detailed view

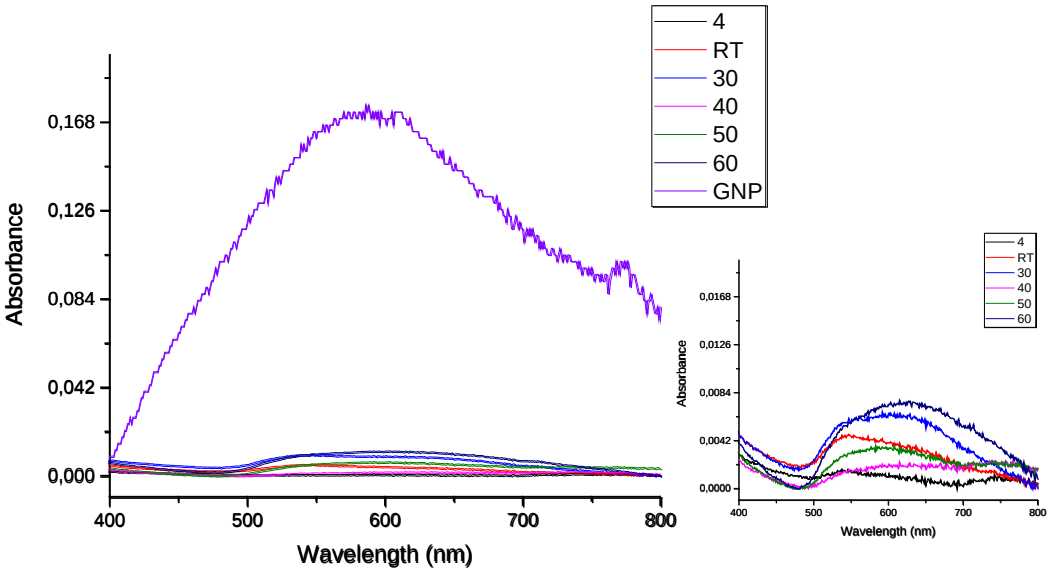

Figure 50. Oxidation spectrum of the melissa extract reduced GNPs for 10^{-7} M cyanide; inset shows the detailed view

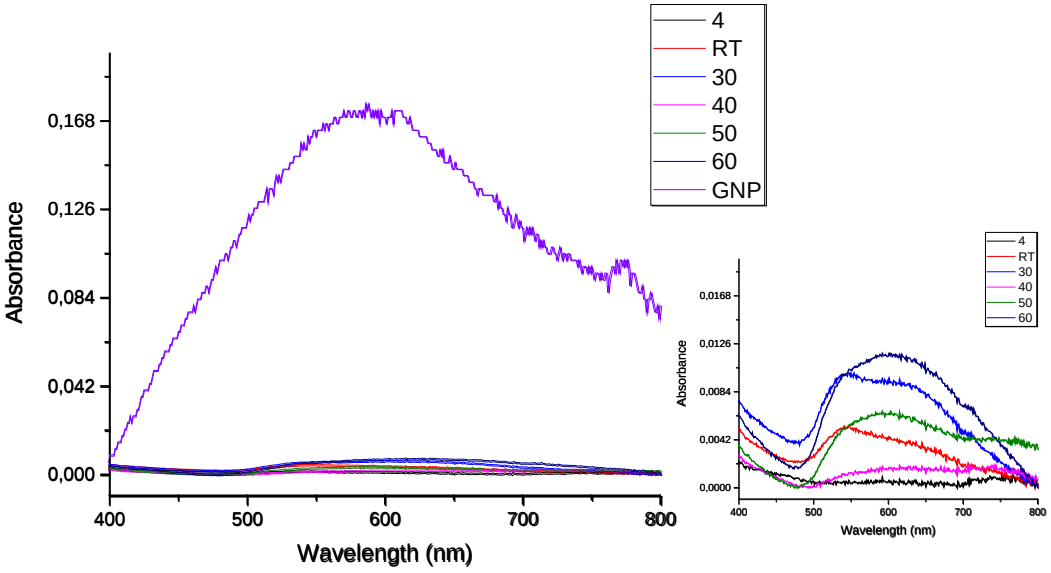

Figure 51. Oxidation spectrum of the melissa extract reduced GNPs for 10^{-8} M cyanide; inset shows the detailed view

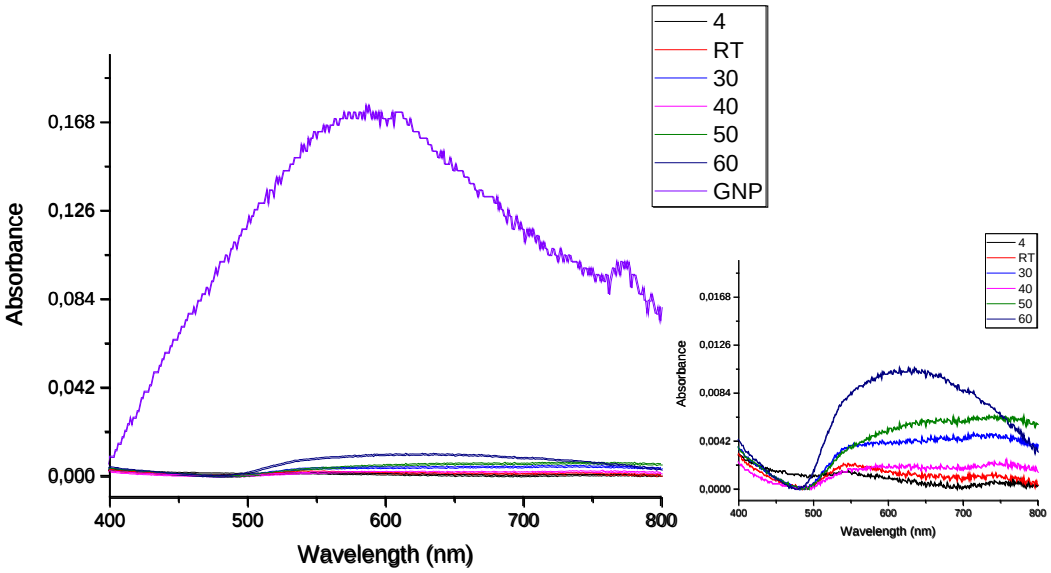

Figure 52. Oxidation spectrum of the melissa extract reduced GNPs for 10^{-9} M cyanide; inset shows the detailed view

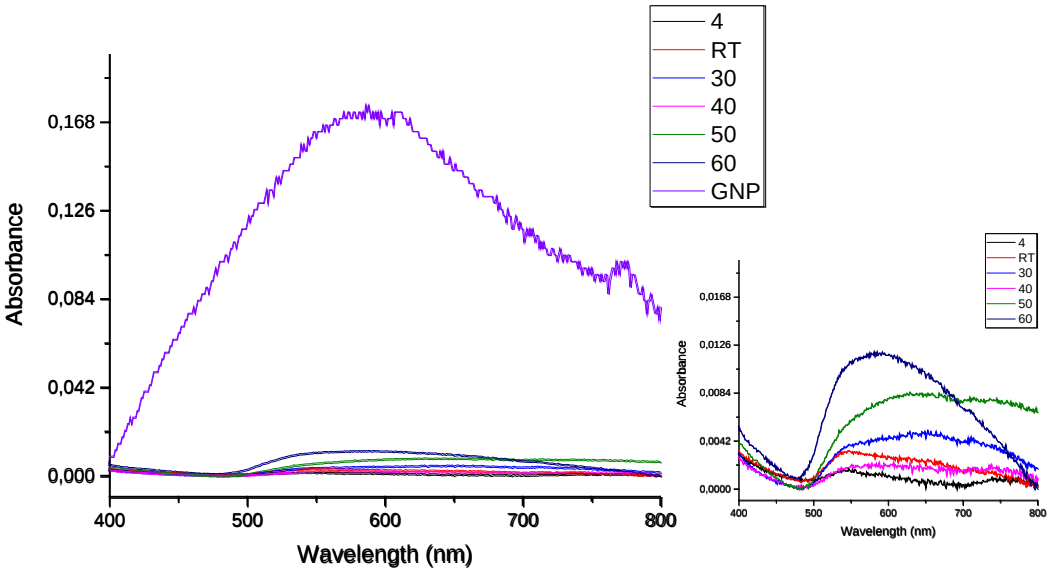

Figure 53. Oxidation spectrum of the melissa extract reduced GNPs for 10^{-10} M cyanide; inset shows the detailed view

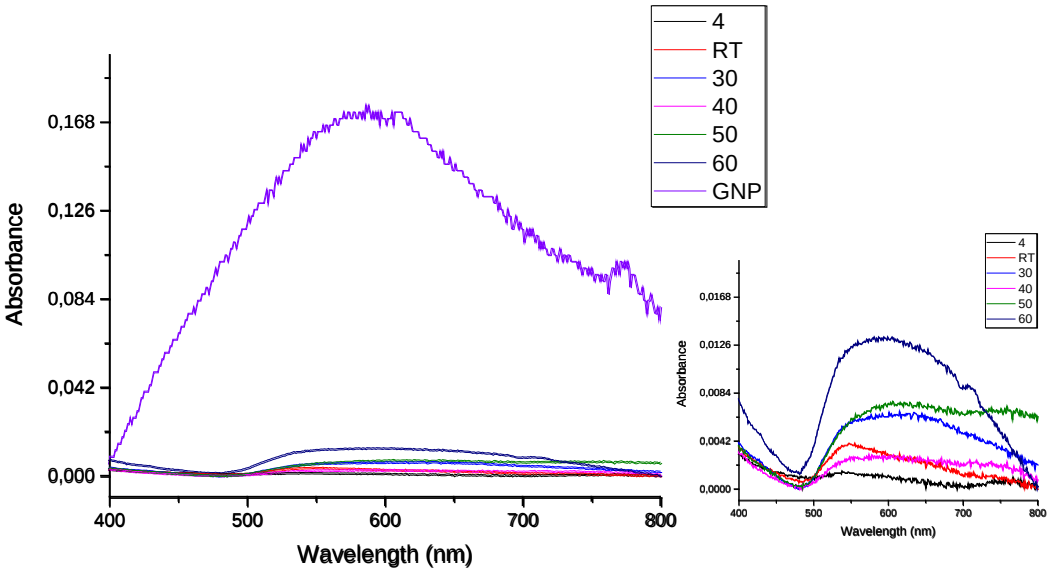

Figure 54. Oxidation spectrum of the melissa extract reduced GNPs for 10^{-11} M cyanide; inset shows the detailed view

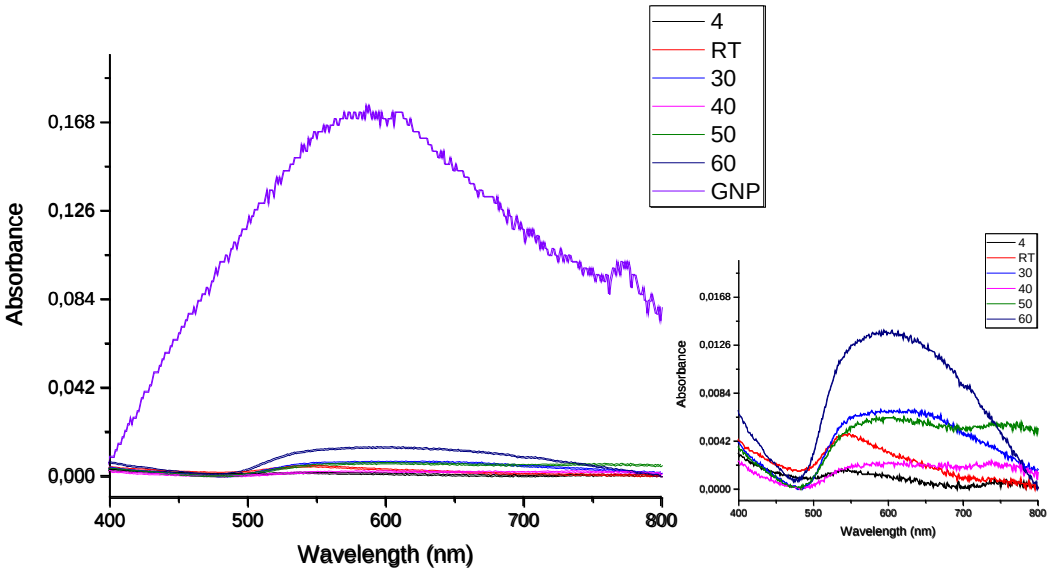

Figure 55. Oxidation spectrum of the melissa extract reduced GNPs for 10^{-12} M cyanide; inset shows the detailed view

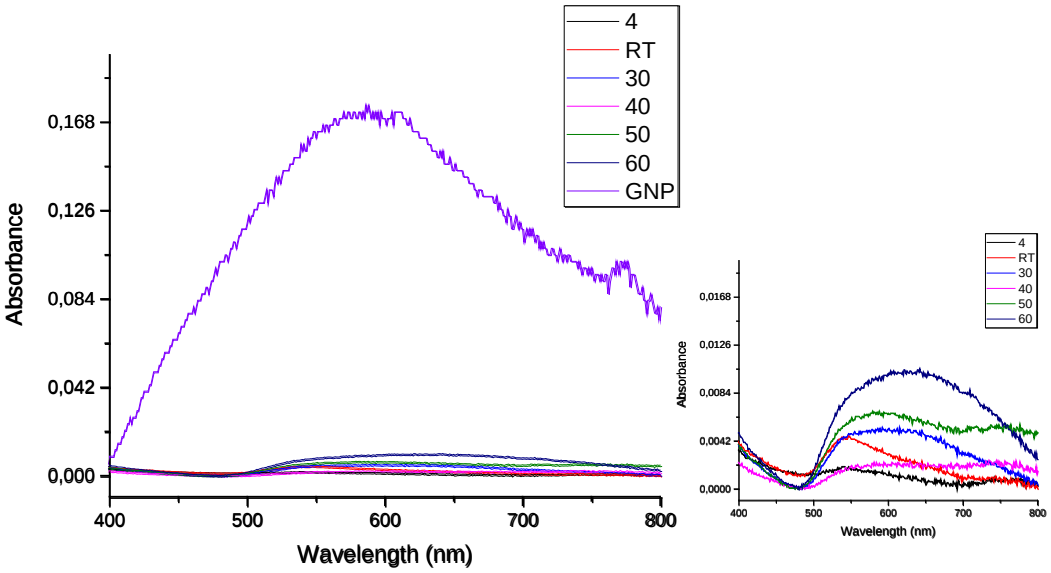

Figure 56. Oxidation spectrum of the melissa extract reduced GNPs for 10^{-13} M cyanide; inset shows the detailed view

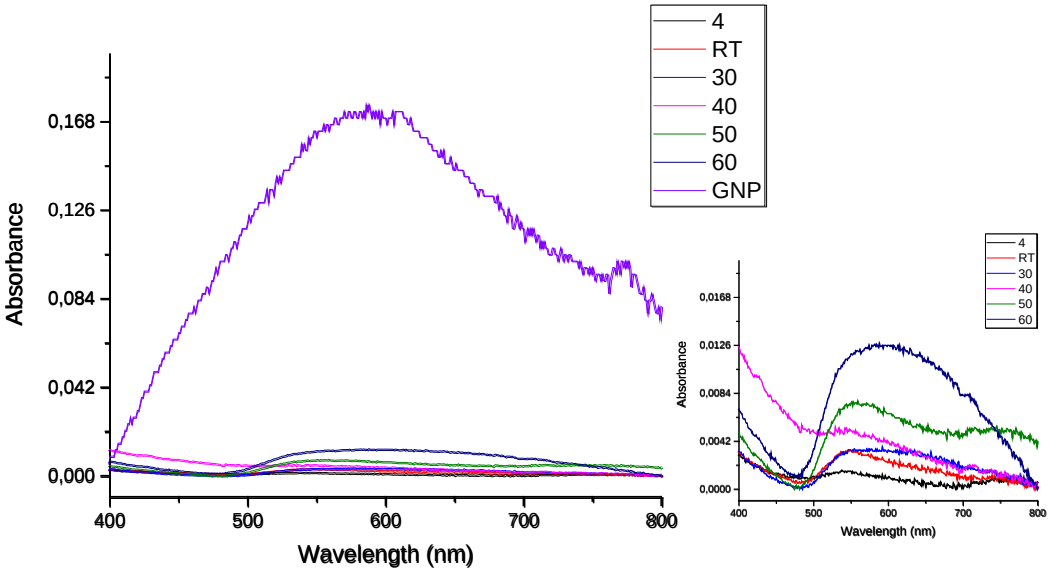

Figure 57. Oxidation spectrum of the melissa extract reduced GNPs for 10^{-14} M cyanide; inset shows the detailed view

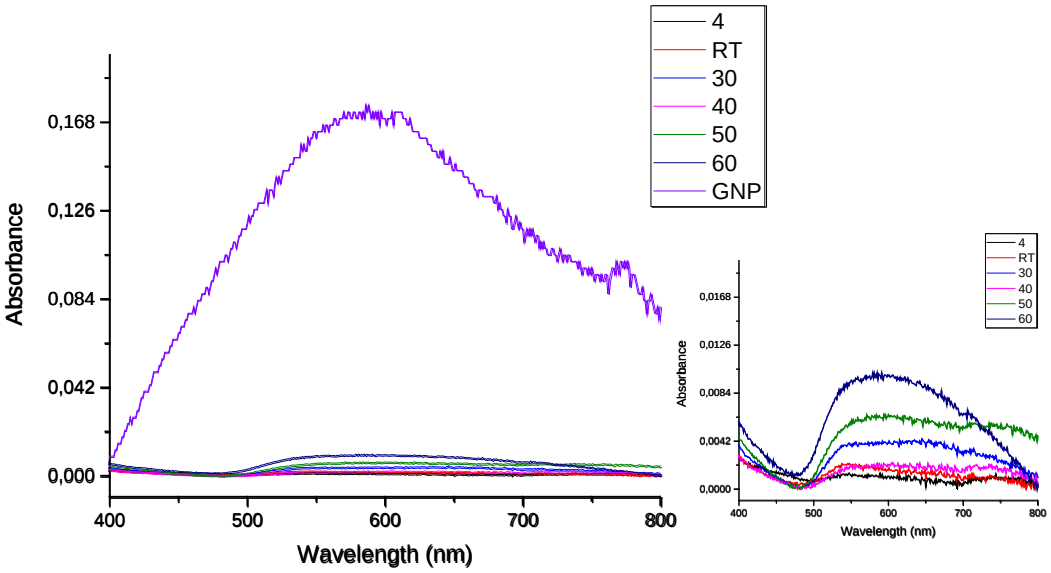

Figure 58. Oxidation spectrum of the melissa extract reduced GNPs for 10^{-15} M cyanide; inset shows the detailed view

3.3.2 Cyanide detection via *Punica granatum* reduced GNPs

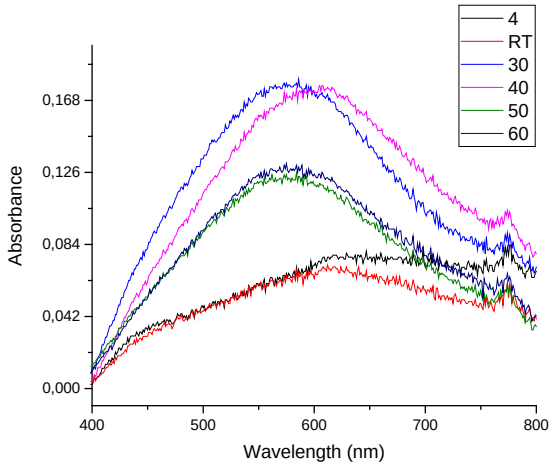

Figure 59. GNPs from the pomegranate extract immobilization on well plate

The UV-Vis spectra of immobilized GNPs, which are synthesized by pomegranate extract reduction at varied temperatures, are shown in Figure 60. As it was observed previously, the size and the structure of GNPs are changing based on synthesis temperatures, so absorbance intensity and also immobilization efficiency is correlating with it.

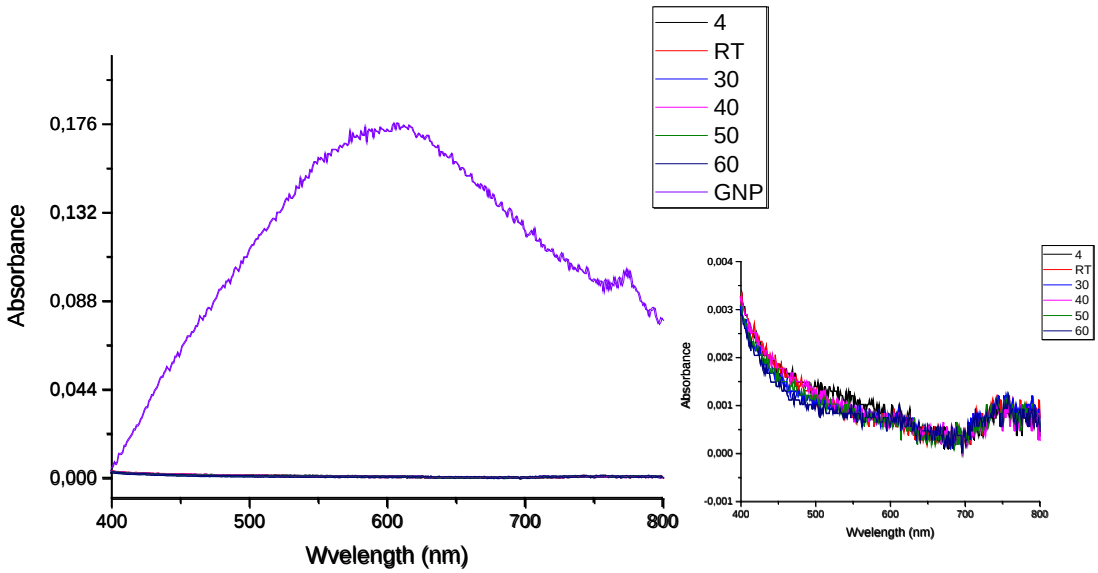

Figure 60. Oxidation spectrum of the pomegranate extract reduced GNPs for 10^{-1} M cyanide; inset shows the detailed view

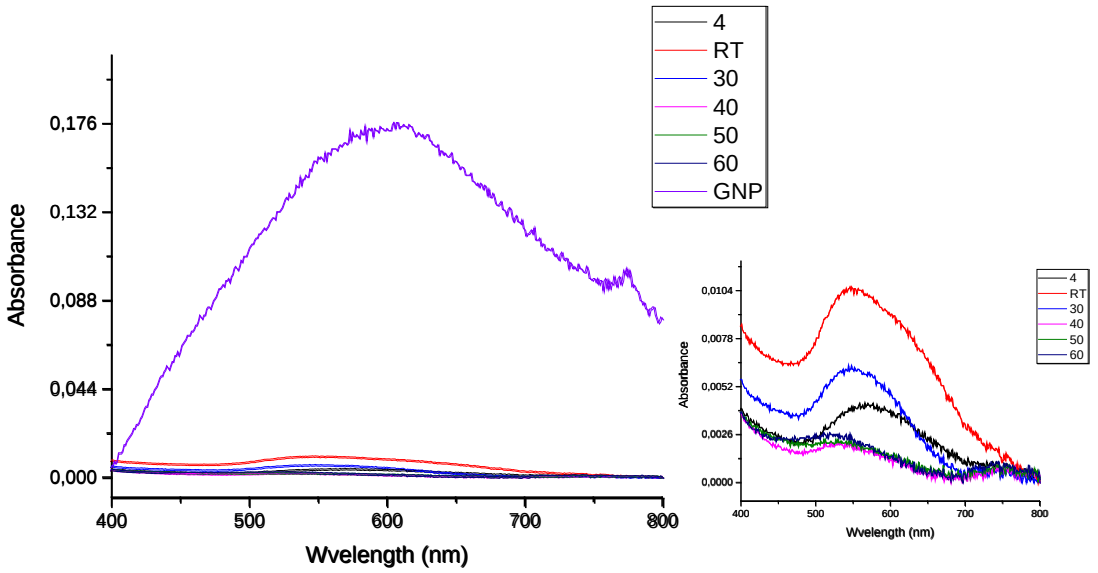

Figure 61. Oxidation spectrum of the pomegranate extract reduced GNPs for 10^{-2} M cyanide; inset shows the detailed view

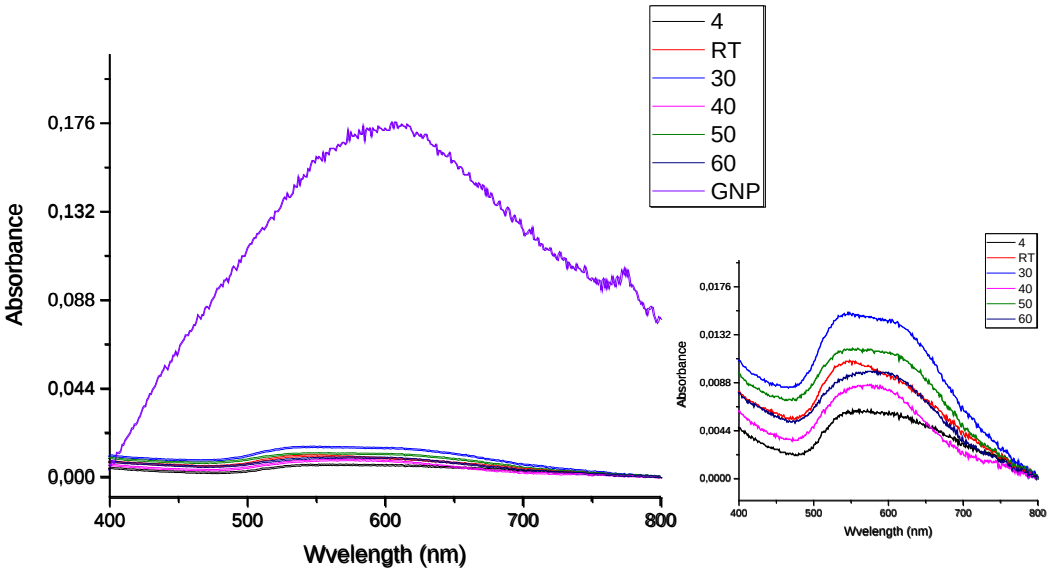

Figure 62. Oxidation spectrum of the pomegranate extract reduced GNPs for 10^{-3} M cyanide; inset shows the detailed view

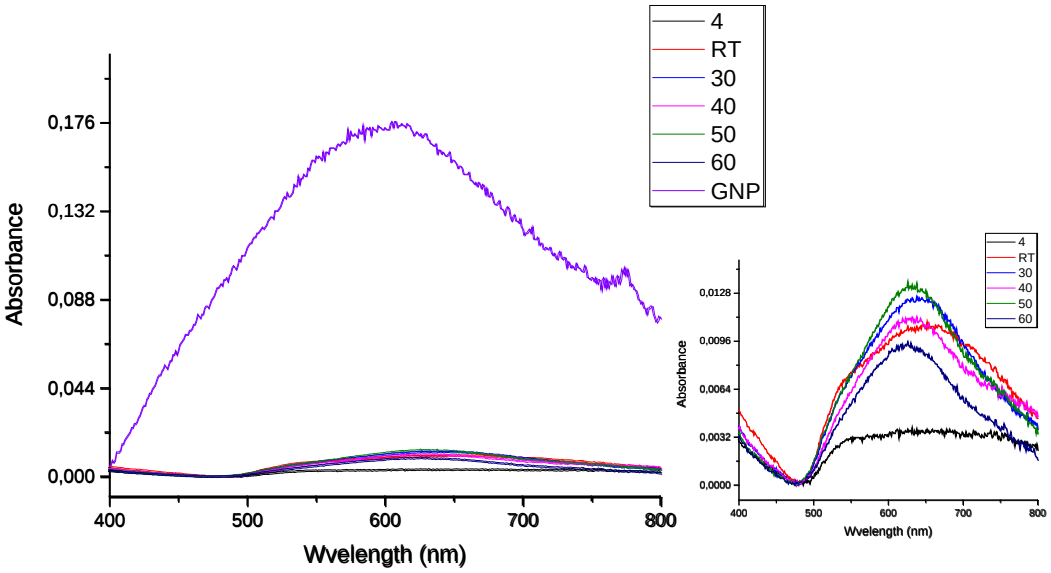

Figure 63. Oxidation spectrum of the pomegranate extract reduced GNPs for 10^{-4} M cyanide; inset shows the detailed view

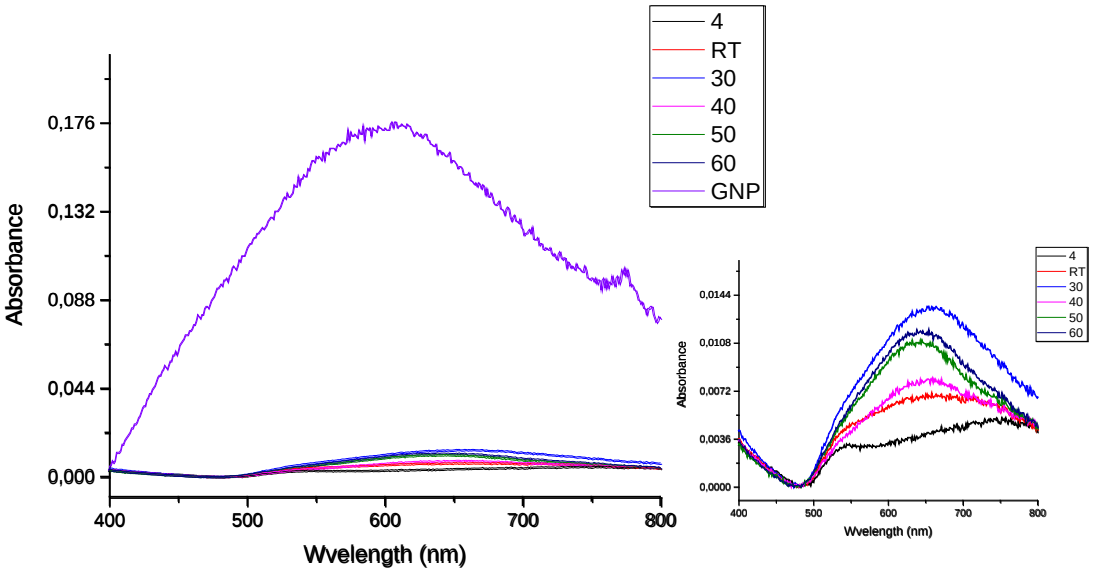

Figure 64. Oxidation spectrum of the pomegranate extract reduced GNPs for 10^{-5} M cyanide; inset shows the detailed view

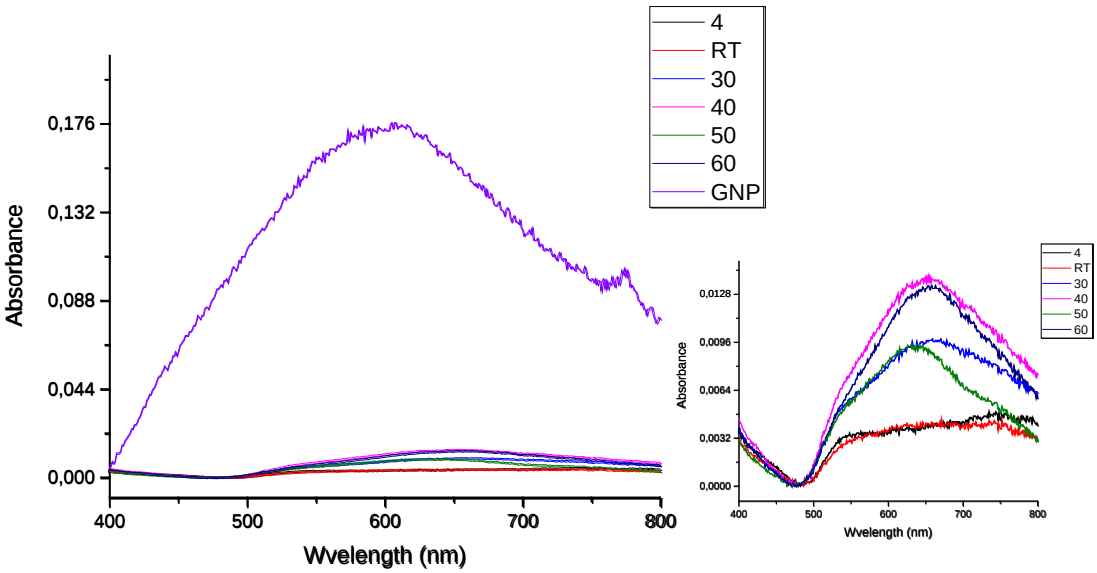

Figure 65. Oxidation spectrum of the pomegranate extract reduced GNPs for 10^{-6} M cyanide; inset shows the detailed view

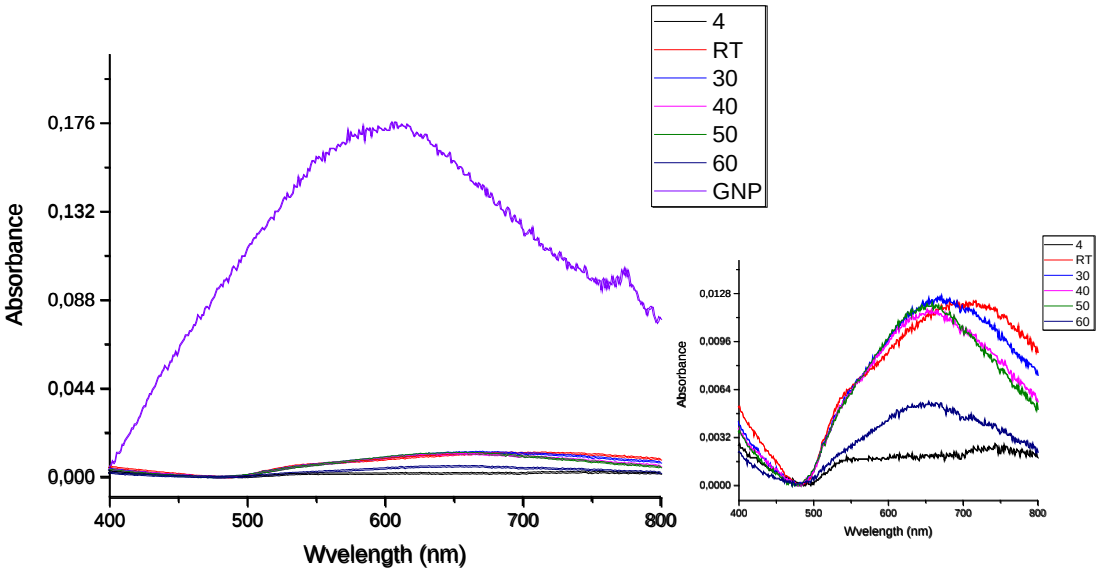

Figure 66. Oxidation spectrum of the pomegranate extract reduced GNPs for 10^{-7} M cyanide; inset shows the detailed view

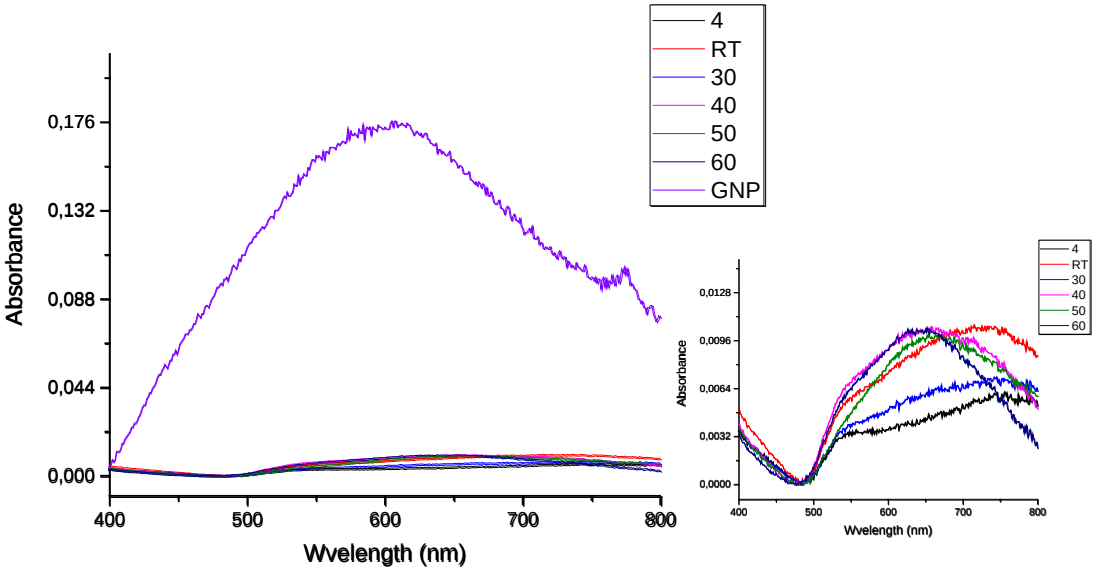

Figure 67. Oxidation spectrum of the pomegranate extract reduced GNPs for 10^{-8} M cyanide; inset shows the detailed view

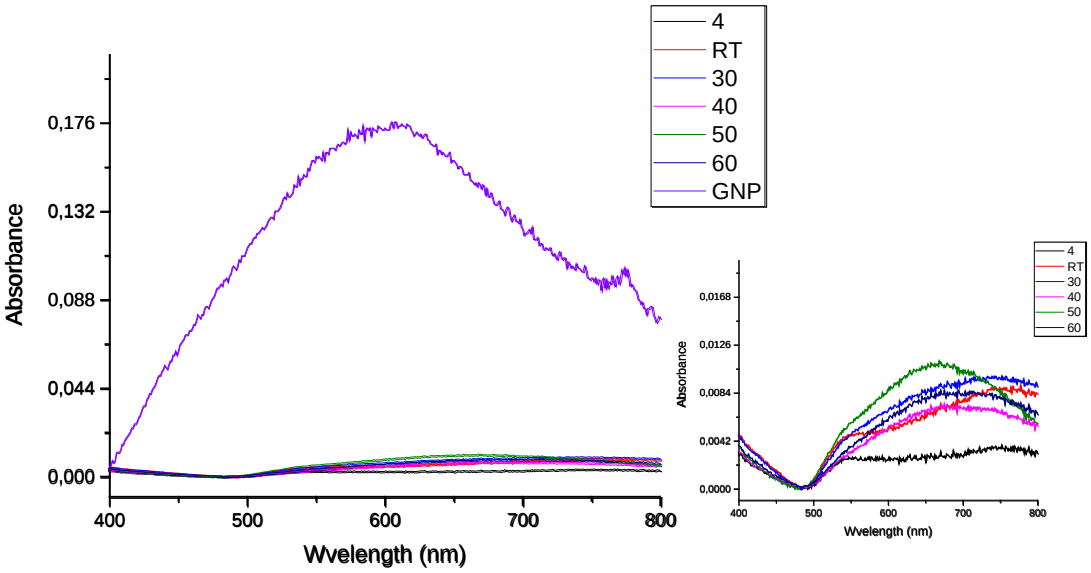

Figure 68. Oxidation spectrum of the pomegranate extract reduced GNPs for 10^{-9} M cyanide; inset shows the detailed view

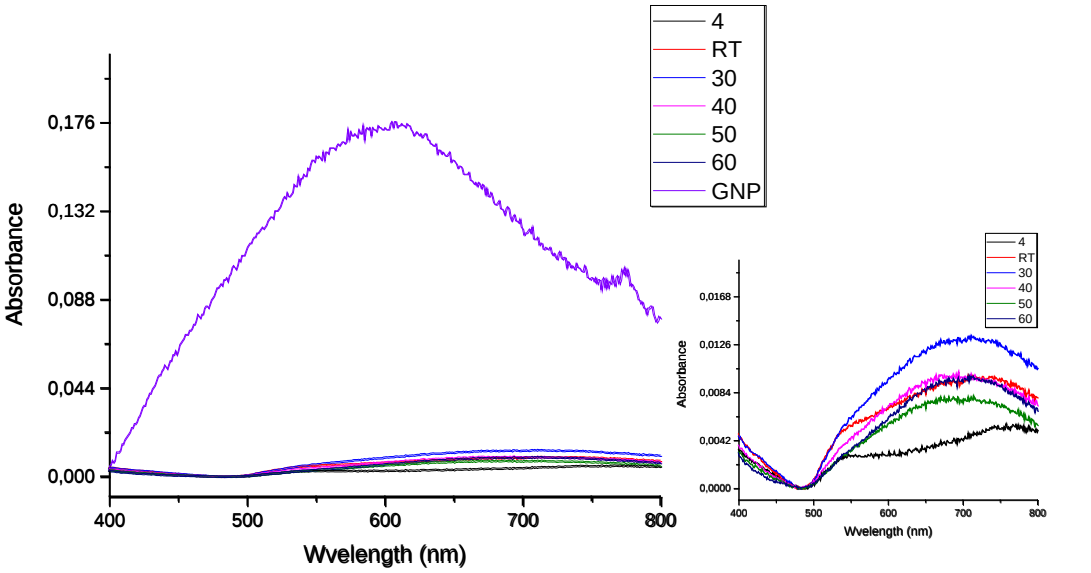

Figure 69. Oxidation spectrum of the pomegranate extract reduced GNPs for 10^{-10} M cyanide; inset shows the detailed view

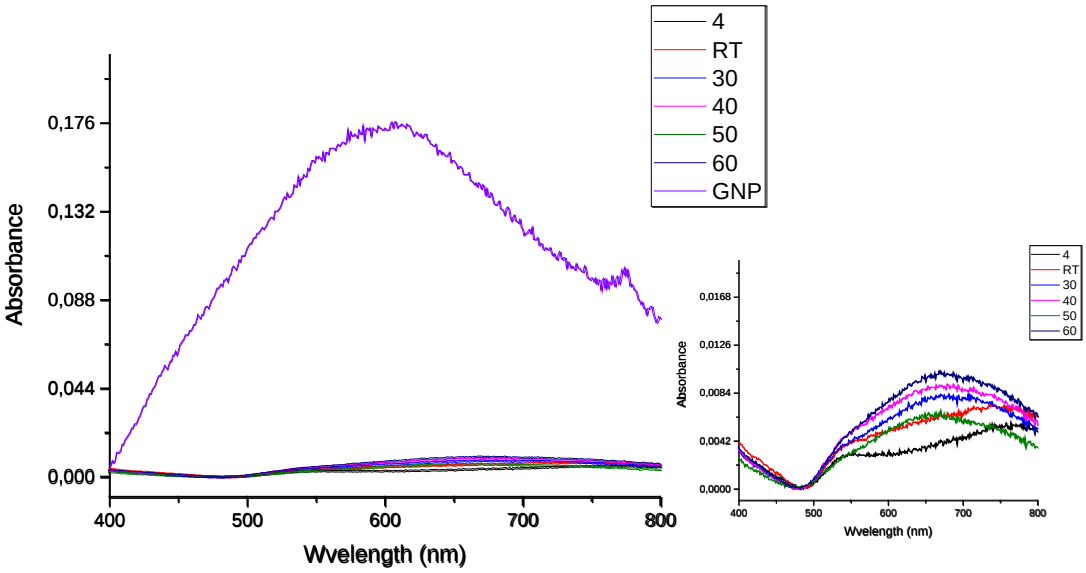

Figure 70. Oxidation spectrum of the pomegranate extract reduced GNPs for 10^{-11} M cyanide; inset shows the detailed view

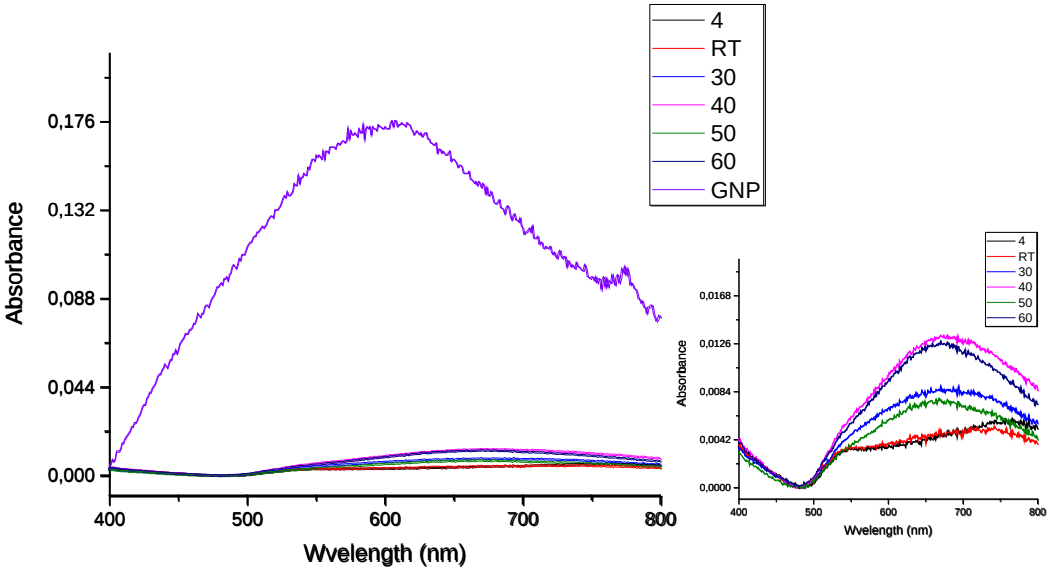

Figure 71. Oxidation spectrum of the pomegranate extract reduced GNPs for 10^{-12} M cyanide; inset shows the detailed view

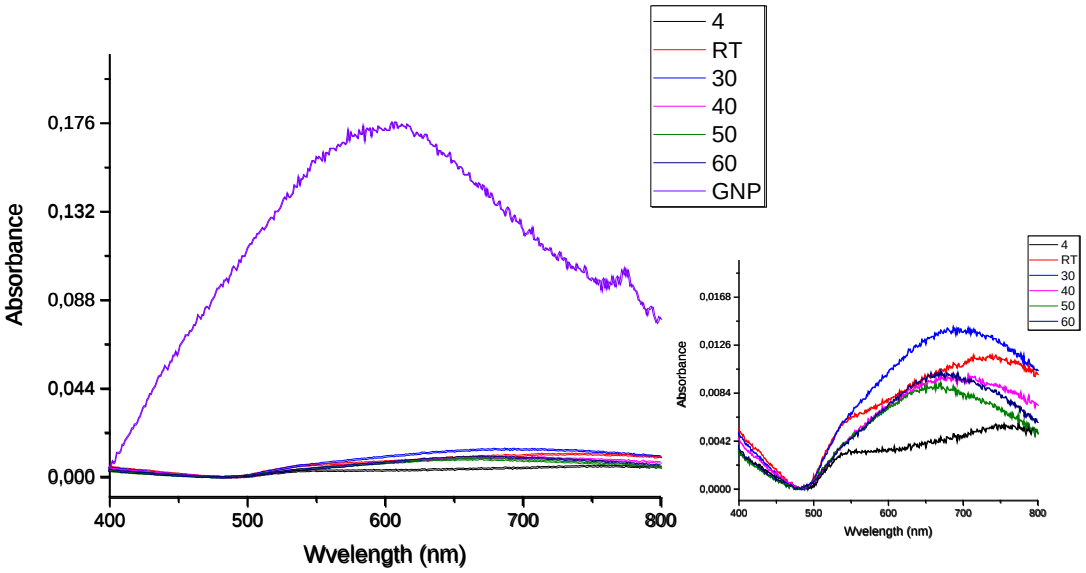

Figure 72. Oxidation spectrum of the pomegranate extract reduced GNPs for 10^{-13} M cyanide; inset shows the detailed view

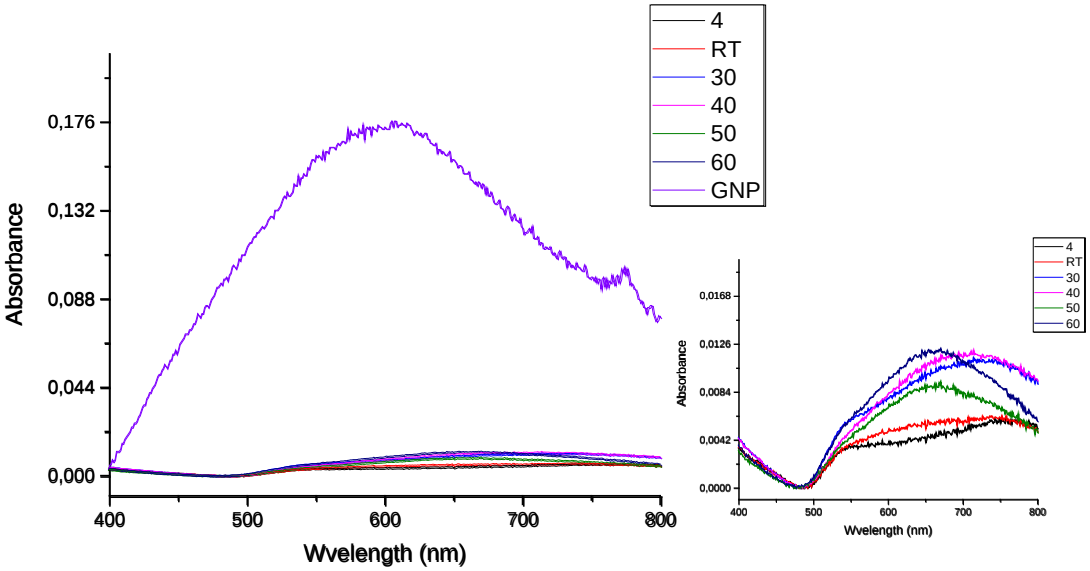

Figure 73. Oxidation spectrum of the pomegranate extract reduced GNPs for 10^{-14} M cyanide; inset shows the detailed view

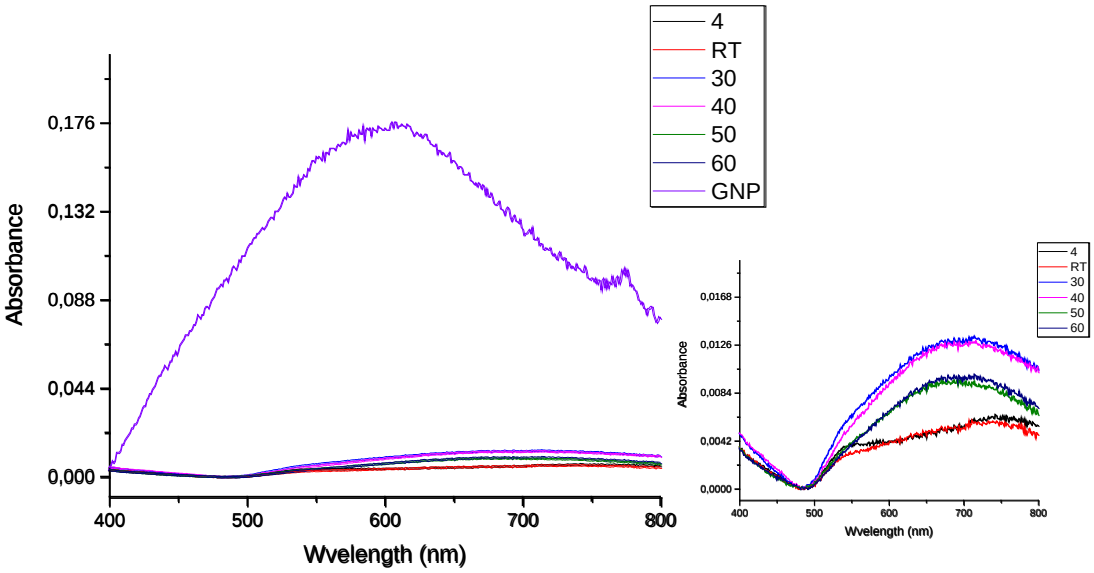

Figure 74. Oxidation spectrum of the pomegranate extract reduced GNPs for 10^{-15} M cyanide; inset shows the detailed view

Figures from 61 to 76, are representing the spectra of CN^- detection at varied CN^- concentrations (from 10^{-1} to 10^{-15}M) via pomegranate extract-reduced GNP oxidation. Similar results were obtained compared to melissa extract-reduced GNPs. The lowest detection limit was 10^{-15} M for CN^- detection via utilizing GNP immobilized plasmonic platform no correlation is observed based on the properties and synthesis conditions of GNPs.

3.3.3 Response of Plasmonic GNP Platform against Cyanide Oxidation via Varying Cyanide Concentrations

Absorbance responses and related intensity differences of immobilized GNPs before and after CN^-oxidation were analysed (Figure 76). It was observed that the most responsive plasmonic platform is the GNPs that were synthesized via melissa extract at lower temperatures such as 4 and RT. Figure 77 also shows the absorbance intensity differences of immobilized GNPs from pomegranate extract before and after CN^- oxidation. Among pomegranate samples 30 °C sample is observed as the most responsive one. However, no correlation is observed for varied synthesis conditions and temperatures.

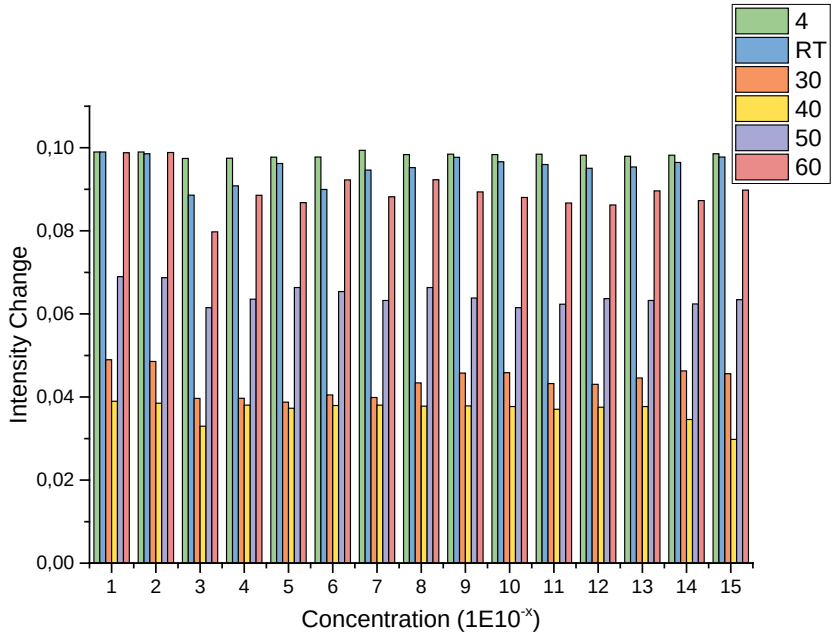

Figure 75. Absorbance intensity differences between immobilized and cyanide oxidized GNPs for the melissa-reduced samples

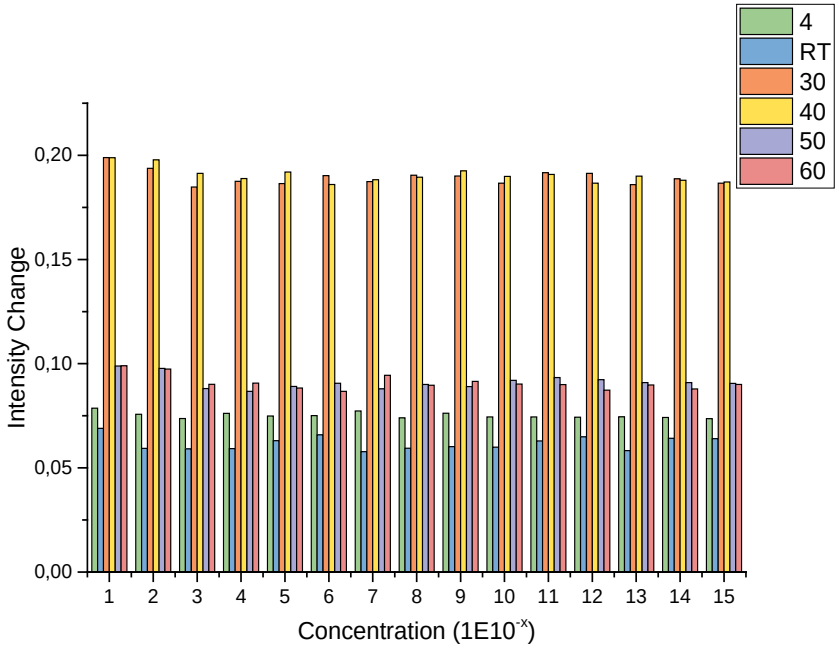

Figure 76. Absorbance intensity differences between immobilized and cyanide oxidized GNPs for the pomegranate-reduced samples

CHAPTER 4

CONCLUSION

GNPs synthesized from the plant extracts is a green synthesis method that uses mild reducing agent. The plant extracts of *Melissa officinalis* and *Punica granatum* were used in this thesis, along with preliminary studies on *Salvia officinalis*. The results from the sage extract induced GNPs, were not satisfactory for the future applications, since synthesis yield was too low. Therefore, characterization and utilization of GNPs were challenging due to the low concentration.

The size of the NPs vary from 6 to 55 nm, while the size of the nanoplates get smaller with increasing temperature; varying from 300 to 365 nm in width. Different nanoplate shapes were obtained from the synthesis such as; triangular, hexagonal and truncated triangular. The presence of nanoplates and shapes were confirmed via SEM analyses. After characterizing the GNPs from the melissa and pomegranate extracts, it can be concluded that the green synthesized GNPs have negative charge on their surfaces. This is caused by the organic molecules inducing the reduction reaction. The immobilization process is also affected from the surface charge. Negatively charged GNPs were immobilized using a positively charged polymer (PLL).

Analysis and detection of CN^- in water samples were the major application step of this work. Different concentrations of CN^- were analysed by using the GNP immobilized plasmonic platform. As a result, the lowest detection limit of the experiments was found to 10^{-15} M. Even though, temperature change, or reducing agent does not affect the detection system, immobilization efficiency of GNPs on a solid surface affects the results. In conclusion, all the CN^- detection trials regarding temperature and reducing agent variables were visually and optically done successfully. It was shown that the green synthesized GNP immobilized plasmonic platform can be utilized as an experimental platform for CN^- detection purpose.

REFERENCES

1. Nath, D.; Banerjee, P., Green nanotechnology - a new hope for medical biology. *Environ Toxicol Pharmacol* **2013,** *36* (3), 997-1014.

2. Sett, A.; Gadewar, M.; Sharma, P.; Deka, M.; Bora, U., Green synthesis of gold nanoparticles using aqueous extract ofDillenia indica. *Advances in Natural Sciences: Nanoscience and Nanotechnology* **2016,** *7* (2).

3. Kharissova, O. V.; Dias, H. V.; Kharisov, B. I.; Perez, B. O.; Perez, V. M., The greener synthesis of nanoparticles. *Trends Biotechnol* **2013,** *31* (4), 240-8.

4. Wu, S.; Zhou, X.; Yang, X.; Hou, Z.; Shi, Y.; Zhong, L.; Jiang, Q.; Zhang, Q., A rapid green strategy for the synthesis of Au “meatball”-like nanoparticles using green tea for SERS applications. *Journal of Nanoparticle Research* **2014,** *16* (9).

5. Shi, G.; Li, Y.; Xi, G.; Xu, Q.; He, Z.; Liu, Y.; Zhang, J.; Cai, J., Rapid green synthesis of gold nanocatalyst for high-efficiency degradation of quinclorac. *J Hazard Mater* **2017,** *335*, 170-177.

6. Sanda, F.; Takata, T.; Endo, T., Synthesis of a Novel Optically-Active Nylon-1 Polymer - Anionic-Polymerization of L-Leucine Methyl-Ester Isocyanate. *J. Polym. Sci. A: Polym. Chem.* **1995,** *33* (14), 2353-2358.

7. I Mudder, T.; M Botz, M., *Cyanide and society: A critical review*. 2003; Vol. 4.

8. Mason, G.; Littin, K., *The humaneness of rodent pest control*. 2003; Vol. 12.

9. Li, H.; Chen, T.; Jin, L.; Kan, Y.; Yin, B., Colorimetric and fluorometric dual-modal probes for cyanide detection based on the doubly activated Michael acceptor and their bioimaging applications. *Analytica Chimica Acta* **2014,** *852*, 203-211.

10. Wei, S. C.; Hsu, P. H.; Lee, Y. F.; Lin, Y. W.; Huang, C. C., Selective detection of iodide and cyanide anions using gold-nanoparticle-based fluorescent probes. *ACS Appl Mater Interfaces* **2012,** *4* (5), 2652-8.

11. Vijayaraghavan, K.; Ashokkumar, T., Plant-mediated biosynthesis of metallic nanoparticles: A review of literature, factors affecting synthesis, characterization techniques and applications. *Journal of Environmental Chemical Engineering* **2017,** *5* (5), 4866-4883.

12. Hornyak, G. L., Moore, J. J., Tibbals, H. F., Dutta, J., Fundamentals of Nanotechnology. **2008**.

13. van der Leeden, M. C.; Frens, G., Surface properties of plastic materials in relation to their adhering performance. *Adv Eng Mater* **2002,** *4* (5), 280-289.

14. Mirkhalaf, F.; Schiffrin, D. J., Surface spectroscopy and electrochemical characterisation of metal dithizonates covalently attached to gold by a self-assembled cysteamine monolayer. *J Chem Soc Faraday T* **1998,** *94* (9), 1321-1327.

15. Hardt, S.; Pennemann, H.; Schonfeld, F., Theoretical and experimental characterization of a low-Reynolds number split-and-recombine mixer. *Microfluidics and Nanofluidics* **2006,** *2* (3), 237-248.

16. Hussain, I., Singh, N. B., singh, A., Singh, H., Singh S.C., Green synthesis of nanoparticles and its potential application. *Biotechnology Letters* **2016,** *38*, 545-560.

17. Zhang, T.; Zhang, X.-Y.; Wang, L.-D.; Song, Y.-J.; Lin, M.-N.; Wang, L.-N.; Zhu, S.-Q.; Li, R.-Z., Fabrication and Optical Spectral Characterization of Linked Plasmonic Nanostructures and Nanodevices. *Materials Transactions* **2013,** *54* (6), 947-952.

18. Mieszawska, A. J.; Mulder, W. J.; Fayad, Z. A.; Cormode, D. P., Multifunctional gold nanoparticles for diagnosis and therapy of disease. *Mol Pharm* **2013,** *10* (3), 831-47.

19. Daniel, M. C., Astruc, D., Gold Nanoparticles: Assembly, Supramolecular Chemistry, Quantum-Size-Related Properties, and Applications toward Biology,Catalysis, and Nanotechnology. *Chemical Reviews* **2004,** *104*, 293-346.

20. Thakor, A. S.; Jokerst, J.; Zavaleta, C.; Massoud, T. F.; Gambhir, S. S., Gold nanoparticles: a revival in precious metal administration to patients. *Nano Lett* **2011,** *11* (10), 4029-36.

21. Faraday, M., X. The Bakerian Lecture. Experimental Relations of Gold (and Other Metals) to Light. *Phil. Trans. R. Soc. Lond.* **1857,** *147*, 145-185.

22. Turkevich, J.; Stevenson, P. C.; Hillier, J., A study of the nucleation and growth processes in the synthesis of colloidal gold. *Discussions of the Faraday Society* **1951,** *11* (0), 55-75.

23. Frens, G., Controlled Nucleation for Regulation of Particle-Size in Monodisperse Gold Suspensions. *Nature-Phys Sci* **1973,** *241* (105), 20-22.

24. Brust, M.; Walker, M.; Bethell, D.; Schiffrin, D. J.; Whyman, R., Synthesis of thiol-derivatised gold nanoparticles in a two-phase Liquid-Liquid system. *Journal of the Chemical Society, Chemical Communications* **1994,** (7), 801-802.

25. Clarke, N. Z.; Waters, C.; Johnson, K. A.; Satherley, J.; Schiffrin, D. J., Size-dependent solubility of thiol-derivatized gold nanoparticles in supercritical ethane. *Langmuir* **2001,** *17* (20), 6048-6050.

26. Waters, C. A.; Mills, A. J.; Johnson, K. A.; Schiffrin, D. J., Purification of dodecanethiol derivatised gold nanoparticles. *Chem Commun* **2003,** (4), 540-541.

27. Abad, J. M.; Sendroiu, L. E.; Gass, M.; Bleloch, A.; Mills, A. J.; Schiffrin, D. J., Synthesis of omega-hydroxy hexathiolate-protected subnanometric gold clusters. *Journal of the American Chemical Society* **2007,** *129* (43), 12932-+.

28. Liang, G.; Jin, X.; Zhang, S.; Xing, D., RGD peptide-modified fluorescent gold nanoclusters as highly efficient tumor-targeted radiotherapy sensitizers. *Biomaterials* **2017,** *144*, 95-104.

29. Sweeney, S. F., Woehrle, G. H., Hutchison, J. E., Rapid Purification and Size Separation of Gold Nanoparticles via Diafiltration. *Journal of American Chemical Society* **2006,** *128*, 3190-3197.

30. Taylor, A.; Verhoef, R.; Beuwer, M.; Wang, Y.; Zijlstra, P., All-Optical Imaging of Gold Nanoparticle Geometry Using Super-Resolution Microscopy. *J Phys Chem C Nanomater Interfaces* **2018,** *122* (4), 2336-2342.

31. Zou, L.; Qi, W.; Huang, R.; Su, R.; Wang, M.; He, Z., Green Synthesis of a Gold Nanoparticle–Nanocluster Composite Nanostructures Using Trypsin as Linking and Reducing Agents. *ACS Sustainable Chemistry & Engineering* **2013,** *1* (11), 1398-1404.

32. Elia, P.; Zach, R.; Hazan, S.; Kolusheva, S.; Porat, Z.; Zeiri, Y., Green synthesis of gold nanoparticles using plant extracts as reducing agents. *Int J Nanomedicine* **2014,** *9*, 4007-21.

33. Lin, Y.-W.; Chen, Y.-C.; Wang, C.-W.; Chen, W.-T.; Liu, C.-M.; Chen, C.-Y.; Chang, H.-T., Gold Nanosponges: Green Synthesis, Characterization, and Cytotoxicity. *Journal of Nanoscience and Nanotechnology* **2013,** *13* (10), 6566-6574.

34. Yulizar, Y.; Ariyanta, H. A.; Abduracman, L., Green Synthesis of Gold Nanoparticles using Aqueous Garlic (Allium sativum L.) Extract, and Its Interaction Study with Melamine. *Bulletin of Chemical Reaction Engineering & Catalysis* **2017,** *12* (2).

35. Luty-Błocho, M.; Wojnicki, M.; Grzonka, J.; Kurzydłowski, K. J.; Fitzner, K., Linking the Gold Nanoparticles Formation Kinetics with Their Morphology. *International Journal of Chemical Kinetics* **2018,** *50* (3), 204-214.

36. Luty-Błocho, M.; Wojnicki, M.; Fitzner, K., Gold Nanoparticles Formation via Au(III) Complex Ions Reduction with l-Ascorbic Acid. *International Journal of Chemical Kinetics* **2017,** *49* (11), 789-797.

37. Mukherjee, S.; Ghosh, S.; Das, D. K.; Chakraborty, P.; Choudhury, S.; Gupta, P.; Adhikary, A.; Dey, S.; Chattopadhyay, S., Gold-conjugated green tea nanoparticles for enhanced anti-tumor activities and hepatoprotection--synthesis, characterization and in vitro evaluation. *J Nutr Biochem* **2015,** *26* (11), 1283-97.

38. Chou, J.; Li, X.; Yin, Y.; Indrisek, N., Determination of antioxidant activities in fruit juices based on rapid colorimetric measurement and characterisation of gold nanoparticles. *International Journal of Environmental Analytical Chemistry* **2015,** *95* (6), 531-541.

39. Alshatwi, A. A.; Athinarayanan, J.; Periasamy, V. S., Green synthesis of bimetallic Au@Pt nanostructures and their application for proliferation inhibition and apoptosis induction in human cervical cancer cell. *J Mater Sci Mater Med* **2015,** *26* (3), 148.

40. Fang, A.; White, S. L.; Masitas, R. A.; Zamborini, F. P.; Jain, P. K., One-to-One Correlation between Structure and Optical Response in a Heterogeneous Distribution of Plasmonic Constructs. *The Journal of Physical Chemistry C* **2015,** *119* (42), 24086-24094.

41. Ziaková, A.; Brandsˇteterová, E., Application of Different Preparation Techniques for Extraction of Phenolic Antioxidants from Lemon Balm (Melissa Officinalis) before Hplc Analysis. *Journal of Liquid Chromatography & Related Technologies* **2002,** *25* (19), 3017-3032.

42. Mohamad, N. A. N.; Arham, N. A.; Jai, J.; Hadi, A., Plant Extract as Reducing Agent in Synthesis of Metallic Nanoparticles: A Review. *Advanced Materials Research* **2013,** *832*, 350-355.

43. Li, S.; Niu, H.; Qiao, Y.; Zhu, R.; Sun, Y.; Ren, Z.; Yuan, H.; Gao, Y.; Li, Y.; Chen, W.; Zhou, J.; Lou, H., Terpenoids isolated from Chinese liverworts Lepidozia reptans and their anti-inflammatory activity. *Bioorganic & Medicinal Chemistry* **2018,** *26* (9), 2392-2400.

44. Jiang, X.; Hansen, H. C. B.; Strobel, B. W.; Cedergreen, N., What is the aquatic toxicity of saponin-rich plant extracts used as biopesticides? *Environmental Pollution* **2018,** *236*, 416-424.

45. Awad, R.; Muhammad, A.; Durst, T.; Trudeau, V. L.; Arnason, J. T., Bioassay-guided fractionation of lemon balm (Melissa officinalis L.) using an in vitro measure of GABA transaminase activity. *Phytother Res* **2009,** *23* (8), 1075-81.

46. Grattan, S. R.; Grieve, C. M., Salinity–mineral nutrient relations in horticultural crops. *Scientia Horticulturae* **1998,** *78* (1), 127-157.

47. Salah, S. M.; Jäger, A. K., Screening of traditionally used Lebanese herbs for neurological activities. *Journal of Ethnopharmacology* **2005,** *97* (1), 145-149.

48. Jaeger, J.; Berns, S.; Uzelac, S.; Davis-Conway, S., Neurocognitive deficits and disability in major depressive disorder. *Psychiatry Research* **2006,** *145* (1), 39-48.

49. Akhondzadeh, S.; Noroozian, M.; Mohammadi, M.; Ohadinia, S.; Jamshidi, A.; Khani, M., Melissa officinalis extract in the treatment of patients with mild to moderate Alzheimer's disease: a double blind, randomised, placebo controlled trial. *Journal of Neurology, Neurosurgery, and Psychiatry* **2003,** *74* (7), 863-866.

50. Soulimani, R.; Fleurentin, J.; Mortier, F.; Misslin, R.; Derrieu, G.; Pelt, J.-M., Neurotropic Action of the Hydroalcoholic Extract of Melissa officinalis in the Mouse. *Planta Med* **1991,** *57* (02), 105-109.

51. Dragland, S.; Senoo, H.; Wake, K.; Holte, K.; Blomhoff, R., Several Culinary and Medicinal Herbs Are Important Sources of Dietary Antioxidants. *The Journal of Nutrition* **2003,** *133* (5), 1286-1290.

52. Triantaphyllou, G. B. D. K., Antioxidative properties of water extracts obtained from herbs of the species Lamiaceae. *International Journal of Food Sciences and Nutrition* **2009,** *52* (4), 313-317.

53. Cohen, R. A.; Kucera, L. S.; Herrmann, E. C., Antiviral Activity of Melissa officinalis (Lemon Balm) Extract. *Proceedings of the Society for Experimental Biology and Medicine* **1964,** *117* (2), 431-434.

54. Patora, J.; Majda, T.; Gora, J.; Klimek, B., Variability in the content and composition of essential oil from lemon balm (Melissa officinalis L.) cultivated in Poland. *Acta poloniae pharmaceutica* **2003,** *60* (5), 395-400.

55. Mikus, J.; Harkenthal, M.; Steverding, D.; Reichling, J., In vitro effect of essential oils and isolated mono- and sesquiterpenes on Leishmania major and Trypanosoma brucei. *Planta Med* **2000,** *66* (4), 366-8.

56. Brieskorn, C. H.; Krause, W., [Further triterpenes from Melissa officinalis L (author's transl)]. *Archiv der Pharmazie* **1974,** *307* (8), 603-12.

57. Sarer, E.; Kökdil, G., Constituents of the Essential Oil from Melissa officinalis. *Planta medica* **1991,** *57* (1), 89-90.

58. Tittel, G.; Wagner, H.; Bos, R., [Chemical composition of the essential oil from melissa]. *Planta Med* **1982,** *46* (2), 91-8.

59. Carnat, A. P.; Carnat, A.; Fraisse, D.; Lamaison, J. L., The aromatic and polyphenolic composition of lemon balm (Melissa officinalis L. subsp. officinalis) tea. *Pharmaceutica Acta Helvetiae* **1998,** *72* (5), 301-305.

60. Allahverdiyev, A.; Duran, N.; Ozguven, M.; Koltas, S., Antiviral activity of the volatile oils of Melissa officinalis L. against Herpes simplex virus type-2. *Phytomedicine : international journal of phytotherapy and phytopharmacology* **2004,** *11* (7-8), 657-61.

61. Karasová, G.; Lehotay, J.; Kłodzinska, E.; Gadzała-Kopciuch, R.; Buszewski, B., Comparison of Several Extraction Methods for the Isolation of Benzoic Acid Derivatives fromMelissa officinalis. *Journal of Liquid Chromatography & Related Technologies* **2006,** *29* (11), 1633-1644.

62. Butterfield, H. M., A history of subtropical fruits and nuts in California. **1963**.

63. Aggarwal, B. B.; Shishodia, S., Molecular targets of dietary agents for prevention and therapy of cancer. *Biochem Pharmacol* **2006,** *71* (10), 1397-421.

64. Hamidpour, M.; Hamidpour, R.; Hamidpour, S.; Shahlari, M., Chemistry, Pharmacology, and Medicinal Property of Sage (Salvia) to Prevent and Cure Illnesses such as Obesity, Diabetes, Depression, Dementia, Lupus, Autism, Heart Disease, and Cancer. *Journal of Traditional and Complementary Medicine* **2014,** *4* (2), 82-88.

65. T., D. C.; L., W. P.; J., F. F., ANTHOCYANINS OF POMEGRANATE, Punica granatum. *Journal of Food Science* **1975,** *40* (2), 417-418.

66. Amakura, Y.; Okada, M.; Tsuji, S.; Tonogai, Y., Determination of phenolic acids in fruit juices by isocratic column liquid chromatography. *J Chromatogr A* **2000,** *891* (1), 183-8.

67. de Pascual-Teresa, S.; Santos-Buelga, C.; Rivas-Gonzalo, J. C., Quantitative analysis of flavan-3-ols in Spanish foodstuffs and beverages. *J Agric Food Chem* **2000,** *48* (11), 5331-7.

68. Karakaplan, M., Özcan, M., Determination of phenolic acids in pomegranate juices by HPLCDAD. *European Journal of Science and Technology* **2017,** *6*, 32-37.

69. Waheed, S., Siddique, N., Rahman, A., Zaidi, J. H., Ahmad, S., INAA for dietary assessment of essential and other trace elements in fourteen fruits harvested and consumed in Pakistan. *Journal of Radioanalytical and Nuclear Chemistry* **2004,** *260* (3), 523-531.

70. Lansky, E. P.; Newman, R. A., Punica granatum (pomegranate) and its potential for prevention and treatment of inflammation and cancer. *J Ethnopharmacol* **2007,** *109* (2), 177-206.

71. Schubert, S. Y.; Lansky, E. P.; Neeman, I., Antioxidant and eicosanoid enzyme inhibition properties of pomegranate seed oil and fermented juice flavonoids. *J Ethnopharmacol* **1999,** *66* (1), 11-7.

72. van Elswijk, D. A.; Schobel, U. P.; Lansky, E. P.; Irth, H.; van der Greef, J., Rapid dereplication of estrogenic compounds in pomegranate (Punica granatum) using on-line biochemical detection coupled to mass spectrometry. *Phytochemistry* **2004,** *65* (2), 233-241.

73. Noda, Y.; Kaneyuki, T.; Mori, A.; Packer, L., Antioxidant activities of pomegranate fruit extract and its anthocyanidins: delphinidin, cyanidin, and pelargonidin. *J Agric Food Chem* **2002,** *50* (1), 166-71.

74. Huang, T. H.; Yang, Q.; Harada, M.; Li, G. Q.; Yamahara, J.; Roufogalis, B. D.; Li, Y., Pomegranate flower extract diminishes cardiac fibrosis in Zucker diabetic fatty rats: modulation of cardiac endothelin-1 and nuclear factor-kappaB pathways. *Journal of cardiovascular pharmacology* **2005,** *46* (6), 856-62.

75. World Health Organization (WHO), U. N. C. s. F. U., Progress on Drinking Water, Sanitation and Hygiene. *Licence: CC BY-NC-SA 3.0 IGO* **2017**.

76. Harikishore Kumar Reddy, D., Water Pollution Control Technologies A2 - Abraham, Martin A. In *Encyclopedia of Sustainable Technologies*, Elsevier: Oxford, 2017; pp 3-22.

77. Yu, L.; Yıldız, İ., 1.24 Energy and Water Pollution A2 - Dincer, Ibrahim. In *Comprehensive Energy Systems*, Elsevier: Oxford, 2018; pp 950-979.

78. Way, J. L., Cyanide Intoxication and its Mechanism of Antagonism. *Annual Review of Pharmacology and Toxicology* **1984,** *24* (1), 451-481.

79. Leavesley, H. B.; Li, L.; Mukhopadhyay, S.; Borowitz, J. L.; Isom, G. E., Nitrite-Mediated Antagonism of Cyanide Inhibition of Cytochrome c Oxidase in Dopamine Neurons. *Toxicological Sciences* **2010,** *115* (2), 569-576.

80. Beasley, D. M.; Glass, W. I., Cyanide poisoning: pathophysiology and treatment recommendations. *Occupational medicine (Oxford, England)* **1998,** *48* (7), 427-31.

81. Organization, W. H.; Safety, I. P. o. C., Guidelines for drinking-water quality. Vol. 2, Health criteria and other supporting information. *Geneva : World Health Organization* **1996**.

82. Dumas, P.; Gingras, G.; LeBlanc, A., Isotope Dilution-Mass Spectrometry Determination of Blood Cyanide by Headspace Gas Chromatography. *Journal of Analytical Toxicology* **2005,** *29* (1), 71-75.

83. Iqbal, J.; Whitney, P., Use of cyanide and diethyldithiocarbamate in the assay on superoxide dismutases. *Free Radical Biology and Medicine* **1991,** *10* (1), 69-77.

84. Organization, W. H., Cyanide in Drinking-water. *WHO Guidelines for Drinking-water Quality* **1996,** *2*.

85. Agency, U. S. E. P., 2012 Edition of the Drinking Water standars and Helath Advisories. **2012**.

86. (ATSDR), A. f. T. S. a. D. R., Toxicological profile for Cyanide. Atlanta. *U.S. Department of Health and Human Services, Public Health Service.* **2006**.

87. Goshman, L. M., Clinical Toxicology of Commercial Products, 5th ed. *Journal of Pharmaceutical Sciences 74* (10), 1139.

88. Hu, J.-W.; Lin, W.-C.; Hsiao, S.-Y.; Wu, Y.-H.; Chen, H.-W.; Chen, K.-Y., An indanedione-based chemodosimeter for selective naked-eye and fluorogenic detection of cyanide. *Sensors and Actuators B: Chemical* **2016,** *233*, 510-519.

89. Batista, R. M. F.; Costa, S. P. G.; Raposo, M. M. M., Selective colorimetric and fluorimetric detection of cyanide in aqueous solution using novel heterocyclic imidazo-anthraquinones. *Sensors and Actuators B: Chemical* **2014,** *191*, 791-799.

90. Isaad, J.; Achari, A. E., A novel glycoconjugated N-acetylamino aldehyde hydrazone azo dye as chromogenic probe for cyanide detection in water. *Analytica Chimica Acta* **2011,** *694* (1), 120-127.

91. Kumar, V.; Kaushik, M. P.; Srivastava, A. K.; Pratap, A.; Thiruvenkatam, V.; Row, T. N. G., Thiourea based novel chromogenic sensor for selective detection of fluoride and cyanide anions in organic and aqueous media. *Analytica Chimica Acta* **2010,** *663* (1), 77-84.

92. Ajayakumar, M. R.; Mandal, K.; Rawat, K.; Asthana, D.; Pandey, R.; Sharma, A.; Yadav, S.; Ghosh, S.; Mukhopadhyay, P., Single Electron Transfer-Driven Multi-Dimensional Signal Read-out Function of TCNQ as an "Off-the-Shelf" Detector for Cyanide. *ACS Applied Materials & Interfaces* **2013,** *5* (15), 6996-7000.

93. Yang, L.; Li, X.; Yang, J.; Qu, Y.; Hua, J., Colorimetric and Ratiometric Near-Infrared Fluorescent Cyanide Chemodosimeter Based on Phenazine Derivatives. *ACS Applied Materials & Interfaces* **2013,** *5* (4), 1317-1326.

94. Parga, J. R.; Valenzuela, J. s. L.; Vazquez, V. c.; Rodriguez, M.; Moreno, H. c., Removal of Aqueous Lead and Copper Ions by Using Natural Hydroxyapatite Powder and Sulphide Precipitation in Cyanidation Process. *Materials Sciences and Applications* **2013,** *Vol.04No.04*, 7.

95. Delaney, M. F., Testing for Cyanide in Drinking Water. *United States Environmental Protection Agency* **2017**.

96. Delgado, A. V.; González-Caballero, F.; Hunter, R. J.; Koopal, L. K.; Lyklema, J., Measurement and Interpretation of Electrokinetic Phenomena (IUPAC Technical Report). *Pure and Applied Chemistry* **2005,** *77* (10), 1753-1805.

97. Huo, Q.; Worden, J. G., Monofunctional gold nanoparticles: synthesis and applications. *Journal of Nanoparticle Research* **2006,** *9* (6), 1013-1025.

98. Hong, S.; Shuford, K. L.; Park, S., Shape Transformation of Gold Nanoplates and their Surface Plasmon Characterization: Triangular to Hexagonal Nanoplates. *Chemistry of Materials* **2011,** *23* (8), 2011-2013.

99. Reimschu.Ac; Frederic.Rj, APPLICATION OF SCANNING ELECTRON MICROSCOPY TO STUDY OF MORPHOLOGY OF MULTICOMPONENT CATALYST SYSTEMS - PETR. *Abstr. Pap. Am. Chem. Soc.* **1970,** (FEB), 42-&.